Fakultät für Medizin
Urologische Klinik und Poliklinik

Establishment of an orthotopic bladder cancer mouse model for the assessment of a YB-1 based viro-immunotherapy *in vivo*

Eva Franziska Philomena Lichtenegger

Vollständiger Abdruck der von der Fakultät für Medizin der Technischen Universität München zur Erlangung des akademischen Grades eines
Doktors der Naturwissenschaften (Dr. rer. nat.)
genehmigten Dissertation

Vorsitzender: Prof. Dr. Roland Rad

Prüfer der Dissertation:

1: Prof. Dr. Per Sonne Holm
2: Prof. Dr. Gabriele Multhoff

Die Dissertation wurde am 15.02.2018 bei der Fakultät für Medizin der Technischen Universität München eingereicht und durch die Fakultät für Medizin am 04.07.2018 angenommen

Abstract

Oncolytic viruses are a novel therapeutic approach for cancer treatment. They cause a tumor-specific cell lysis and induce an immune stimulatory effect. T-Vec, a genetically modified herpes simplex virus carrying a gene for GM-CSF, is the first oncolytic virus approved for cancer treatment. In a recent study, excellent results were obtained by combining T-Vec with PD-L1 blockade demonstrating the highly effective therapeutic impact of oncolytic virotherapy in combination with immune checkpoint blockade.

In this project, we generated the novel virus XVir-N-31-aPD-L1, a YB-1 dependent oncolytic adenovirus containing a transgene for an anti-PD-L1 antibody which combines XVir-N-31 with a PD-L1 specific immune checkpoint blockade. XVir-N-31-aPD-L1 showed efficient replication and cell lysis in the human bladder cancer cell line UMUC3. Further on, we demonstrated the transgene expression, antibody synthesis and secretion and the specific binding of the antibody to its antigen.

In order to analyze the therapeutic effect of XVir-N-31-aPD-L1 in an immunocompetent, syngeneic mouse model, we tested if the murine MB49 cells are suitable for adenoviral replication. We were able to overcome the low permissiveness of murine MB49 cells for human adenovirus by use of the Mdm2 inhibitor nutlin-3a. Nutlin-3a led to a significant increase in viral replication, cell killing effect and antibody synthesis in XVir-N-31-aPD-L1 infected cells. To identify the underlying mechanism, we analyzed the biochemical effects and found that nutlin-3a induced a G1 arrest and downregulated pRb and E2F1 suggesting that E2F1 downregulation supports adenoviral replication.

In order to investigate XVir-N-31 as a new therapeutic approach for bladder cancer, we established an orthotopic, ultrasound guided xenograft mouse model for bladder cancer using the human UMUC3 cells. This method is minimally invasive and uses an ultrasound-based technique for highly precise tumor cell injections into the lamina propria of the bladder. We found that our YB-1 based virotherapy is able to significantly reduce tumor growth by 42 % in the orthotopic mouse model. Furthermore, we successfully established a syngeneic, immunocompetent model using MB49 cells. This model can be used in the future to evaluate the impact of the immune system on the therapeutic effect of our YB-1 based viro-immunotherapy.

Considering the recent achievements of virotherapy in combination with immune checkpoint blockade, our findings are an important step in translating the YB-1 based virotherapy into the clinic for bladder cancer therapy.

Zusammenfassung

Onkolytische Viren sind ein neuer therapeutischer Ansatz für die Krebsbehandlung, welche eine selektive Lyse von Tumorzellen induzieren und dadurch das Immunsystem stimulieren. T-Vec, ein genetisch verändertes, GM-CSF exprimierendes Herpes simplex Virus, ist das erste für die Behandlung von Tumoren zugelassene onkolytische Virus. In einer neuen Studie wurden hervorragende Ergebnisse durch die Kombination von T-Vec mit einer PD-L1 Blockade erzielt. Diese Resultate demonstrieren die hocheffektive therapeutische Wirkung der onkolytischen Virotherapie in Kombination mit Immuncheckpointblockade.

In diesem Projekt wurde das neue Virus XVir-N-31-aPD-L1 generiert, welches für einen anti-PD-L1 Antikörper kodiert und somit das YB-1 abhängige onkolytische Adenovirus XVir-N-31 mit einer PD-L1 spezifischen Immuncheckpointblockade kombiniert. XVir-N-31-aPD-L1 zeigte effektive Replikation und Zelllyse in den humanen Blasenkarzinomzellen UMUC3. Außerdem konnte die Transgenexpression, die Synthese und Sekretion des Antikörpers sowie die spezifische Bindung des Antikörpers an das Antigen nachgewiesen werden.

Um den therapeutischen Effekt von XVir-N-31-aPD-L1 in einem immunkompetenten syngenen Mausmodell zu untersuchen, wurde die murine Zelllinie MB49 auf ihre Eignung für adenovirale Replikation untersucht. Die geringe Empfänglichkeit von murinen MB49 Zellen für humane Adenoviren konnte durch die Verwendung des Mdm2 Inhibitors Nutlin-3a überwunden werden. Nutlin-3a führte zu einer signifikant erhöhten Replikation, Zelllyse und Antikörpersynthese von XVir-N-31-aPD-L1 infizierten Zellen. Um den zugrundeliegenden Mechanismus zu verstehen, wurden die biochemischen Effekte von Nutlin-3a untersucht. Dabei konnte gezeigt werden, dass Nutlin-3a einen G1 Arrest induziert und pRb und E2F1 runterreguliert, was zu der Vermutung führte, dass eine reduzierte E2F1 Expression adenovirale Replikation unterstützt.

Um XVir-N-31 als neuen therapeutischen Ansatz für das Blasenkarzinom zu untersuchen, wurde ein orthotopes, ultraschallgesteuertes xenograft Mausmodell unter Verwendung der humanen UMUC3 Zellen etabliert. Diese Methode ist minimalinvasiv und mithilfe der ultraschallbasierten Technik können hochpräzise Injektionen in die Lamina Propria der Blasenwand durchgeführt werden. In dem orthotopen Mausmodell führte die YB-1 basierte Virotherapie zu einer signifikanten Reduzierung des Tumorwachstums um 42%. Des Weiteren wurde ein syngenes, immunkompetentes Mausmodell unter Verwendung der murinen MB49 Zellen etabliert. Dieses Model kann in Zukunft verwendet werden, um den Einfluss des Immunsystems auf den therapeutischen Effekt unserer YB-1 basierten Viro-Immuntherapie zu untersuchen.

Diese Ergebnisse sind angesichts der neusten Errungenschaften der Virotherapie in Kombination mit Immuncheckpointblockade ein wichtiger Schritt, um die YB-1 basierte Virotherapie zur Behandlung von Blasenkrebs in die Klinik zu übertragen.

Acknowledgement

First and foremost, I want to thank Prof. Dr. Gschwend for giving me the opportunity to work in his department.

I would like to express my sincere gratitude to my advisor PD Per Sonne Holm. He gave me the opportunity to work on a project that was innovative, up to date and exceptional. He has taught me many aspects of scientific research. I appreciated all his contributions to the difficulties of the project. His supervision helped me to learn a broad spectrum of scientific methodology, patience and critical thinking. He taught me to plan and manage my project independently. The joy and enthusiasm he has for his research were motivational for me and I am very happy and thankful about the experiences I made in his lab.

Thanks also to PD Roman Nawroth for his advices and help. I always enjoyed the discussions with him.

I am deeply grateful to the members of the urological research group. You have contributed immensely to my time in this lab. Dear Klaus, thank you for your cloning advice, your guidance and your persistent help. Your optimism motivated me throughout the last three years. Dear Jana, Judith, Pan Qi and Zhichao, you were wonderful colleagues. Thank you for your constructive comments and your encouragement. I also want to thank Angelika for her help in the lab and all the past and present members of the Holm and Nawroth group. The atmosphere was always friendly and cooperative and I enjoyed working there.

I would like to offer my greatest appreciation to Igor Moscalev from the Prostate Cancer Centre in Vancouver for his patience, guidance and precious help during learning and establishing the ultrasound guided orthotopic bladder cancer model. Special thanks also to Helena for her support in generating this mouse model and my brother for constructing the needle mounting.

I also want to thank Prof. Gabi Multhoff for the time in her lab and her supportive comments. I extent my gratitude to Prof. Klaus-Peter Janssen and PD Melanie Laschinger. Thank you for your help and your motivating words.

Thanks also to the DFG for financial support for this project.

My deepest appreciation goes to Yoshi, my family and all my friends. Thank you for your love, trust and patience. Your optimism and support encouraged me to pursue my goal.

Contents

List of Figures

List of Tables

List of Symbols and Abbreviations

µl	microliter
ml	milliliter
l	liter
nm	nanometer
µm	micrometer
cm	centimeter
m	meter
fg	femtogram
ng	nanogram
µg	microgram
mg	milligram
nM	nanomolar
µM	micromolar
mM	millimolar
fmol	femtomole
nmol	nanomole
µmol	micromole
mmol	millimole
V	volt
°C	degree Celsius
sec	seconds
min	minute
h	hour
w/v	weight/volume

ADP	Adenoviral death protein
APC	Antigen presenting cell
APS	Ammonium persulfate
ATP	Adenosine triphosphate
BCG	Bacillus Galmette-Guerin
Bcl-2	B cell lymphoma-2
Bp	Base pair
BSA	Bovine serum albumin
$CaCl_2$	Calcium chloride
CAR	Coxsackie adenovirus receptor
CD	Cluster of differentiation

CIS	Carcinoma in situ
CPE	Cytopathic effect
CRT	Calreticulin
CsCl	Caesium chloride
CTLA-4	Cytotoxic T-lymphocyte associated-protein 4
CTLs	Cytotoxic T lymphocytes
DAMP	Danger associated molecular pattern
DC	Dendritic cell
DMEM	Dulbecco's modified eagle medium
DMSO	Dimethyl sulfoxide
DNA	Deoxyribonucleic acid
dNTPs	Deoxynucleotide triphosphate
DTT	Dithiothreitol
ECL	Enhanced chemiluminescence
EDTA	Ethilenediaminetetraacetic acid
ER	Endoplasmatic reticulum
FACS	Fluorescence activated cell sorting
FBS	Fetal bovine serum
FDA	Food and drug administration
FITC	Fluorescein isothiocyanate
FoxO1	Forkheadbox protein O1
Fw primer	Forward primer
GM-CSF	Granulocyte- macrophage - colony stimulating factor
GSTM1	Glutathione S-transferase
H_2O_2	Hydrogen peroxide
HCl	Hydrochloride acid
HMGB1	High-mobility group box 1
HSV-1	Herpes simplex virus 1
ICB	Immune checkpoint blockade
ICD	Immunogenic cell death
IF	Immunofluorescence
IFNγ	Interferon- γ
IHC	Immunohisto chemistry
IRF3/7	Interferon regulatory factor 3/7
IVC	Individual ventilated cage
Jak/STAT	Janus kinase/signal transducer and activator of transcription
kDa	Kilo Dalton
LAG-3	Lymphocyte activation gene 3
MgCl	Magnesium chloride
MHC	Major histocompatibility complex

MIBC	Muscle-invasive bladder cancer
MLP	Major late promoter
MMF	Medetomidine, midazolam, fentanyl
MMR	Mismatch repair
mRNA	Messenger RNA
mTOR	Mechanistic target of rapamycin
Mdm2	Mouse double minute homologue 2
MyD88	Myeloid differentiation primary response 88
NaCl	Sodium chloride
NAT2	N-acetyltransferase-2
NEAA	Non-essential amino acids
NLR	Nucleotide oligomerization domain (NOD)-like receptor
NMIBC	Non muscle-invasive bladder cancer
NOD	Nucleotide oligomerization domain
ORR	Objective response rate
OVT	Oncolytic virotherapy
P2RX7	Purinoreceptor 7
PBS	Phosphate buffered saline
PCR	Polymerase chain reaction
PD-1	Programmed death protein 1
PD-L1/2	Programmed death-ligand 1/2
PFU	Plaque forming units
PI3K	Phosphoinositide 3-kinase
PTEN	Phosphatase and tensin homolog
qPCR	Quantitative PCR
Ras	Rat sarcoma
Rb	Retinoblastoma
Rev primer	Reverse primer
RGD	Arginine-Glycine-Aspartic acid
RIG-1	Retinoic acid inducible gene-
RNA	Ribonucleic acid
ROS	Reactive oxygen species
RPMI	Roswell park memorial institute
SDS	Sodium dodecyl sulfate
SDS-PAGE	SDS - Polyacrylamide gel electrophoresis
SHP2	Src-homology 2 domain-containing phosphatase
SRB	Sulforhodamine B
STING	Stimulator of interferon genes
TAAs	Tumor associated antigens
TBS	Tris buffered saline

TBS-T	Tris buffered saline with Tween-20
TCA	Trichloric acid
TCR	T cell receptor
TEMED	Tetramethylethylenediamine
TIL	Tumor infiltrating lymphocyte
TIM-3	T-cell immunoglobin and mucin-domain containing-3
TLR4	Toll-like receptor 4
TNM	Tumor, node and metastasis
TP	Terminal protein
Tregs	Regulatory T cells
Tris	Tris(hydroxymethyl)-aminomethane
TSA	Tumor-specific antigen
T-VEC	Talimogene laherparepvec
WB	Western Blot
WtAd	Wild type adenovirus
YB-1	Y-box binding protein 1
ZAP70	Zeta-chain-associated protein kinase 70

1 Introduction

Bladder cancer is defined as a neoplastic lesion originating from the tissue of the urinary bladder. More than 95 % of bladder tumors arise from the epithelium and the majority of these are urothelial carcinomas affecting the urothelium (Tanaka et al. 2011).

The approval of different immune checkpoint inhibitors has opened a new field in cancer therapy. Targeting the Programmed death protein 1 (PD-1) or Programmed death 1 ligand 1 (PD-L1) with antibodies is becoming standard of care treatment for multiple tumor entities, including metastatic melanoma, lung, kidney and also bladder cancer (Sharma und Allison 2015). It unlocks immune suppressive pathways and induces a consistent anti-tumor immune response. However, the use of PD-1/PD-L1 inhibitors clearly showed that the majority of patients (60 – 80 %) is resistant and does not benefit from this therapy. Immense research activity on this field brought light into the mechanisms of resistance and showed that the expression of target molecules on both tumor cells and immune cells is unstable but can be induced by intrinsic as well as extrinsic factors (Ritprajak und Azuma 2015). In addition, it was also shown that the presence of $CD8^+$ T cells is mandatory (Pardoll 2012). These results serve as the rational to combine immune checkpoint blockade (ICB) with an immune stimulatory therapy like virotherapy (Ribas et al. 2017).

Oncolytic viruses were underestimated for decades. However, the approval of Talimogene laherparepvec (T-Vec) demonstrates their immense power in cancer therapy (Rehman et al. 2016). Oncolytic viruses induce cancer cell lysis and thereby cause a strong immune stimulatory effect (Guo et al. 2017). The hypothesis of combining PD-1/PD-L1 specific immune checkpoint blockade (ICB) and oncolytic virotherapy was just recently proven right (Ribas et al. 2017). This study achieved an outstanding objective response rate of 62 % with a complete response rate of 33 %. It demonstrated that oncolytic viruses change the tumor microenvironment due to their immune stimulatory effect and thereby improve ICB (Ribas et al. 2017).

These exceptional findings are clinically highly important and serve as a basis for new and auspicious combinatorial viro-immunotherapy-approaches in a variety of cancers, including bladder cancer. In this project, we aimed to develop and characterize the novel combination therapy using YB-1 based virotherapy and a PD-L1 specific immune checkpoint blockade.

1.1 Epidemiology of bladder cancer

Bladder cancer is the ninth most common cancer worldwide and the second most common genitourinary cancer. There were an estimated 429 000 patients diagnosed for bladder cancer and 165 000 deaths from bladder cancer in 2012 (Ferlay et al. 2015). It occurs more often in man than in women (worldwide sex ratio of 3,5:1) and 60 % of all incident cases are diagnosed in more developed countries (Ferlay et al. 2015). Risk factors for developing bladder cancer are mainly environmental with cigarette smoking as one of the best-established factors. Approximately 50 % of all BLCA are associated with

smoking (Freedman et al. 2011). There is an almost linear correlation between the risk of bladder cancer and the duration of smoking. 20 years of smoking increases the risk for bladder cancer roughly about 100 % and 60 years of smoking about 500 % (Brennan et al. 2000). The second most important risk factor for bladder cancer is the exposure to carcinogens like polycyclic aromatic hydrocarbons, aromatic amines and chlorinated hydrocarbons. These factors occur mainly in industrial areas and are associated with roughly 20 % of all bladder cancer cases (Burger et al. 2013). There is also a genetic susceptibility for bladder cancer. First degree relatives to bladder cancer patients have a two-fold increased risk of developing bladder cancer (Burger et al. 2013). Some inherited genetic defects like in the carcinogen detoxifying genes N-acetyltransferase-2 (NAT2) and glutathione S-transferase (GSTM1) are additional risk factors to the exposure of carcinogens or tobacco for developing bladder cancer (Burger et al. 2013; Knowles und Hurst 2015). Single nucleotide polymorphisms (SNPs) close to genes like MYC, TP63 or FGFR3 are also moderate risk factors for bladder cancer (Knowles und Hurst 2015).

1.2 Bladder cancer staging and grading

Bladder cancer stages are defined by the tumor, node and metastasis (TNM) classification which describes the extent of invasion (figure 1.1) (Knowles und Hurst 2015; Witjes et al. 2014). T describes the size of the tumor and whether it has invaded nearby tissue. N describes if proximate lymph nodes are involved and M scores distant metastasis formation (Witjes et al. 2014). Flat tumors localized to the epithelium are classified as carcinoma in situ (CIS). Stage Ta describes non-muscle invasive bladder cancer which make up the majority of bladder cancer at diagnosis (roughly 60 %). Stage Ta tumors are papillary tumors of low grade, they are described as non-muscle-invasive bladder cancer (NMIBC). Stage T1 tumors penetrate the epithelium but do not invade into the muscle layer. Tumors of stages T2a and T2b invade the superficial and deep muscle. T3 stage tumors already penetrate perivesical tissue and T4 tumors are those that invade adjacent tissues and organs. Tumors belonging to stages T1 up to T4 are described as muscle-invasive bladder cancer (MIBC) and high-grade tumors. NMIBCs have a five-year survival of roughly 90 %, they mostly recur and rarely progress to invasive forms. MIBCs often progress and develop metastasis, they have a five-year survival of less than 50 % (Knowles und Hurst 2015).

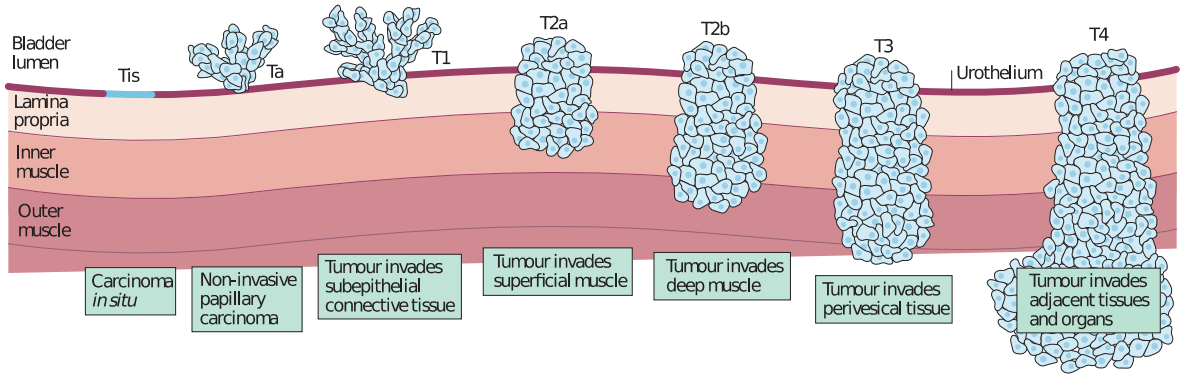

Figure 1.1: Bladder cancer staging. Tis describes local epithelial dysplasia. Ta includes non-invasive tumors. Invasive tumors are staged fromT1 to T4 depending on their invasive growth into surrounding tissue. Figure adapted from (Knowles und Hurst 2015).

1.3 The biology of adenoviruses

Human adenoviruses are double stranded, non-enveloped DNA viruses that can infect a variety of human tissues (Ghebremedhin 2014). They belong to the family of Adenoviridae and the genus Mastadenovirus. About 60 serotypes are known which can be classified into seven species (A-G). Adenoviruses are DNA viruses that have a characteristic icosahedral structure (figure 1.2). The icosahedral capsid consists of a number of minor proteins, VI, VIII, IX, IIIa, IVa2 and the three major proteins hexon (II), penton base (III) and a knobbed fiber (IV) (Russell 2000). There are 240 hexons in one capsid which can be grouped into four types, H1 to H4, according to their different environment. The penton capsomere consists of the penton base and the fiber which binds non-covalently to the penton base. The fiber protein is essential in the early event of infection as it binds to adenoviral receptors on the host cell and mediates cell entry (Russell 2009). The linear, double stranded genome has a size of 26 to 44 kilo base pairs and is covalently attached to the terminal protein (TP) at its 5' termini (Russell 2000). In addition, the DNA is associated with the three core proteins V, VII and Mu (μ). Within the virion, the DNA is organized in a central dense core (Giberson et al. 2012). This work focuses on Adenovirus species C, serotype 5.

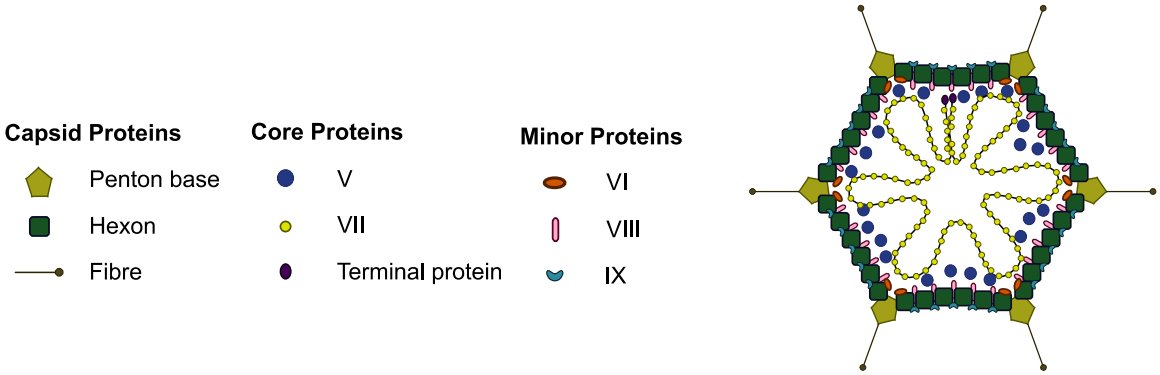

Figure 1.2: Adenovirus structure. A schematic depiction of the adenoviral structure shows the icosahedral capsid comprising hexon proteins, penton base proteins and fibre proteins. The dsDNA within the core is stabilized by core proteins and the terminal protein (Russell 2000). Figure adapted from (Russell 2009).

1.3.1 Adenoviral infection, life cycle and host tropism

During the initial phase of infection, the fiber protein interacts with the given host by binding to the primary receptor which differs among the subgroups (Sharma et al. 2009). The most used receptor is the coxsackie and adenovirus receptor (CAR) (Russell 2009). It belongs to the immunoglobin superfamily and is supposed to be involved in tight junction formation in epithelial cells (Cohen et al. 2001; Philipson und Pettersson 2004). Further adenoviral receptors are, besides other, CD46, CD80/86 or sialic acid (Arnberg et al. 2000). For successful infection of the host cell, not only receptor attachment but also rapid internalization is important. This occurs with binding of the highly conserved Arginine-Glycine-Aspartic acid (RGD) motif on the penton base to αvβ3 or αvβ5 integrins. The virus is completely internalized by clathrin-coated vesicles or endosomes (Russell 2009; Nemerow 2000). To facilitate this process cellular signaling molecules like Rho GTPases and phosphatidylinositol-4,5-biphosphate 3-kinase (PI3 kinases) help to disrupt the cytoskeleton. Within the endosome, the viral particle breaks apart and the endosome is destroyed via endosomal acidification which reveals the hexon coated core in the cytoplasm. There, it binds to the nuclear pore (NP) on the nucleus and injects the DNA containing central core into it (Russell 2009; Giberson et al. 2012). This process is mediated by the association of the viral core to the cellular protein p32 (Matthews und Russell 1994). Within the nucleus, the primary transcription events are initiated and virus DNA replication is activated. After successful DNA replication, the nuclear membrane is disrupted and the viruses are released in the cytoplasm. Disintegration of the plasma membrane allows the release of new viruses (Russell 2000).

Adenovirus subgroups show differences in their tissue tropisms. It is thought that initial attachment of the virus to its subgroup specific receptors is one determinant for tissue tropism. In general, adenoviruses mostly cause mild, flue-like symptoms and respiratory infections but can also cause gastrointestinal, kidney and urinary tract infections. In immune or nutritionally compromised individuals, adenoviral infection can lead to acute respiratory infections with life-threatening viral spread (Robinson et al. 2013).

1.3.2 Adenoviral genome regulation

The genome of the adenovirus 5 comprises roughly 36 000 base pairs. It is organized in early and late genes depending on their expression before or after viral DNA replication (figure 1.3) (Saha et al. 2014).

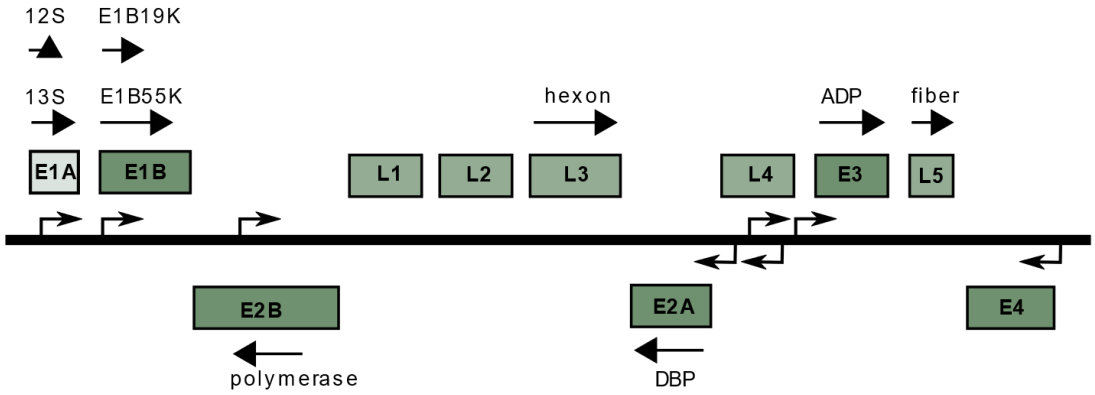

Figure 1.3: A simplified overview of the wild type adenoviral genome. The adenoviral genome consists of early genes (E1 to E4) and late genes (L1 to L5). Early genes get activated in the first 8 hours after infection, they encode for regulatory proteins which are necessary for viral replication. The transcription of late genes starts at the end of the infection process, they encode for structural proteins.

The early genes E1A, E1B, E2, E3 and E4 are the first genes transcribed, they encode for proteins which are necessary for altering the cellular environment to enable viral DNA replication and virus production. E1A messenger RNAs (mRNAs) have been detected as early as 30 minutes after infection. Therefore, the E1A gene is defined as immediate early gene (Boulanger und Blair 1991). It encodes for the five proteins 9S (55 amino acids), 10S (171 amino acids), 11S (217 amino acids), 12S (243 amino acids) and 13S (289 amino acids). The 12S and the 13S protein play important roles in genome regulation and transcriptional control (Nervins 1987). They share the two conserved regions CR1 and CR2, the CR3 domain is unique to the 13S protein. The E1A proteins optimize the cellular milieu for viral replication by inducing mitotic activity in the host cell, counteracting defense mechanisms against the virus and inducing expression of remaining early genes (Saha et al. 2014; Boulanger und Blair 1991).

The E1B transcript comprises two splice variants. They encode for two structural unrelated proteins with molecular masses of 19 kDa and 55 kDa, both mediating anti apoptotic effects. Together with E4orf6, the E1B55K protein inhibits a p53 mediated cell cycle arrest and apoptosis, whereas E1B19K, a B cell lymphoma-2 (Bcl-2) homologue protein, limits Bcl-2 induced cell death.

The E2 gene encodes for the viral DNA polymerase, the 5’ precursor terminal protein (pTP) which serves as a primer for adenoviral DNA replication and the DNA binding protein (DBP) that unwinds the DNA template and is important in the control of early and late gene transcription (Stuiver, van der Vlient 1990; Hay et al. 1995).

The E3 gene codes for several proteins that are involved in modulating the host immune system in favour of viral replication and for proteins involved in cell lysis (Yun et al. 2005). Major E3 proteins are the adenoviral death protein (ADP) and the E3gp19K protein. ADP is important during host cell lysis and the release of new viruses whereas E3gp19K interferes in the process of antigen presentation via MHC molecules (Russell 2000). The E3 RID protein inhibits Fas-induced cell lysis during viral replication (Yun et al. 2005).

The E4 proteins have different functions during infection, they are involved in viral DNA synthesis, inhibition of cellular protein synthesis and they regulate mRNA shuttling and cell death (Braithwaite und Russell 2001). As mentioned above, E4orf6 together with E1B55K is known to inhibit p53 mediated cell death. E4orf4 is involved in protein phosphatase 2A (PP2A) mediated apoptosis and E4orf6/7 interacts with E2F1 to stabilize its E2 promoter binding ability (Braithwaite und Russell 2001).

Approximately 10 hours after infection, the major late promoter (MLP) is fully active and allows transcription of the late genes L1 to L5. They encode for structural proteins, most important ones are the hexon protein, penton and fiber proteins (Russell 2009).

Table 1: Important adenoviral proteins and their function.

Protein	Function
E1A	Transactivation of early viral gene promoters
E1B19K	Inhibition of Bcl-2 mediated cell death
E1B55K	Inhibition of p53 mediated cell cycle arrest together with E4orf6
E2A, E2B	Provide the replication machinery for viral DNA
E3 ADP	Initiation of cell lysis
E3gp19K	Interference in MHC mediated antigen presentation
E3 RID	Inhibition of Fas induced cell lysis
E4orf4	Induction of apoptosis
E4orf6/7	DNA synthesis

1.3.3 Adenoviral interference in cell cycle regulation

Viruses are not autarchic. They need cellular mechanisms and proteins for genome replication and are therefore dependent on cellular resources. To generate an ideal environment for their replication and production, viruses manipulate progression through the cell cycle and interfere in checkpoint signaling. In this regard, the p53 and Rb pathway are two crucial pathways that are utilized by adenoviruses (Chaurushiya und Weitzman 2009).

The pRb protein is a well-known tumor suppressor protein, it inhibits cell cycle progression and induces arrest in G1 stage by binding to E2Fs (Dyson 1998; Sherr und McCormick 2002). The E2F family

comprises sequence-specific DNA binding transcription factors which induce expression of genes necessary for S phase entry (Trimarchi und Lees 2002). After initiation of the cell cycle and progression to the S phase via cyclin D expression, activated CDK4/6 hyperphosphorylates pRb (Ewen et al. 1993). This releases the transcription factor E2F from pRb and induces target gene transcription and cell cycle progression. The adenoviral E1A protein is known to target the E2F-Rb complex in order to disrupt it. This frees E2F which can promote spontaneous S phase transition (Bellacchio und Paggi 2013).

Another option to mediate G1/S phase transition is via p53 inactivation. Due to the E1A induced release of E2F, E2F1 activates transcription of p14/ARF, a Mouse double minute 2 homolog (Mdm2) neutralizing protein (Ben-Israel 2002). This causes inhibition of Mdm2 function and consequently elevated p53 levels (Zhang et al. 1998). To counteract this effect, the adenoviral proteins E1B55K and E4orf6 induce inhibition, ubiquitination and proteasomal degradation of p53 and thereby prevent cell cycle arrest and apoptosis of infected cells (Ben-Israel 2002). E1B55K binds to p53 and blocks its transcriptional activation and growth suppressive function (Martin und Berk 1998). E4orf6 either interacts directly with p53 or binds to it in a complex with E1B55K and induces p53 degradation (Querido et al. 1997).

1.3.3.1 The cell cycle inhibitors nutlin-3a and PD-0332991

Deregulation of the cell cycle and a subsequent uncontrolled proliferation are prominent occurrences in cancer cells which belong to the hallmarks of cancer (Hanahan und Weinberg 2000). Targeting the unguided cell cycle using small molecules is one approach to treat cancer.

The protein p53 plays an essential role in cell cycle regulation by inducing apoptosis as well as G1 arrest (Shaw 1996). It is regulated by the oncoprotein Mdm2 by targeting p53 for proteasome mediated degradation (Walsh et al. 2015). The specific p53-Mdm2 interaction is a highly coveted target for inhibitors that regulate the cell cycle. Nutlins are a group of small molecules that were found to disrupt the p53-Mdm2 interaction by binding to the p53 binding domain in the N terminal region of Mdm2 (Vassilev et al. 2004). Thereby, p53 is released from its negative regulator and can activate pathways that mediate cell cycle arrest and apoptosis. Nutlin-3a is the most potent and active member of this group and its p53-activating function has been proofed in various cancer cell lines expressing wild type p53 (Walsh et al. 2015). In this context it has been shown that p21 which is upregulated by p53 is important in mediating cell death (Drakos et al. 2011). In addition, nutlin-3a downregulates E2F1 and total Rb levels by mainly affecting hypophosphorylated Rb in p53 wild type cells (Walsh et al. 2015). It has been reported that nutlin-3a has promising effects in p53 wild type tumors (Vassilev et al. 2004). However, about 50 % of all tumor entities express mutated p53. In these malignancies, the therapeutic effect of nutlin-3a is p53 independent, it upregulates E2F1 by inhibiting the binding of Mdm2 to E2F1 (Ambrosini et al. 2007). Therefore, nutlin-3a represents a promising molecule for targeted therapy that is currently tested in various clinical trials as monotherapy and also in combinatorial approaches (Walsh et al. 2015).

Besides this, CDKs are another target to stop uncontrolled cell proliferation. Inhibition of CDKs can prevent Rb phosphorylation, repress the release of E2F and block S phase entry. PD-0332991 is reported to be a CDK4/6 inhibitor which has been tested in pre-clinical models for various tumor

entities including breast, lung, prostate and bladder cancer. These data provide evidence that CDK4/6 inhibition using PD-0332991 is a potential therapeutic approach for Rb positive bladder cancer whereas Rb mutated bladder cancer cells are resistant to PD-0332991 treatment (Sathe et al. 2016). Its mechanism of action is based on the induction of a G0/G1 arrest by inhibiting Rb mediated G1-S phase transition in Rb wild type cells (Asghar et al. 2015).

1.4 Oncolytic viruses for cancer therapy

Oncolytic virotherapy (OVT) is a therapeutic approach for cancer treatment that uses native or genetically modified viruses which selectively replicate in cancer cells. The principle behind this new therapeutic class of immunotherapy is based on two effects, the selective tumor cell killing and the induction of a local and systemic anti-tumor immune response (Kaufman et al. 2015). OVT was born in the beginning of the 20th century and there were first data published in the 1950th (Moore 1952). However, the first phase III study using a viral-based therapy for melanoma has only just been published (Andtbacka et al. 2015). The interest in virotherapy has increased dramatically in the last decade, with a research focus on tumor immunology, virus biology and combination therapies (Kaufman et al. 2015). Up to now, poxviruses, HSV-1, coxsackie viruses, polioviruses, measles viruses and adenoviruses have entered clinical trials (Kaufman et al. 2015).

1.4.1 The concept of oncolytic virotherapy

The concept of OVT as a therapy against cancer switched from a virotherapeutic to an immunological approach (Guo et al. 2017). Originally, it was thought that the exclusive effect of virotherapy is a selective tumor cell lysis (Kirn 2005). The tremendous research intensity on this field showed that there is also an immunological aspect of virotherapy which was shown to be essential for the therapeutic effectiveness (Sobol et al. 2011; Diaz et al. 2007; Prestwich et al. 2008). Thus, the current concept of OVT includes two major effects: the direct infection and selective lysis of cancer cells and the stimulation of an anti-tumor (and anti-viral) immune response (figure 1.4) (Guo et al. 2017).

After infection of both healthy tissue and tumor tissue, the virus replicates selectively and exclusively in tumor cells. When the viral life cycle within the host cell is completed, viral proteins mediate cell lysis to release newly produced viruses. This is mainly mediated by the E3 ADP protein (Yun et al. 2005). Unlike other E3 proteins, ADP is solely expressed in the late phase of viral infection (Tollefson et al. 1996). It induces cell death and thereby releases newly produced viruses which spread within the tumor and infect nearby tumor cells (bystander effect) (Tollefson et al. 1996). The destruction of tumor cells by the virus is the first major effect of virotherapy, followed by a consequent

immune stimulatory effect which is the second main effect of virotherapy (Woller et al. 2014). The immune stimulatory effect is, among other mechanisms, a consequence of the virus induced immunogenic cell death (ICD) which does not share the classical mechanism of apoptosis or necrosis. Apoptosis is one form of programmed cell death that is defined by morphological changes like chromatin condensation, shrinkage of the cytoplasm, nuclear fragmentation and formation of apoptotic bodies (Tesniere et al. 2008). Apoptotic bodies are rapidly removed by phagocytic cells to avoid a local immune reaction. Necrosis is a further form of programmed cell death but is considered to be immunogenic, as the swelling of the cytoplasma leads to an uncontrolled release of damaged cell organelles and cell debris (Tesniere et al. 2008). In contrast to these two forms of cell death, distinctive features for ICD are changes in the cell surface composition as well as the release of soluble immunogenic mediators (Kroemer et al. 2013). An endoplasmic reticulum (ER) stress response and the production of reactive oxygen species (ROS) are necessary for these cellular processes (Adkins et al. 2014). Dying cells transport calreticulin (CRT) and heat shock protein 70 and 90 to their outer cell membrane to show immunogenicity. In addition, they release tumor associated antigens (TAAs) as well as danger associated molecular patterns (DAMPs) like high-mobility group box 1 (HMGB1) and adenosine triphosphate (ATP). HMGB1, ATP and CRT bind to toll-like receptor 4 (TLR4), P2X purinoreceptor 7 (P2RX7) and cluster of differentiation (CD91), respectively, and stimulate immature antigen presenting cells (APCs) for antigen uptake and presentation. Moreover, molecules like ATP act as “find-me” signals and induce immune cell recruitment. The cross presentation of TAAs to T cells leads to interleukin-1β (IL-1β) and interleukin-17 (IL-17) release, an activation of γδ T cells and cytotoxic $CD8^+$ T lymphocytes (CTLs) and an interferon γ (IFNγ) mediated potent immune response specifically against tumor cells (Kroemer et al. 2013).

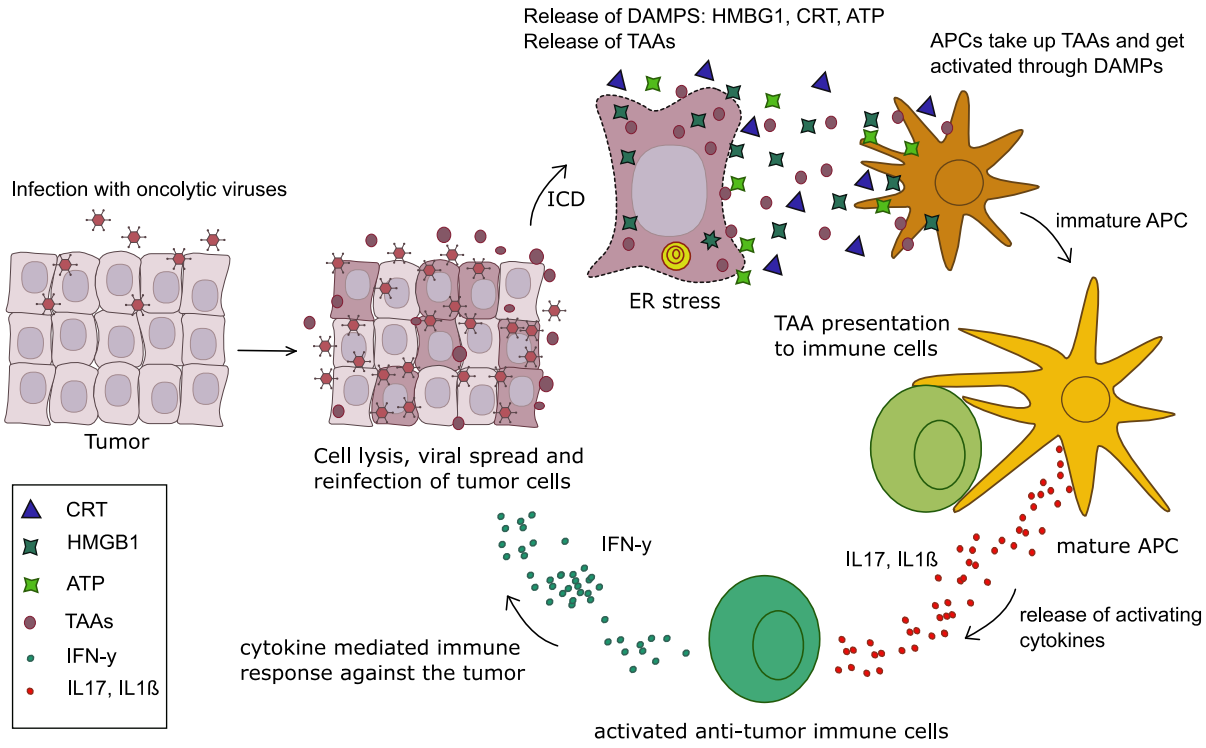

Figure 1.4: The concept of virotherapy for cancer treatment. After infection of tumor cells, the virus replicates within the cell. This induces cell lysis and an immunogenic cell death. Within this process, new viruses as well as DAMPS and TAAs are released and can stimulate APCs. Mature APCs activate immune cells and release activating cytokines. Stimulated immune cells form an anti-tumor immune response mediated by cytokines. Figure modified from (Kroemer et al. 2013).

1.4.2 Overview of current clinical trials using virotherapy

At the moment more than 80 clinical trials are using oncolytic viruses for cancer therapy (clinical trials virotherapy, 2017). The breakthrough in the area of virotherapy was the approval of T-Vec in 2015, the first oncolytic virus to treat cancer. T-Vec is a genetically modified and granulocyte-macrophage colony-stimulating factor (GM-CSF) armed herpes simplex virus (HSV) for the treatment of melanoma. It is also tested in several other tumor entities as a single therapy or in combination with radiotherapy, chemotherapy or immune checkpoint blockade (Kohlhapp et al. 2015). Table 2 gives an overview over the latest and most relevant oncolytic viruses in clinical trials. The listed viruses are in different phases of clinical trials and they are tested as single therapy or in combinatorial approaches for safety and efficacy, spreading and immune stimulating effects in various tumor entities (clinical trials virotherapy, 2017) (Guo et al. 2017).

Table 2: Most relevant clinical trials using virotherapy. Table modified from (Guo et al. 2017)

Virus		Combination	Tumor entity
Herpes simples virus 1	T-Vec (Gangi und Zager 2017)		Pancreatic cancer, melanoma
	T-Vec (Rehman et al. 2016)	Radiotherapy + Cisplatin	Untreated stage III/IV squamous cell carcinoma of head and neck
	T-Vec (Puzanov et al. 2016)	Ipilimumab	Melanoma
Reovirus	Reolysin (Galanis et al. 2012)		Advanced melanoma, prostate cancer, malignant glioma, metastatic colorectal cancer, multiple myeloma, breast cancer
	Reolysin (Noonan et al. 2016)	Paclitaxel/ Carboplatin	Pancreatic adenocarcinoma, metastatic and/or recurrent head and neck cancer, lung cancer
Adenovirus	OAMCGT (Freytag et al. 2014)		Prostate cancer
	CG0070 (Fukuhara et al. 2016)		Non-muscle invasive bladder cancer after BCG failure
Vaccinia virus	JX-594 (Guo et al. 2017; Fukuhara et al. 2016)		Advanced hepatocellular carcinoma, melanoma, lung cancer, renal cell carcinoma, head and neck cancer, colorectal cancer

1.4.3 Oncolytic adenoviruses

Using viral agents to treat cancer needs certain requirements to achieve a therapeutic utility. These are high stability and efficient infection of host cells, the possibility to manipulate viral DNA, the capability to avoid detection and clearance by the immune system and, most important, a selective replication and propagation only in tumor cells. In this context, adenoviruses have many suitable attributes that recommend their use (Curiel 2000). They are ubiquitous, have a low pathogenicity, they can be easily manipulated and their genome can be deleted and gives space for relatively large transgenes. Additionally, adenoviruses are very stable and production of high titers is established (Vorburger und Hunt 2002).

1.4.3.1 Engineering oncotropic adenoviruses

One major aspect in engineering oncolytic adenoviruses is the tumor selective replication, also called oncotropism (Aben et al. 2000). Oncotropic properties can be achieved by basically two strategies: replication specificity based on tumor biology or based on transcriptional control (Curiel 2000). Specificity based on certain tumor biological mutations or alterations uses the knowledge of interaction between viral and cellular proteins, for example inhibitory effects of E1B55K on p53. Based on this, dl1520 (ONYX-015) which has two deletions in the E1B55K gene was developed. It is supposed to replicate only in p53 negative tumor cells (Bischoff et al. 1996). However, latest findings show that replication of this virus is not dependent on the presence of functional p53 (Rothmann et al. 1998). Another example is the interplay between Rb, E1A and E2F. In healthy tissue, Rb bound to E2F blocks viral replication which can be restored when E1A binds to Rb. AdΔ24 is deleted in the Rb binding region in E1A, thus viral replication occurs only in cancer cells with abnormal Rb levels (Fueyo et al. 2003).

Using transcriptional control to achieve oncotropism means that viral promoters are replaced by tissue-specific or tumor specific promoters (Alemany et al. 2000). Examples are the use of the human telomerase reverse transcriptase promoter (hTERT), the hypoxia responsive element or the E2F promoter to control E1A gene transcription (Jounaidi et al. 2007).

1.4.3.2 The YB-1 dependent oncolytic adenovirus XVir-N-31

XVir-N-31 is a YB-1 dependent oncolytic adenovirus that was developed in our lab (Mantwill et al. 2013). It is deleted in the CR3 region of the E1A 13S gene and has further deletions in the E1B19K gene and the E3 region. In addition, it has an RGD motif in the fiber encoding gene to improve infection of tumor cells that have poor CAR expression (Dmitriev et al. 1998).

The mechanism of action of XVir-N-31 is based upon the multifunctional protein YB-1. It belongs to the family of cold-shock proteins, all of which bind both DNA and RNA via a conserved nucleic-acid binding motif (Wolffe et al. 1992; Lasham et al. 2013). YB-1 has diverse functions, it is highly expressed in embryonic tissue and malignant, neoplastic tissue but poorly expressed in healthy adult tissue (Bargou et al. 1997; Holm et al. 2002). In tumor cells, YB-1 supports a variety of the hallmarks of cancer (Lasham et al. 2013; Hanahan und Weinberg 2000). YB-1 is involved in maintaining proliferative signaling by inducing the transcription of activator E2Fs (E2F1, E2F2, E2F3) while inhibiting the transcription of repressor E2Fs (E2F5, E2F7). Furthermore, it is thought to enable replicative immortality by most possibly mediating hyperphosphorylation of Rb and consequently a release of E2F1. It can directly bind to p53 and thereby resisting p53 mediated cell death and growth suppression. YB-1 deregulates cellular energetics and can induce angiogenesis by activating transcription of pro-angiogenic genes under reduced oxygen conditions and it stimulates invasion and metastasis by transcription of genes necessary for epithelial-mesenchymal transition (Lasham et al. 2013).

In the context of adenoviruses, the expression and nuclear localization of YB-1 is indispensable, since the E2late promoter has three YB-1 binding motifs and its activation is YB-1 dependent (Holm et al. 2002). Immediately after infection, wildtype adenoviruses (WtAd) activate E1A transcription and

expression and thereby enable transcription of E1B55K and E4orf6. Both E1B55K and E4orf6 are necessary to translocate YB-1 into the nucleus of healthy cells so that it can bind to the E2late promoter and induce E2 gene transcription (Holm et al. 2002). In cancer cells, YB-1 is already in the nucleus and an E1A mediated nuclear translocation of YB-1 is not needed for successful viral replication (Bargou et al. 1997; Holm et al. 2002; Holm et al. 2004). For this reason, XVir-N-31 can selectively replicate in nuclear YB-1 positive cancer cells but cannot replicate in normal cells. This is the main principle of the tumor selectivity of XVir-N-31 (Holm et al. 2004; Rognoni et al. 2009; Mantwill et al. 2013).

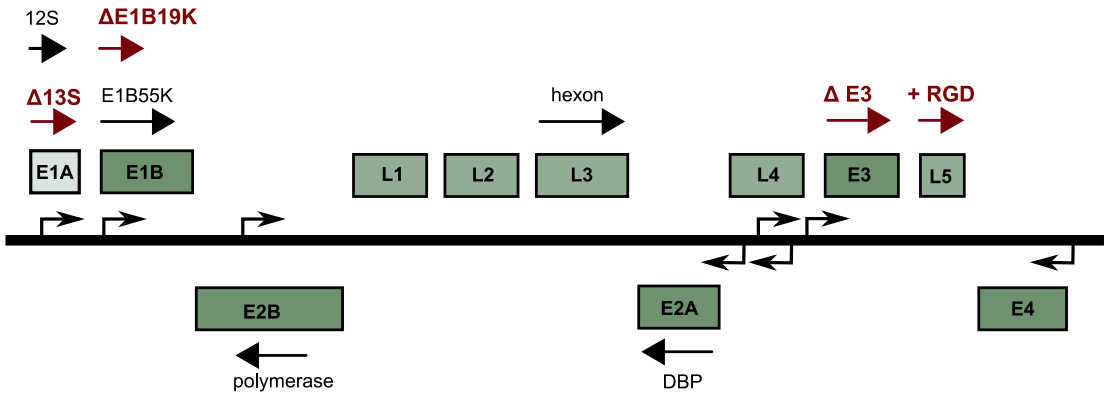

Figure 1.5: A simplified overview of the genome of XVir-N-31. The oncolytic adenovirus XVir-N-31 contains partial deletions in E1A and E1B19K. It is deleted in E3 and has an additional RGD motif in the fiber encoding region. XVir-N-31 replicates selectively in nuclear YB-1 positive cancer cells (Mantwill et al. 2013; Rognoni et al. 2009;).

1.4.4 Virotherapy for the treatment of bladder cancer

Bladder cancer is for several reasons a practical tumor entity for virotherapy. The application of the virus via the urethra, called intravesical instillation, is easy and allows direct exposure of the tumor to high virus titers (Shen et al. 2008). The effortless access to the bladder is convenient for repeated evaluation of treatment effects and tissue sampling. Additionally, the bladder is an isolated organ that is protected by multiple layers of various tissues which reduces systemic spreading to a minimum (Taguchi et al. 2017). Bladder cancer is a highly immunogenic tumor and the success of Bacillus Calmette-Guérin (BCG) therapy has already proofed suitability for immunotherapy (Burke 2010; Potts et al. 2012). So far, four clinical trials using two different viruses have been carried out in bladder cancer patients.

CG0070 is a GM-CSF armed oncolytic adenovirus in which the human E2F1 promoter drives viral E1A gene expression (Ramesh et al. 2006). The mechanism of CG0070 is based on Rb which is commonly mutated in bladder cancers, and its regulatory function on E2F1 (Bandara und La Thangue 1991). A phase I trial in patients with non-muscle-invasive bladder cancer, who failed BCG therapy, showed an overall response rate of 48.6 % and 63.6 % in the single and multidose cohort, respectively.

Doses up to $3x10^{13}$ viral particles were applied every 28 days with three repetitions or weekly for six repetitions. Based on these results, a phase II/III randomized controlled trial is currently performed in patients with non-muscle-invasive bladder cancer who failed BCG therapy to compare CG0070 treatment with mitomycin C, IFN, valrubicin or gemcitabine (www.clinicaltrials.gov, NCT01438112) (Taguchi et al. 2017). In another phase II trial, patients with non-muscle-invasive bladder cancer who failed BCG therapy or refused cystectomy, are treated with CG0070 at a dose of 10^{12} viral particles weekly for 6 weeks which will continue for 18 months if they achieve a partial or complete response after 6 months (www.clinicaltrials.gov, NCT02365818) (Taguchi et al. 2017).

Wildtype vaccinia virus was tested in a phase I study in four patients with muscle-invasive bladder cancer. Patients received three times over two weeks a maximum dose of 10^8 particle forming units (PFU) prior to cystectomy (Potts et al. 2012). No serious treatment-related adverse events were reported which shows the potential use of vaccinia wildtype virus for virotherapy (Taguchi et al. 2017).

1.5 Immunological aspects of adenovirus-host interaction

1.5.1 Immunological barriers to oncolytic virotherapy

Immunological defense mechanisms of the host against adenoviruses, like activation of an innate and adaptive immune response as well as pre-existing immunity, are major barriers that limit the effectiveness of adenovirus based virotherapy (Fausther-Bovendo und Kobinger 2014). The innate immune response is an immediate answer to adenoviral infection mediated by macrophages, dendritic cells (DC), neutrophils, natural killer cells (NK) and proteins like chemokines and cytokines (Liu und Muruve 2003). After cell entry of the virus via CAR or integrin binding, nuclear factor kappa-light-chain-enhancer of activated B cells (NFκB) gets activated via PI3K mediated pathways and gene transcription of chemokines and cytokines such as interleukin-1 (IL-1), IL-18, IL-8, regulated on activation, normal T cell expressed and secreted (RANTES) and tumor necrosis factor-α (TNF-α) starts. Among these pro-inflammatory factors, IL-1 and type I IFNs play a predominant role as they induce positive feed-back loops which produce additional inflammatory stimulators (Fausther-Bovendo und Kobinger 2014). Once the virus is internalized, viral DNA located either in the cytoplasm or in endosomes, acts as strong immunological activator. Within the endosome, toll-like receptor 9 (TLR9) detects viral DNA and activates transcription of pro-inflammatory mediators via myeloid differentiation primary response 88 (MyD88) (Thaci et al. 2011). DNA binding molecules like stimulator of interferon genes (STING), retinoic acid inducible gene-I (RIG-1), nucleotide oligomerization domain (NOD)-like receptor (NLR) or DNA-dependent activator of IFN-regulatory factors (DAI) detect and bind cytoplasmic viral DNA and RNA (Kawai and Akira, 2009). These sensors induce interferon regulatory factor 3/7 (IRF3/7) translocation into the nucleus and transcriptional activation of powerful antiviral chemokines such as type I IFNs and interleukin-1 (Barber 2011). The release of these immunological factors serves as a chemoattractant to other immune cells which will migrate to the site of infection and fight the virus.

In contrast to the rapid and direct innate immune response, the adaptive immune response needs about one week to become effective (Zaiss et al. 2009). Macrophages and dendritic cells which have internalized the virus, act as antigen presenting cells and migrate to lymph nodes where they present viral antigens to B cells and stimulate antibody production. In case of a pre-existing immunity, re-challenging with the same adenoviral vector will induce a neutralization and elimination through specific antibodies and memory B cells (Zaiss et al. 2009).

1.5.2 Immune evasion strategies of adenoviruses

Adenoviruses rely on a healthy and functional host cell. Because viral infection of cells induces a strong immune reaction that would lead to elimination of the infected cell, adenoviruses dampen host immune response to prevent their own elimination and the damaging consequences for the host cell. Adenoviruses express several proteins that can mediate immune evasion at different levels.

One of the first reactions of host cells to viral infection is type I IFN expression (IFNα, IFNβ) (Leonard und Sen 1997). Binding of IFNs to their receptors causes activation of the Janus kinase/signal transducer and activator of transcription (JAK/STAT) pathway which leads to transcription of antiviral genes. The adenoviral E1A protein can block the functions of type I IFNs via blocking downstream signaling of IFNs by interfering in the JAK/STAT pathway and also by transcriptional inhibition of IFNα and IFNβ encoding genes (Mahr und Gooding 1999).

TNF signaling is another pathway that is addressed by adenoviruses for immune evasion. TNFs are pro-inflammatory cytokines that are secreted by macrophages and T cells, they bind to their widely expressed receptors TNFR1 and TNFR2 and induce cell death (Wohlleber et al. 2012). E1B19K, E3 14.7k and E3RIDα/β can block TNF mediated cytolysis (Wold 1993; Mahr und Gooding 1999). E3RIDα/β also downregulates cell surface receptors of the TNF family, e.g. Fas, tumor necrosis factor related apoptosis inducing ligand (TRAIL) receptor 1 and 2 and inhibits thereby Fas and TRAIL mediated apoptosis (Lichtenstein et al. 2002).

A third pathway that is targeted by adenoviruses to circumvent an anti-viral immune reaction is the presentation of antigens on MHC molecules to activate $CD8^+$ cells. The loading of viral peptides onto the MHCI molecule occurs within the ER (Ressing et al. 2013; Mahr und Gooding 1999). There, the TAP protein transports the viral peptide into the ER lumen where it can bind to MHCI. This TAP mediated transport is inhibited by the adenoviral protein E3gp19K, whereby loading of MHCI and cell surface presentation of antigens to activate $CD8^+$ cytotoxic T cells is prevented (Ressing et al. 2013; Purcell und Elliott 2008).

1.6 Immunotherapy

Immunotherapy is besides surgery, radiation, chemotherapy and target therapy one of the five pillars of cancer therapy. The strategy of immune evasion and immune editing are well known but the knowledge of the underlying mechanism has only just been grown in the last years. Immunotherapy uses different approaches to stimulate the immune system specifically against the cancer with the ulterior motif of a long-lasting tumor specific memory.

1.6.1 Different immunotherapeutic approaches for cancer

Immunotherapeutic approaches comprise therapeutic cancer vaccines, immune cell therapy, immune system modulators and ICB (Farkona et al. 2016).

Therapeutic cancer vaccines stimulate and augment adaptive immune reactions. Thereby, three methods exist: a whole cell vaccine uses a variety of tumor-associated antigens and leads to a broader immune response. Vaccination with protein antigens uses intact peptides derived from tumor associated antigens that can directly bind to MHCI molecules. A third method is the vaccination with *ex vivo* antigen-pulsed patient derived DCs (Makkouk und Weiner 2015). The idea of the vaccination approach is to increase the presentation of tumor specific antigens (TSAs) or TAAs on antigen presenting cells to B and T cells in order to improve an anti-tumor immune response (Velcheti und Schalper 2016).

Immune cell therapy includes adoptive T cell therapy, NK cell therapy and the chimeric antigen receptor (CAR) method. The rationale behind immune cell therapy is to enrich and improve T cells or NK cells that are able to recognize the tumor (Velcheti und Schalper 2016). The adoptive NK cell therapy was initially tested in leukemia patients. Recent studies focus on the improvement of NK cell activity and specificity. Adoptive T cell therapy is the *ex vivo* culturing and expansion of patient derived lymphocytes under certain growth factors. An advancement is the CAR method. CARs are designed T cell receptors that consist of an antigen binding T cell receptor (TCR) exodomain and the cytoplasmatic TCR ζ chain. This receptor recognizes unprocessed antigens as well as glycoproteins, carbohydrates and gangliosides. After transfection of T cells with the CAR encoding plasmid, the CAR expressing T cells are reinjected into the patient (Dotti et al. 2014). So far, clinical trials were mostly disappointing because of the limited migration of reinjected T cells to the tumor site and the highly immunosuppressive milieu within the tumor (Velcheti und Schalper 2016).

Immune modulators like chemokines and cytokines are well known in their immune stimulating functions. Therefore, they find application in various immunotherapeutic approaches and also in combination therapies. For example, members of the IL-2 family, like IL-7, IL-15 or IL-21 are injected into cancer patients to activate their immune system (Sim und Radvanyi 2014). Type I IFNs are also used in immunotherapy as they activate NK cells, macrophages, cytotoxic T cells and mediate pro-inflammatory cytokine production (Lee und Margolin 2011).

1.6.2 Immune checkpoints as new therapeutic targets for cancer therapy

The initial immune activation is a multistep process. After antigen processing by APCs or dendritic cells, the antigen is presented on a MHC class II receptor to the T cell receptor. To achieve full T cell activation, a second co-stimulatory signal via CD28 on the T cell and CD80/86 on the APC is necessary. Only in the presence of both signals, a full immune response against the presented antigen including cytokine release, antibody production and recruitment of other immune cells can be generated. In addition, inhibitory signals ensure immune homeostasis and modulate the duration and amplitude of immune reactions. These negative stimuli are known as inhibitory immune checkpoints, prominent examples are cytotoxic T-lymphocyte associated protein 4 (CTLA-4), PD-1, T-cell immunoglobin and mucin-domain containing-3 (TIM-3) and lymphocyte activation gene-3 (LAG-3) (figure 1.6) (Cogdill et al. 2017). In a physiological situation, immune checkpoints are necessary to prevent autoimmunity and overwhelming immune reactions.

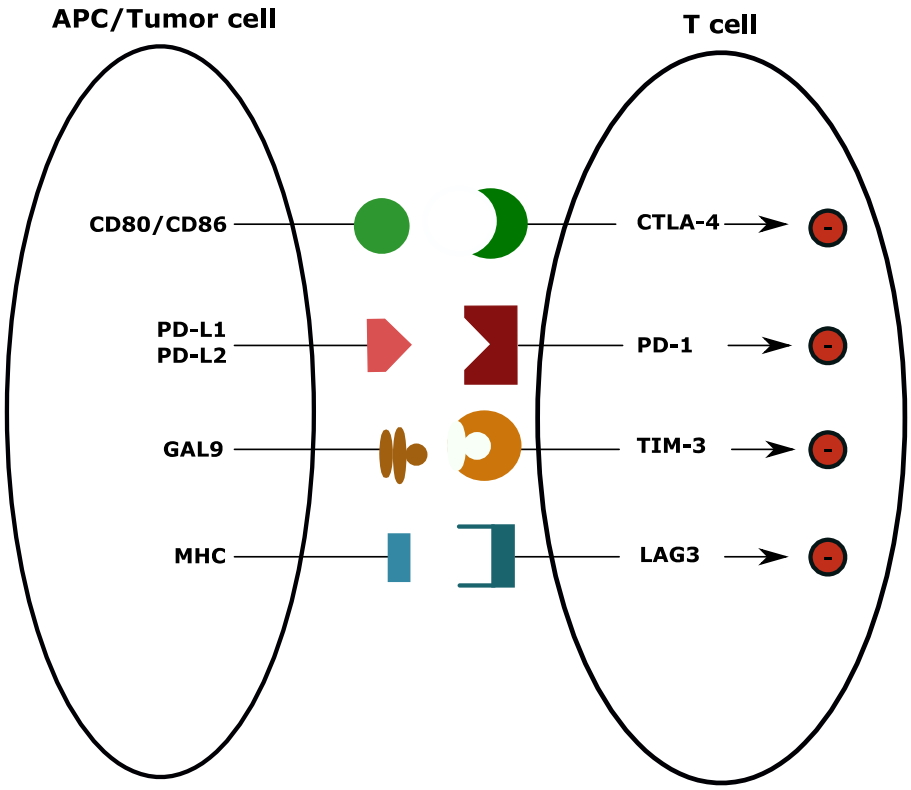

Figure 1.6: Inhibitory immune checkpoint molecules. Immune checkpoint molecules are regulators of the immune system. They prevent overwhelming immune reactions and control their duration by mediating immunosuppressive pathways. Cancer cells abuse these checkpoints to escape from immune reactions against the tumor. (CD80/86: cluster of differentiation, GAL9: galectin 9, MHC: major histocompatibility complex)

However, the tumor co-opts immune checkpoints to take advantage of its inhibitory functions. Cancer cells as well as tumor infiltrated immune cells overexpress immune checkpoint molecules to evade immune recognition (Pardoll 2012). The seminal observation, that the blockade of immune

checkpoint molecules like CTLA-4 is able to mediate tumor regression was the birth of the era of ICB for cancer therapy (Leach et al. 1996). Subsequently, various antibodies targeting different immune checkpoint receptors and ligands were developed and showed promising effects in different tumor entities. Most prominent examples for approved immune checkpoint inhibitors and their application are listed in table 3.

Table 3: Overview of approved antibodies for immune checkpoint blockade.

Target	Drug name	Tumor entity
CTLA-4	Ipilimumab	Melanoma
PD-1	Nivolumab	NSCLC, Locally advanced or metastatic urothelial carcinoma
	Pembrolizumab	Melanoma, NSCLC (in combination with carboplatin and pemetrexed)
PD-L1	Atezolizumab	NSCLC, Locally advanced or metastatic urothelial carcinoma
	Durvalumab	Locally advanced or metastatic urothelial carcinoma
	Avelumab	Merkel cell carcinoma

1.6.3 Immunotherapeutic approaches for bladder cancer

Bladder cancer has been treated with BCG as an immunotherapeutic approach for nearly 4 decades (Fuge et al. 2015). The mechanism of action is traced back to the immune-stimulatory effect of BCG. Thereby, the infection of urothelial as well as bladder cancer cells and internalization of BCG leads to an increase in antigen presenting cells as well as antigens. Activated immune cells response via cytokine release and in this process, the acquired Th1 mediated immune response as well as the innate Th2 mediated immune response are implicated. The induced immune reaction and finally the established antitumor immune response is mainly mediated by NK cells, dendritic cells, macrophages and $CD8^+$ as well as $CD4^+$ T lymphocytes. The result is improved recognition and subsequent destruction of tumor cells (Fuge et al. 2015).

BCG is one of the most successful immunotherapies ever used. Adjuvant BCG in high grade NMIBC reduces risk of recurrence by 70 % compared to transurethral resection alone and in CIS it induces a complete response in 70-90 % of all cases. BCG is the only intravesical therapy that is known to reduce tumor progression in intermediate and high-risk groups (Saluja und Gilling 2017). Besides this, it is safe and well tolerated (Fuge et al. 2015). The success of this therapy showed that the principle of immunotherapy is working for bladder cancer and it serves as a rationale to verify and establish ICB for

bladder cancer therapy. In addition, several other characteristics of BLCA make it an excellent tumor entity with promising prerequisites for ICB, e.g. the immunogenicity of bladder cancer with the presence of tumor infiltrated immune cells (TILs) and the high mutational load resulting in increased levels of neoantigens (Bidnur et al. 2016; Kandoth et al. 2013). It has been shown that neoantigen burden and neoantigen specific T cell reactivity are a marker for successful immunotherapy (Schumacher und Schreiber 2015). In a study with non-small cell lung cancer patients, PD-1 treatment efficacy was correlated with a higher mutational load in the tumor and another study with melanoma patients showed that a higher mutational landscape supports CTLA-4 therapy (Rizvi et al. 2015; Snyder et al. 2014). Mismatch repair (MMR) deficiency seems to be a further marker for successful ICB. Cancers with MMR deficiency show extreme high levels of somatic mutations and these cancers are sensitive to immune checkpoint blockade (Le et al. 2017). Certainly, expression of target immune checkpoint molecules on cancer cells as well as infiltrated immune cells can predict responders and efficacy of ICB but they are not yet reliable markers (Nishino et al. 2017). In general, it is known that PD-L1 and PD-1 expression is associated with high grade tumors, tumor infiltration of mononuclear cells and that PD-L1 positive tumors have a reduced overall survival (Boorjian et al. 2008; Inman et al. 2007). Analyzing the PD-L1/PD-1 status of tumors to select for responders brought contradictory results. Clinical trials suggested a benefit of PD-L1 positive tumor cells and tumor infiltrated immune cells to PD-L1/PD-1 blockade compared to PD-L1 negative tumors (Herbst et al. 2014; Apolo et al. 2017; Massard et al. 2016). However, there are also data showing that not all PD-L1 positive tumors responded to PD-L1 blockade (Ribas und Hu-Lieskovan 2016). The major issues using PD-L1 as a selector for responders are the dynamic of target molecule expression, the lack of standardized assays and the different interpretation of PD-L1 staining (Apolo 2016). If and to what extent PD-L1 expression can serve as a useful and trustworthy biomarker for ICB is still a matter of intensive research.

Up to now, five checkpoint inhibitors (nivolumab, atezolizumab, pembrolizumab, avelumab and durvalumab) demonstrated therapeutic efficacy with objective response rates (ORRs) ranging from 15-20 % in patients with metastatic urothelial cancer in a second-line setting. Atezolizumab and pembrolizumab were also tested in a first-line setting in cisplatin ineligible patients. The FDA approved durvalumab, nivolumab and atezolizumab for treatment of locally advanced or metastatic urothelial carcinoma (Davarpanah et al. 2017).

1.6.4 The PD-1/PD-L1 immune checkpoint pathway

The PD-1/PD-L1 pathway is a prominent example for immune checkpoint pathways, its inhibitory role was first published in 2000 (Freeman et al. 2000). PD-1 is a transmembrane receptor with a cytoplasmic immunoreceptor tyrosine-based inhibitory motif (ITIM) and an immunoreceptor tyrosine-based switch motif (ITSM). It has been detected on T cells in the thymus, regulatory T cells, exhausted T cells, B cells, dendritic cells and NK cells.

PD-1 expression is not constitutive but can be induced upon activation and its broad expression on various immune cell types indicates wide-ranging functions in diverse immune responses (Okazaki und Honjo 2007). The receptor PD-1 binds to its ligands PD-L1 and PD-L2 (Li et al. 2016). PD-L2 expression is limited to dendritic cells and macrophages and seems to play a minor role in PD-1 signaling. The

expression of PD-L1 is abundant in immune cells, epithelial cells and cancer cells which signifies a role in secondary lymphoid organs as well as target organs (Okazaki und Honjo 2007). PD-L1 expression can be controlled via intrinsic and extrinsic mechanisms. Extrinsic up-regulation of PD-L1 is strongly dependent on TLR mediated signaling and pro-inflammatory cytokines like IFNγ, GM-CSF, TNF-α. In bladder cancer cell lines, it was shown that TLR-4 signaling upregulates PD-L1 expression which can be attenuated by extracellular-signal regulated kinase (ERK) and c-Jun N terminal kinases (JNK) inhibitors (Qian et al. 2008). IFN-γ induces PD-L1 expression via signaling through the JAK/STAT pathway and IRF-1 (Ritprajak und Azuma 2015). Additionally, microRNAs (miRNAs) have been shown to regulate post-transcriptionally PD-L1 transcription. For example, miR-513 interacts with the 3'-untranslated region of PD-L1 mRNA which results in translational repression (Gong et al. 2009). Moreover, also intrinsic pathways regulate PD-L1 expression. Ki-67 expression and loss of phosphate and tensin homolog (PTEN) as well as activating epidermal growth factor receptor (EGFR) mutations have been correlated to PD-L1 expression (Ritprajak und Azuma 2015). Furthermore, activation of the mitogen activated protein kinase (MAPK) and PI3K/Akt pathway upregulate PD-L1 expression in cancer cells (Chen et al. 2016).

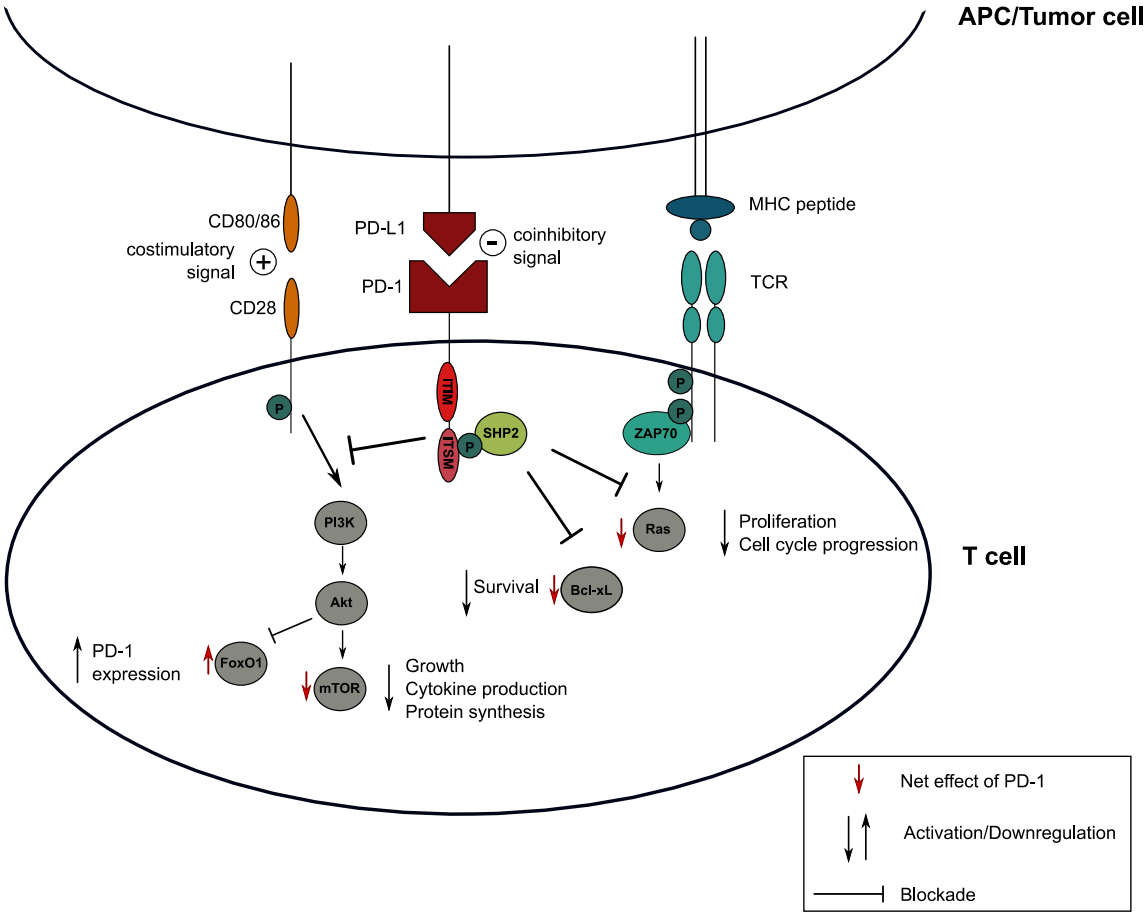

Figure 1.7: The PD-1/PD-L1 pathway. Engagement of PD-1, expressed on T cells, by PD-L1, e.g. expressed on tumor cells, initiates immune inhibitory signaling pathways. They lead to reduced cytokine production and protein synthesis and induce blockade of cell cycle progression and proliferation. These effects finally cause a suppression of T cell activation and prevent an immune response. Figure modified from (Chinai et al. 2015).

After receptor-ligand engagement, PD-1 recruits the Src-homology 2 domain-containing phosphatase (SHP2). SHP2 inhibits phosphorylation of the intracellular domains of the T cell receptor as well as dephosphorylates the CD3ς chain which leads to the inhibition of various T cell activating pathways. This includes inhibition of Ras signaling which suppresses cell cycle progression and proliferation, inhibits pro-survival proteins like Bcl-xl and blocks the PI3K/Akt pathway causing a decrease in protein synthesis, proliferation and cytokine production (especially IL-2). PI3K/Akt suppression leads in addition to the upregulation of FoxO1 which induces PD-1 upregulation. Finally, PD-1/PD-L1 signaling decreases T cell receptor signaling and results in suppressed T cell activity (figure 1.7) (Nirschl und Drake 2013).

1.7 Combining virotherapy and immune checkpoint blockade

Latest insights in the fields of virotherapy and ICB demonstrate the substantial role of the immune system in the fight against cancer (Lichty et al. 2014). The excellent therapeutic success of T-Vec clearly demonstrates the power of combining virotherapy with immunotherapy and clinical studies showed that limited antitumor immunity constrains the effectiveness of virotherapy (Lichty et al. 2014). This can be overcome by unlocking immune inhibitory pathways like immune checkpoints (Zamarin et al. 2014). Additionally, priming with immune stimulating agents induces higher expression of immune checkpoint molecules in the tumor, leading to increased response rates to ICB. This is the leading rationale for a combination therapy using oncolytic viruses with immune checkpoint blockade (Zamarin et al. 2014).

1.8 Difficulty of evaluating oncolytic adenoviruses in mouse models

The difficulty in finding an appropriate *in vivo* model to test oncolytic adenoviruses bases on their strict species specificity (Russell 2000). Human adenoviruses replicate and produce infectious new particles almost exclusively in human cells. In most murine cell lines, they cannot effectively infect and replicate and consequently, a syngeneic, immunocompetent mouse model to study adenoviral virotherapy for cancer treatment is not feasible (Ginsberg et al. 1991). This is the reason why human tumor xenografts were used to study OVT for cancer treatment. This model uses human tumor cells implanted in an immunodeficient mouse which allows viral replication in human tumor cells but does not reflect the host's immune system. The lack of a functional immune system in xenografts is a major disadvantage of this model, especially regarding the fact that the immune stimulatory effect of OVT is known to play a dominant role in therapeutic effectiveness (Zhang et al. 2015). Although there are attempts to solve this problem, e.g. by using the Syrian hamster model, there is still no applicable

model that fulfills the requirements of a syngeneic, immunocompetent system. Recently, the murine lung adenocarcinoma cell line ADS-12 was found to support adenoviral replication, particle formation and to respond to adenoviral oncolysis (Zhang et al. 2015). Other murine cell lines like the murine bladder cancer cell line MB49 and MBT2 were mostly used to study adenoviral gene therapy (Summerhayes und Franks 1979; Loskog et al. 2005; Horinaga et al. 2005). The humanized mouse model presents a possibility to study oncolytic adenoviruses, however, it is highly challenging, time consuming, artificial and limited in time due to the development of a graft versus host disease (GvHD) (Shultz et al. 2007). This shows the urgent need for a syngeneic, immunocompetent mouse model to study adenoviral virotherapy regarding its oncolytic as well as immune stimulatory effects in cancer therapy.

Orthotopic cancer models are the best models to represent the physiological situation in humans and they are important for testing novel therapies. For bladder cancer, there exist several animal models which can be categorized into spontaneous and non-spontaneous models. Spontaneous models are chemically induced or genetically modified. These tumors are rare, time consuming, complicated and repeatability is not guaranteed (Zhang et al. 2015). Non-spontaneous models comprise heterotopic and orthotopic xenograft models. Heterotopic xenograft models are generated by injecting tumor cells non-orthotopic under the skin. This method is fast and easy in handling but does not represent the organ specific physiology and natural environment within the mouse. Development of orthotopic bladder cancer models needs surgical implantation, instillation or ultrasound based injection of tumor cells (Jäger et al. 2014). Surgical injection is very time consuming, risky and not reliable. The instillation of tumor cells needs pretreatment of the bladder and develops only superficial tumors. The new ultrasound based model allows precise injections of tumor cells into the lamina propria and forms invasive bladder tumors. It simulates human pathology and tumor biology within the natural environment at its best. Additionally, it enables straightforward and precise tumor monitoring and treatment (Jäger et al. 2014).

1.9 Aims and objectives

OVT gained attention with the approval of T-Vec as the first oncolytic virus for cancer therapy. The enormous research activity in this field brought new insights in the principle effects of virotherapy and showed the importance and necessity of its immune stimulatory effect. However, the tumor has highly effective mechanisms to block the immune activating effect of virotherapy and limits thereby its effectiveness. The immune checkpoints, such as the PD-L1/PD-1 pathway, are a prominent example for immune evasion mechanisms that repress immune stimulation. This leads to the rationale for combining oncolytic viruses with immune checkpoint blockade to restore the full power of virotherapy.

The aim of this work was to study a new therapeutic approach for bladder cancer that combines OVT and PD-L1 specific immune checkpoint blockade. This project included the development and production of a novel oncolytic adenovirus encoding for an anti-PD-L1 specific antibody, named XVir-N-31-aPD-L1. Further on, we intended to characterize the new virus *in vitro* regarding its replication

behavior, its cell killing effect and its transgene expression. In addition, we wanted to analyze the therapeutic effect of XVir-N-31-aPD-L1 in a mouse model. Therefore, we aimed to establish an orthotopic, invasive mouse model for bladder cancer. Since adenoviral replication is limited in mouse cells, we investigated several approaches including cell cycle inhibitors regarding their capacity to enhance viral replication and transgene expression in a murine, immunocompetent mouse model.

2 Material and methods

2.1 Material

2.1.1 Multiple use equipment

Multiple use equipment	Source
3M durapore surgical tape	3M, Saint Paul, MN, USA
Analytical balance AT250	Mettler, Toledo, GIessen, Germany
Analytical balance Sartorium 2254	Sartorius, Goettingen, Germany
Autoclave Systec DX-65	System GmbH, Linden, Germany
Automatic film processor Curtix CP1000	Agfa Healthcare, Mortsel, Belgium
Bag sealer Folio FS3602	Severin Elektrogeräte GmbH, Sundern, Germany
BD FACS Calibur Flow Cytometry System	DB Bioscience, San Lose, CA, USA
Biological safety cabinet Herasafe KS12	Thermo Scientific, Waltham, MA, USA
BVC professional laboratory fluid aspirator	Vacuubrand GmbH, Wertheim, Germany
Centrifuge 5810R	Eppendorf GmbH, Hamburg, Germany
Centrifuge ROTINA 35R	Hettich, Tuttlingen, Germany
Chemidoc XRS Imaging System	BioRad, Hercules, CA, USA
CO_2 incubator HERA Cell240	Thermo Scientific, Waltham, MA, USA
CO_2 incubator HERA Cell240i	Thermo Scientific, Waltham, MA, USA
Cryogenic Freezing Container, 1° C	Nalgene, Rochester, NY, USA
Electrophoresis Power Supply EPS 601	Amersham Pharmacia Biotech., Uppsala, Sweden
Embedding center Leica EG1150	Leica Microsystems GmbH, Wetzlar, Germany
Glasware	Schott AG, Mainz, Germany
Heating and drying oven Heraeus Function Line B6	Thermo Scientific, Waltham, MA, USA
Heating and drying oven Heraeus Function Line UT20	Thermo Scientific, Waltham, MA, USA
Heating block thermostat BT100	Kleinfeld Labortechnik, Gehrden, Germany
Ice Machine Manitowic	Manitowic Ice, Manitowic, WI, USA
Imaging station	FUJIFILM Visual Sonics, Inc. Toronto, ON, Canada
Intellimixer RM-2L	Elmi Ltd. Laboratory Equipment, Calabasas, CA, USA
Isofluran evaporator	Uno, Netherlands
Magnetic Stirrer	Heidolph Instruments GmbH, Schwabach, Germany

Multiple use equipment	**Source**
Microcentrifuge 5430R	Eppendorf GmbH, Hamburg, Germany
Microcentrifuge QickSpin QS7000 personal	Edwards Instruments CO., Narellan NSW, Australia
Micropipettes PIPETMAN P2, P10, P20, P20, P1000	Gilson Inc., Middleton, WI, USA
Microplate reader Vmax Kinetic	Molecular Devices, Sunnyvale, CA, USA
Microscope Axio Vert.135	Carl Zeiss, Oberkochen, Germany
Microscope Axio Vert.A1	Carl Zeiss, Oberkochen, Germany
Microscope camera Axio Cam ERc 5s	Carl Zeiss, Oberkochen, Germany
Mini Protean System	BioRad, Hercules, CA, USA
Mini Trans-blot cell transfer system	BioRad, Hercules, CA, USA
Mini-Protean Tetra Cell gel system	BioRad, Hercules, CA, USA
Minishaker IKA MS2	IKA Works Inc., Staufen, Germany
Multilabel plate reader VICTOR X3	Perkin Elmer, Waltham, MA, USA
Neubauer chamber	LO Laboroptik, Lancing, England
Orbital shaker K15	Edmund Buehler GmbH, Hechinger, Germany
Perfect Blue Gelsystem Mini M	PEQLAB Biotechnologie GmbH, Erlangen, Deutschland
pH Meter 691	Metrohm, Filderstadt, Germany
Power supply PowerPac HC	BioRad, Hercules, CA, USA
Spectrophotometer Nanodrop 2000c	Thermo Scientific, Waltham, MA, USA
Surgical instruments	Timesco, Essex, United Kingdom
Thermal cycler C1000 CFX96	BioRad, Hercules, Ca, USA
Thermal cycler iCycler iQ Real-time PCR detection system	BioRad, Hercules, Ca, USA
Thermo cycler MJ Research PTC-200	BioRad, Hercules, CA, USA
Tissue processor Leica ASP200 S	Leica Microsystems GmbH, Wetzler, Germany
Ultracentrifuge Optima LE-80K, rotor SW32 Ti	Beckman Coulter GmbH, Krefeld, GER
Vevo 2100 Ultrasound	FUJIFILM Visual Sonics, Inc. Toronto, ON, Canada
Vortex-Genie 2	Scientific Industries, Inc., Bohemia, NY, USA
Water bath W350	Memmert, Schwabach, Germany
Water purification system, Purelab	Elga Lab water, Celle, Germany

2.1.2 Disposable equipment

Disposable equipment	Source
Amersham hybond-P PVDF-Membrane	GE-Healthcare, Buckinghamshire, England
Cell culture plates 24 well, 15 cmm	TPP, Techno Plastic Products AG, Trasadingen, Schweiz
Cell culture plates 96 well, 24 well, 12 well, 6 well, 10 cm	Coming Incoporated, Coming, NY, USA
Chromatography paper Whatman	GE Healthcare, Buckinghamshire, England
Conical bottom polystyrene tubes	Elkay, Hampshire, United Kingdom
Conical tubes 15ml, 50ml Falcon	Greiner GmbH, Frickenhausen, Germany
Cryogenic vials 1.8 ml Nunc	Sigma-Aldrich Chemie GmbH, Munich, Germany
Desalting sephadex PD-10 columns	GE Healthcare, Buckinghamshire, England
Embedding cassettes Rotilabo	Carl Roth, Karlsruhe, Germany
Hard-Shell PCR Plates 96-well	BioRad, Hercules, CA, USA
Lens cleaning paper	The Tiffen company, Hauppauge, NY, USA
Microscope coverslips	Thermo Scientific Waltham, MA, USA
Microscope slides Superfrost plus	Thermo Scientific Waltham, MA, USA
Needles 27 Gauge	BD Biosciences, San Jose, CA, USA
Needles 30 Gauge, ¾" Monoject	Medtronic, MA, USA
PCR reaction tube 0.5 ml	Biozym Scientific, Oldendorf, Germany
PCR sealers Microseal 'B' Film	BioRad, Hercules, CA, USA
Pipette tips with and without filter	Sarstedt, Nuembrecht, Germany
Reaction tubes 0.5ml, 1.5ml, 2ml	Sarstedt, Nuembrecht, Germany
Round bottom polystyrende tubes	Croning Incorporated, Corning, NY, USA
Serological pipettes	Greiner Bio-One International AG, Kremsmuenster, Austria
Silicone sheet, 0.5mm thick	Sahlberg GmbH&Co., KG, Munich, Germany
Sterile filter Nalgene 0.25µm, 0.45µm	Thermo Scientific, Waltham, MA, USA
Syringes 1ml Omnifix	B. Braun Melsungen AG, Melsungen, Germany
Ultracentrifugation tube Ultra-Clear 25x89 mm	Beckmann&Coulter GmbH, Krefeld, Germany
X-ray film CEA RP New	Agfa Healthcare, Mortsel, Belgium

2.1.3 Chemicals and reagents

Chemicals and reagents	Source
2-mercaptoethanol	Sigma-Aldrich Chemie GmbH, Munich,
7-Aminoactinomycin	Thermo Scientific, Waltham, MA, USA
96% Ethanol	Otto Fischer GmbH, Saarbrücken, Germany
Acetic acid	Merck Chemicals GmbH, Hessen, Germany
Agarose Ultrapure	Thermo Scientific, Waltham, MA, USA
Ammonium persulfate (APS)	Sigma-Aldrich Chemie, GmbH, Munich, Germany
Ampicillin	Sigma-Aldrich Chemie GmbH, Munich, Germany
Biocoll separating solution	Biochrom, Berlin, Germany
Boric acid	Sigma-Aldrich Chemie GmbH, Munich, Germany
Bovine serum albumin (BSA)	Sigma-Aldrich Chemie GmbH, Munich, Germany
Bromophenol blue	Serva Electrophoresis GmbH, Heidelberg, Germany
Caesium chloride(CsCl)	Sigma-Aldrich Chemie GmbH, Munich, Germany
CD293 Media	Thermo Scientific, Waltham, MA, USA
Chlorophorm	Sigma-Aldrich Chemie GmbH, Munich, Germany
Color Prestained Protein Standard, Broad Range	New England Biolabs, Ipswich, MA, USA
Cresol Red	Sigma-Aldrich Chemie GmbH, Munich, Germany
DAB-Chromogen and Substrate buffer	Agilent, Santa Clara, CA, USA
DAKO REAL antibody diluent	Dako, Hamburg, Germany
Deoxynucleotide tri-phosphate (dNTPs)	Thermo Scientific, Waltham, MA, USA
Developing and fixation solutions Vision X GV60	Roentgen bender GmbH&Co. KG, Baden-Baden, Germany
Dimethyl sulfoxide (DMSO)	Sigma-Aldrich Chemie GmbH, Munich, Germany
Dithiothreitol (DTT)	Cell-Signaling, Cambridge, England
DNA ladder 100bp, 1kb	Thermo Scientific, Waltham, MA, USA
DNA loading buffer 6x	Thermo Scientific, Waltham, MA, USA
Dulbecco's Modified Eagle's Medium (DMEM)	Biochrom, Berlin, Germany
E. coli, DH10B	PD Per Sonne Holm, Experimental Urology, Klinikum rechts der Isar, TUM
ECM from Engelbert-Holm – Swarm murine sarcoma	Sigma-Aldrich Chemie GmbH, Munich, Germany
Ethanol absolut	Merck Chemicals GmbH, Hessen, Germany
Ethidiumbromide, 10 mg/ml	Sigma-Aldrich Chemie GmbH, Munich, Germany
Ethylenediaminetetraacetic acid (EDTA), 0,5 M	AppliChem, Darmstadt, Germany
Fetal Bovine Serum	Biochrom, Berlin, Germany
Fugene HD	Promega, Madison, WI, USA

Chemicals and reagents	Source
Glycine	Sigma-Aldrich Chemie GmbH, Munich, Germany
GoTaq Green PCR master mix	Promega, Madison, WI, USA
GoTaq qPCR master mix	Promega, Madison, WI, USA
Haematoxylin solution, Mayer's	Krankenhausapotheke, Klinikum rechts der Isar, Munich, Germany
Hydrogen chloride (HCl)	Merck Chemicals GmbH, Hessen, Germany
Hydrogen peroxide	Merck Chemicals GmbH, Hessen, Germany
Immobilized Protein A Plus	Thermo Scientific, Waltham, MA, USA
Interleukin 2	Sigma-Aldrich Chemie GmbH, Munich, Germany
Isocitrate monohydrate	Sigma-Aldrich Chemie GmbH, Munich, Germany
Isopropanol	Sigma-Aldrich Chemie GmbH, Munich, Germany
Kanamycin	Sigma-Aldrich Chemie GmbH, Munich, Germany
L-Glutamin 200mM	Sigma-Aldrich Chemie GmbH, Munich, Germany
Lipofectamin 2000	Invitrogen, Carlsbad, CA, USA
Lipopolysaccharide	Sigma-Aldrich Chemie GmbH, Munich, Germany
Magnesium Chloride (MgCl)	Sigma-Aldrich Chemie GmbH, Munich, Germany
Methanol	Sigma-Aldrich Chemie GmbH, Munich, Germany
Mounting medium Entellan-new	Merck Chemicals GmbH, Hessen, Germany
Non-essential amino acids (NEAA), 100x	Biochrom, Berlin, Germany
Opti-MEM	Sigma-Aldrich Chemie GmbH, Munich, Germany
Opti-MEM Media	Thermo Scientific, Waltham, MA, USA
Paraformaldehyde solution	Sigma-Aldrich Chemie GmbH, Munich, Germany
p-Coumeric acid	Sigma-Aldrich Chemie GmbH, Munich, Germany
PEI-Mag2	A kind gift from Christian Plank (Tresilwised et al. 2012)
Penicillin/Streptomycin	Sigma-Aldrich Chemie GmbH, Munich, Germany
Phenol:Chlorophorm:Isoamylalcohol	Sigma-Aldrich Chemie GmbH, Munich, Germany
Phosphate buffered saline (PBS), 1x, 10x	Biochrom, Berlin, Germany
Precision Plus Protein Standard	Bio-Rad, Hercules, CA, USA
Restriction enzyme buffers	Thermo Scientific, Waltham, MA, USA; New England Biolabs, Ipswich, MA, USA
Roswell Park Memorial Institute medium (RPMI)	Biochrom, Berlin, Germany
Rotiphorese gel 30	Carl Roth, Karlsruhe, Germany
Select agar	Sigma-Aldrich Chemie GmbH, Munich, Germany
Skimmed milk powder	Nestle, Vevey, Switzerland
Sodium acetate	Merck, Darmstadt, Germany
Sodium azide	Sigma-Aldrich Chemie GmbH, Munich, Germany
Sodium chloride (NaCl)	Merck Chemicals GmbH, Hessen, Germany
Sodium dodecyl sulfate	Sigma-Aldrich Chemie GmbH, Munich, Germany

Chemicals and reagents	Source
Sodium orthovanadate	Sigma-Aldrich Chemie GmbH, Munich, Germany
Sulforhodamin B (SRB)	Sigma-Aldrich Chemie GmbH, Munich, Germany
Tetramethylethylenediamine (TEMED)	Carl Roth, Karlsruhe, Germany
Trichloroacetic acid	Sigma-Aldrich Chemie GmbH, Munich, Germany
Tris(hydroxymethyl)-aminomethane	Merck, Darmstadt, Germany
Triton-X-100	Sigma-Aldrich Chemie GmbH, Munich, Germany
Trypan blue, 0,5%	Biochrom, Berlin, Germany
Trypsin/EDTA	Biochrom, Berlin, Germany
Tryptone	Sigma-Aldrich Chemie GmbH, Munich, Germany
Tween-20	Serva Electrophoresis GmbH, Heidelberg, Germany
Virus lysis buffer	Biochrom, Berlin, Germany
Virus storage buffer	Biochrom, Berlin, Germany
Yeast Extract	Sigma-Aldrich Chemie GmbH, Munich, Germany

2.1.4 Enzymes

Enzymes	Source
BamHI	Thermo Scientific, Waltham, MA, USA
Benzonase	Sigma-Aldrich Chemie GmbH, Munich, Germany
BGlII	New England Biolabs, Ipswich, MA, USA
Complete mini-protease inhibitor	Roche, Basel, Switzerland
EcoRV	New England Biolabs, Ipswich, MA, USA
FastAP phosphatase	Thermo Scientific, Waltham, MA, USA
NdeI	Thermo Scientific, Waltham, MA, USA
PacI	New England Biolabs, Ipswich, MA, USA
Phosphatase inhibitor mix II	Serva Electrophoresis GmbH, Heidelberg, Germany
PmeI	New England Biolabs, Ipswich, MA, USA
Proteinase K	Sigma-Aldrich Chemie GmbH, Munich, Germany
SpeI	New England Biolabs, Ipswich, MA, USA
T4 DNA ligase	Thermo Scientific, Waltham, MA, USA
T4 DNA polymerase	Thermo Scientific, Waltham, MA, USA
Taq DNA polymerase	Thermo Scientific, Waltham, MA, USA
XhoI	Thermo Scientific, Waltham, MA, USA

2.1.5 Buffers and solutions

Buffer	Components
0.1 % $CaCl_2$	0.9 mM $CaCl_2$ in dH_2O
0.5 % (W/V) SRB staining solution	0.5 % SRB in 1% acetic acid
1 % BSA	1 % BSA in PBS
1 % SDS Protein lysis buffer	10 mM Tris/HCl, pH 7.2 1 % SDS 1 mM Na orthovanadate Add one Complete Mini-Protease Inhibitor tablet and 100 µl phosphatase inhibitor per 10 ml of protein lysis buffer
100 % TCA	0.3 M TCA 22,7 ml dH_2O
10x SDS running buffer	25 nM Tris 192 mM Glycine 0.1 % w/v SDS pH 8.3
10x TBE	1 M Tris 1 M Boric acid 0.02 M EDTA
10x TBS	0.5 M Tris/HCl, pH 7.6
10x Transfer buffer	25 nM Tris 192 mM Glycine
1x Transfer buffer	10 % 10x Transfer buffer 20 % Methanol
4x Protein loading buffer	0.25 M Tris/HCl, pH 6.8 8 % SDS 0.04 % Bromophenol blue 40 % Glycine Add 100 µl of 1 M DTT to 500 µl of 4xprotein loading buffer prior to use
Chemiluminescence reagent A	0.1 M Tris/HCl, pH 8.5 2.5 mM Luminol 0.4 mM p-Coumeric acid
Chemiluminescence reagent B	0.1 M Tris/HCl, pH 8.5 0.18 % H_2O_2
CsCl heavy solution p=1.45 g/cm^3	609.0 g/L CsCl in 10 mMTris (pH 7.8)
CsCl light solution p=1.33 g/cm^3	454.2 g/L CsCl in 10 mM Tris (pH 7.8)
DNA Lysis buffer	10 mM Tris/HCl pH8 100 mM NaCl 25 mM EDTA pH8 0.5 % SDS

Buffer	Components
DNA precipitation solution	588 mM $NH_4C_2H_3O_2$ 100 % Ethanol
Immunoblotting antibody dilution buffer	5 % BSA in TBS-T with 0.02 % Sodium azide
Immunoblotting blocking buffer	5 % non-fat milk powder in TBS-T
IP elution buffer:	0.15 M NaCl 0.05 M Tris/HCl 1 % Triton X-100 5 mM EDTA 1x protein loading buffer
IP protein lysis buffer	0.15 M NaCl 0.05 M Tris/HCl 1 % Triton X-100 5 mM EDTA
LB agar	LB Medium 1.5 % select agar
LB medium	0.01 % Tryptone 0.005 % Yeast extract 0.01 % NaCl
PCR buffer	1xTaq Puffer $(NH_4)_2SO_4$ 8 % Glycerol 25 mM $MgCl_2$ 10 mM dNTPs Cresol Red
RIPA protein lysis buffer	0.15 M NaCl 0.05 M Tris/HCl 1 % Triton X-100 0.05 % SDS 5 mM EDTA
Separating gel buffer	1.5 M Tris/HCl, pH 8.8
SRB solubilizing solution	10 mM Tris, pH 10
Stacking gel buffer	0.5 M Tris/HCl, pH 6.8
TBS-T	1x TBS 0.001 % Tween-20
Virus storage buffer	20 mM NaCl 25 mM Tris 2.5 % Glycerol

2.1.6 Commercial kits

Commercial kits	Source
HiSpeed Plasmid Midi Kit	Qiagen, Hilde, Germany
Pierce BCA Protein Assay	Thermo Scientific, Waltham, MA, USA
QIAquick gel extraction kit	Qiagen, Hilde, Germany
QIAprep Spin Miniprep Kit	Qiagen, Hilde, Germany
IFNy ELISA	BioLegend, San Diego, CA, USA

2.1.7 Antibodies and peptides

Target protein, Clon	Application	Dilution	Source
Actin (A2066)	WB	1:1000	Sigma-Aldrich Chemie GmbH, Munich, Germany
CAR, RcmcB	FACS	1:40	Merck Chemicals GmbH, Darmstadt, Germany
E1A, M73	IF	1:100	Santa Cruz Biotechnology, INC., Dallas, TX, USA
E2F1	WB	1:250	Santa Cruz Biotechnology, INC., Dallas, TX, USA
GAPDH (2118)	WB	1:1000	CST, Beverly, MA, USA
h PD-L1, E1L3N	WB	1:1000	CST, Beverly, MA, USA
Hexon AB1056	WB	1:500	Merck Chemicals GmbH, Darmstadt, Germany
Hexon, G097	IHC	1:500	abm, Richmond, BC, Canada
m PD-L1, (179711)	WB	1 µg/ml	R&D
P53, 1C12	WB	1:1000	CST, Beverly, MA, USA
PD-L1, MIH1	Functional assay		Thermo Scietific, Waltham, MA, USA
pRb (Ser780), D59B7	WB	1:1000	CST, Beverly, MA, USA
Rb, 554136	WB	2 µg/ml	BD Bioscience, San Jose, CA, USA

Target protein, Clon	Application	Dilution	Source
YB-1	WB, IF	1:2000, 1:80	Eurogentec GmbH, Köln, Deutschland (Vroni Girbinger 2013)
Alexa 488 conjugated goat-anti-rabbit IgG, 4412	IF	1:500	CST, Beverly, MA, USA
FITC conjugated rabbit-anti mouse IgG, F0232	FACS	10µg/µl	Agilent, Santa Clara, CA, USA
Cy3 conjugated goat-anti-mouse IgG, A10521	IF	5µg/µl	Thermo Scietific, Waltham, MA, USA
FITC conjugated swine-anti-rabbit IgG, F0205	IF	1:100	Agilent, Santa Clara, CA, USA
Peroxidase conjugated anti-rabbit IgG, 711-036-152	WB	1:10 000	Dianova GmbH, Hamburg, Germany
Peroxidase conjugated anti-mouse IgG, 715-036-150	WB	1:10 000	Dianova GmbH, Hamburg, Germany
Peroxidase conjugated goat-anti-mouse IgG, P0447	IHC	1:1000	Agilent, Santa Clara, CA, USA
Mouse gamma globulin Isotype control	FACS	1:40	Dianova GmbH, Hamburg, Germany
Murine Fc block: anti-mouse CD16/32	FACS	1:200	Thermo Scientific, Waltham, MA, USA
Human Fc block	FACS	2.5 µg/1x10^6 cells	Dianova GmbH, Hamburg, Germany

2.1.8 Primer sequences

All primers were synthesized by Life Technologies or Metabion and dissolved in H_2O to a final stock concentration of 10 µM.

Target gene	Forward primer	Reverse primer
E1b19k	CGTGAGAGTTGGTGGGCGT	CTTCGCTCCATTTATCCT
E3	GTTAATGTCAGGTCGCCTAAGTCG	GTGTGTTGCCCGCGACCATT
RGD	CTGCCGCGGAGACTGTTTC	CTGCAATTGAAAAATAAACACG
E1A	ACGGTTGCAGGTCTTGTC	TTTACACCTTATGGCCTGGGGC
E1A 13s	GGCATGTTTGTCTACAGTAAG	GCCATGCAAGTTAAACATTATC
E3 ADP	ATGTCAGCATCTGACTTTG	CTCGAGGAATCATGTCTC
PD-L1-Fc	AAGGTGGAAATCAAGAGAGG	CCAGTTGAACTTGACCTCAG
E3	GAACAATTCAAGCAACTCTAC	GCAGTCTACTTCGATGTGAG

Target gene	Forward primer	Reverse primer
Fiber	AAGCTAGCCCTGCAAACATCA	CCCAAGCTACCAGTGGCAGTA
Human actin	AAAGTGCAAAGAAC CGGCTAAG	TAAGTAGGTGCACAGTAGGTCTGA
Human GAPDH	TGGCATGGACTGTGGTCATGAG	ACTGGCGTCTTCACCACCATGG
Murine actin	CTGCTCTGGCTCCTAGCAC	TGAATGGTGAGCTCTCTGGGT
Murine GAPDH	TTTGGCATTGTGGAAGGGCT	ACCCCTCTACCCAAAAGGGA

2.1.9 Plasmids

Plasmid	Source
pcDNA3.1-IgG1	Kind gift from PD Melanie Laschinger
pShuttle Clontech DraO-WtE3	Cloned by Klaus Mantwill
pMK-RQ-a-PD-L1	Thermo Scientific, Waltham, MA, USA
pUC18-XVir-E3-RGD	Cloned by Klaus Mantwill
pXVir-N-31	Cloned by Klaus Mantwill

2.1.10 Viruses

The wild type adenovirus AdWT serotype 5 species C is well characterized and served as positive control for replication, cell lysis and particle formation in this work. All oncolytic adenoviruses used in this work are derived from AdWT.

dl703 has a 3.2 kb deletion in the E1 region and is replication incompetent (Bett et al. 1994). It served as a negative control in this thesis.

The oncolytic adenovirus XVir-N-31 has an 11 bp deletion in the E1A-CR3 region, a partial deletion in the E1B19K gene and a deletion in the E3 region. It has an additional RGD motif in the fiber encoding gene (Rognoni et al. 2009; Mantwill et al. 2006).

The oncolytic virus XVir-N-31/E2Fm is mutated in its E2F1 binding sites in the E2 early promoter. This mutation was integrated into the backbone of XVir-N-31.

2.1.11 Cell culture

2.1.11.1 Cell lines

Cell line	Source
HEK293	American type culture collection, Manassas, VA, USA
J82	American type culture collection, Manassas, VA, USA
MB49	A kind gift from Dr Breul from the Uniklinikum Essen
MBT2	A kind gift from Dr Breul from the Uniklinikum Essen
T24	American type culture collection, Manassas, VA, USA
UMUC3	American type culture collection, Manassas, VA, USA

2.1.11.2 Cell culture media

Medium	Formulation
Growth medium for cells at 5 % CO2	RPMI 5 % FBS 1 % NEAA 1 % Penicillin/Streptomycin
Growth medium for cells at 10 % CO2	DMEM 5 % FBS 1 % Penicillin/Streptomycin
Growth medium for HEK293 suspension cells	CD293 1 % L-Glutamine
Freezing medium DMEM	50 % growth medium DMEM 40 % FBS 10 % DMSO
Freezing medium RPMI	50 % growth medium RPMI 40 % FBS 10 % DMSO
Infection medium DMEM	DMEM
Infection Medium RPMI	RPMI

2.1.12 Mice

Mouse strain	Source
Foxn1$^{nu/nu}$	Charles River
C57BL/6	Charles River

2.1.13 Software

Software	Company
FlowJo	FlowJo LLC, Ashland, OR, USA
Zen Lite 2012	Carl Zeiss, Oberkochen, Germany
Vevo LAB 2000	FUJIFILM Visual Sonics, Inc. Toronto, ON, Canada

2.2 Methods

2.2.1 Molecular biology techniques

2.2.1.1 Preparation of competent bacteria

E.coli (DH10B) were cultured in 2ml LB medium in a shaker at 37° C overnight. The next day, 100 ml LB medium were inoculated with the starter culture and incubated at 37°C. As soon as cells reached the exponential growth phase, bacteria were put on ice for 30 minutes. Cells were centrifuged for 10 minutes at 4°C with 3000g and pellet was resuspended in 35 ml pre-cooled 0.1 M $CaCl_2$. Resuspended cells were incubated again on ice for 30 minutes and centrifuged for 10 minutes at 4°C with 3000 g. Then, pellet was resuspended in 0.1 M pre-cooled $CaCl_2$ + 10 % Glycerol. Competent bacteria were aliquoted in pre-cooled tubes and stored at -80°C.

2.2.1.2 Purification of plasmid DNA

LB Medium containing selective antibiotic (100µg/ml ampicillin, 50µg/ml kanamycin) was inoculated with single colonies of the plasmid containing bacteria and cultured overnight in a shaker at 37°C. 800 µl bacterial culture was mixed with 400µl glycerol:LB mixture (ratio 3:2) as a glycerol stock. Bacteria were harvested by centrifugation at 3000g for 15 minutes in a pre-cooled centrifuge. Pelleted bacteria were lysed according to the QIAprep Spin Miniprep Kit manual. Plasmid DNA was isolated either by using QIAprep Spin Miniprep columns or by DNA precipitation using isopropanol. Isolation of DNA using columns was performed according to the instruction manual. For isopropanol precipitation of DNA, lysed bacteria were centrifuged for 10 minutes at full speed in a pre-cooled centrifuge. DNA containing supernatant was transferred to a new tube, 0,7 x volume of isopropanol and one drop of glycogen were added and DNA was precipitated by carefully inverting the tube 4 to 6 times. Precipitated DNA was centrifuged at full speed for 30 minutes at 4° C. Pelleted DNA was washed twice with 300 µl of 70 % ethanol and again centrifuged. Air dried DNA pellet was dissolved in 20 to 50 µl water at 55° C for 1 to 2 hours or at 4° overnight. DNA concentration was measured using the NanoDrop 200c. Plasmid DNA was stored at 4°C. Plasmid identity was confirmed by sequencing which was performed by GATC Biotech AG, Constance, Germany.

2.2.1.3 Isolation of DNA from tumor cells

For isolation of cellular and viral DNA in 6 well plates, infected cells were washed once with PBS and lysed with 200 µl of DNA lysis buffer. The lysate was transferred into a 1.5 ml tube, 3 µl of proteinase K were added and the lysate was digested at 56° C under vigorous shaking for 8 to 12 hours. For

purification, 200 µl Phenol:Chlorphorm:Isoamylalcohol was added and mixed by vortexing for 30 seconds. The lysate was incubated on ice for 5 minutes and centrifuged at 16430 g for 5 minutes at 4° C. The upper phase (200 µl) was transferred to a new tube, 200 µl chlorophorm and 2 µl cresol red were added and the sample was mixed by vortexing for 30 seconds. After incubation on ice for 5 minutes, samples were centrifuged at 16430 g for 5 minutes at 4° C. The upper phase (200µl) was again transferred to a new tube and DNA was precipitated by adding 850 µl DNA precipitation solution and centrifugation at 16430 g for 30 minutes at 4° C. Pelleted DNA was washed with 400 µl of 70 % ethanol. After incubation for 10 minutes, DNA was centrifuged at 500 g for 5 minutes at room temperature. DNA was dried and dissolved in 50 to 100 µl 0.1xTE buffer at 40° C for 1 to 5 hours.

2.2.1.4 Restriction digestion

For analysis and digestion of plasmids, an appropriate amount of DNA was digested with the required enzyme for 1 hour or overnight at 37° C. If needed, the restriction enzyme was heat inactivated according to the manufacturer's protocol. Digested DNA was analyzed by agarose gel electrophoresis.

2.2.1.5 Agarose gel electrophoresis and gel extraction of DNA

0.8 to 1.5 % agarose gels were prepared using 1xTBE buffer and 0.5 µg/ml ethidium bromide. DNA was loaded using 6x loading buffer. Gels were run in 1xTBE buffer at 70 to 110 V until bands were separated as needed. The bands were visualized in a UV transillumination and the analysis was documented by the Chemidoc XRS system.

2.2.1.6 Dephosphorylation, ligation and transformation of competent bacteria

Dephosphorylation of digested vectors was performed according to the manufacturer's manual at 37° C for 1 to 2 hours. The phosphatase was heat inactivated at 65° C for 15 minutes. Vector and insert were ligated in ratios varying from 1:3 to 1:7 using T4 DNA ligase by incubating at room temperature for 1 hour. For transformation, competent bacteria were thawed on ice. 15 µl of ligation mixture was added to bacteria, incubated on ice for 30 minutes, followed by a 30s heat shock at 42°C and a 10-minute incubated on ice. Bacterial cells were resuspended in pre-warmed LB medium and incubated for 1 hour at 37°C. Various amounts of the transformed bacteria were streaked onto LB agar plates and incubated at 37° C for 12 to 18 hours.

2.2.1.7 Colony polymerase chain reaction (PCR) to screen clones

Single colonies were picked using a sterile pipette tip to inoculate 100 µl LB medium. Infected medium was incubated at 37° C for 2 to 6 hours. Bacterial cells were pelleted, resuspended in 20 µl PCR master mix and lysed at 100° C for 10 minutes. Cell debris was pelleted by centrifugation and 5 µl of plasmid DNA containing supernatant was used for the PCR. PCR conditions are listed in tableTable 6. Primer combination and their application in various cloning steps are listed in table 4.

Table 4: Primer combinations for colony PCR.

Cloning step	Primer combination	Primer binding site	Product size
Ligation of transgene into shuttle plasmids	311, 310	311: in aPD-L1 fragment 310: in Fc-fragment	613 bp
Ligation of transgene into pShuttle Clontech	310, 81	81: in pShuttle backbone 310: in Fc-fragment	1188 bp
Integration of transgene into pXVir-N-31	324, 325	324: 3’ of BamHI restriction site at bp 26171 325: 5’ of BamHI restriction site at bp 26171	657 bp

2.2.1.8 Identity PCR to verify virus identity

Purified viral DNA was diluted with water to a concentration of 0.1 to 1 ng/µl, purified virus was heat inactivated at 100° C for 10 minutes and diluted 1:10 with nuclease-free water. The PCR reaction mix for one sample includes 18.5 µl PCR master mix, 2.5 µl forward primer and 2.5 µl reverse primer (final primer concentration 12.5 pM) and 0.5 µl Taq polymerase. 24 µl PCR reaction mix was dispensed into 0.2 ml PCR reaction tubes prior to the addition of 1 µl viral DNA or inactivated virus. Primer combinations for the identity PCR are listed in table 5.

The PCR cycling conditions are shown in Table 6. The PCR was analyzed by agarose gel electrophoresis.

Table 5: Primer combinations for identity PCR.

PCR number	Gene	Forward primer	Reverse primer	Product size	
				XVir	WT
1	E1A	H303	H216	540 bp	540 bp
2	E1A13S deletion	H231	H38		548 bp
3	E1B19k deletion	H3	H4	387 bp	587 bp
4	E3 deletion	H36	H37	No amplicon	380 bp
5	E3 ADP	H301	H253	No amplicon	384 bp
6	RGD	H34	H6	176 bp	No amplicon
7	aPD-L1	H311	H310	613 bp	No amplicon
	Fc	H81	H310	337 bp	

Table 6: PCR cycling conditions.

Step	Time, Temperature
Initial denaturation	1 min, 95° C
Annealing (30 cycles)	40 sec, 95° C
	40 sec, 58° C
	40sec, 72° C
Final extension	5 min, 72° C
Hold	∞, 4° C

2.2.1.9 Fiber qPCR to quantify viral replication

To quantify viral DNA, 5 µl of 20 ng/µl purified DNA were used in a fiber qPCR. PCR mix was prepared using the GoTaq Green PCR master mix according to manufacturer's protocol, using 500 nM of forward and reverse primers for fiber, murine and human actin as well as murine GAPDH. Primers against human GAPDH were used at a concentration of 250 nM. For each PCR reaction, 10 µl PCR master mix were used.

The PCR cycling conditions are shown in Table 7.

Table 7: Cycling conditions for fiber qPCR.

Step	Time, Temperature
Initial denaturation	2 min, 94° C
Annealing (45 cycles)	15 sec, 94° C
	15 sec, 60° C
	15 sec, 72° C
Final extension	15 min, 94° C
Melt curve	15 min, 94°C
	5 sec, 60°C
	5 min, 95°C

To quantify viral fiber DNA, the ΔΔCt method was used. For the relative quantification of viral fiber DNA, actin and GAPDH were used as reference genes. The 4 hour fiber value served as control and was used for normalization (Livak and Schmittgen, 2001).

$$\Delta Ct = Ct\ (\text{reference gene}) - Ct\ (\text{fiber gene})$$

$$\Delta\Delta Ct = \Delta Ct\ (\text{sample}) - \Delta Ct\ (\text{control sample})$$

$$\text{Normalized gene expression} = 2^{-\Delta\Delta Ct}$$

2.2.2 Cell culture

2.2.2.1 Cultivation of cell lines

Cells were cultured under sterile conditions at 37°C under saturated humidity in a laminar flow biological safety cabinet. All cell lines were used in early passages and passaged at 80 % confluency. For all experiments, media and trypsin were pre-warmed to 37° C. For passaging, cells were washed with PBS-5% 0.5 M EDTA and incubated with trypsin until they detached. Trypsin was inactivated using fresh medium and cells were centrifuged at 300 RCF for 5 minutes at room temperature. The pelleted cells were resuspended in 10 ml fresh medium and a fraction was transferred onto a new cell culture dish for culturing the subsequent passage. UMUC3, HEK293, MB49 were maintained at 10 % CO_2, while T24, J82 and MBT2 were maintained at 5 % CO_2.

2.2.2.2 Counting of cells

Cell solution was diluted 1:1 in 0.5 % trypan blue solution and counted in a Neubauer chamber. Unstained cells were considered to be viable.

2.2.2.3 Thawing and freezing of cells

For thawing cells, the cryovial was thawed in the water bath and then immediately transferred to a tube containing fresh media. After centrifugation, cells were resuspended in medium and cultured as described in 2.2.2.1. For cryopreservation, cells at 70-80 % confluency were pellet as described in 2.2.2.1. Cell pellet was resuspended in 3 ml of freezing media, transferred into two cryovials and vials were stored in a freezing container at -80° C for 24 to 48 hours and then transferred to liquid nitrogen.

2.2.3 *In vitro* experiments

2.2.3.1 Treatment with inhibitors

Nutlin-3a was dissolved in DMSO and stored as a 5 mM stock solution at -20° C. Cells were seeded 24 hours before treatment. Working dilutions were prepared fresh using pre-warmed medium. The highest DMSO concentration was used as a control.

2.2.3.2 Dose response assay

$5x10^4$ cells per well were seeded on a 12 well plate. 24 hours after seeding, cells were treated with various concentrations of the inhibitor as described in 2.2.3.1. The cells were fixed three days after treatment and the assay was continued as described in 2.2.5.2.

2.2.3.3 Cell cycle analysis by flow cytometry

$2x10^4$ cells per well were seeded on a 6 well plate. 24 hours after seeding, cells were treated with inhibitors or infected with virus. For harvesting, the cells were trypsinized, transferred into FACS tubes and spun down. Then, cells were washed 2 times with PBS and fixed with 70% ice cold ethanol at 4°C

for 12 hours or at -20°C for 1 hours. After fixation, cells were washed with PBS-1 % BSA and total DNA was stained with 4 µg/ml 7-AAD. 5000 events were recorded on the flow cytometer using a low speed. Data were analyzed using the FlowJo software.

2.2.4 Virus generation and production

2.2.4.1 Transfection of linearized, viral plasmids

To generate virus, $2{,}5x10^4$ and $5x10^4$ HEK293 cells were seeded on 24 well and 12 well plates, respectively. After 24 hours, cells were transfected with linearized viral plasmid DNA using FuGene®. Therefore, a FuGene® to DNA ratio of 3:2 with a total DNA amount of 2 µg was used. 25 µl or 50 µl of the transfection mixture were added to the cells on 24 well or 12 well plates, respectively, and medium was changed after 24 hours.

2.2.4.2 Generation of crude virus stocks

After successful transfection, a cytopathic effect (CPE) became visible on day 7 to 14. Cells and supernatant were harvested and applied to 3 freeze and thaw cycles before centrifuged at 600 g for 5 minutes. Virus containing supernatant was transferred into a new tube. 200 µl were used for reinfection of HEK293 on one 15 cm cell culture plate, residual supernatant was mixed with 200 µl glycerin, aliquoted and stored as G1 stock at -80° C. As soon as the reinfected cells showed a CPE, cells and supernatant were harvested. After three freeze and thaw cycles, cells and supernatant were centrifuged at 600 g for 5 minutes. The supernatant was mixed with 200 µl glycerol, aliquoted and stored as G2 stock at -80° C.

2.2.4.3 Virus production

For virus production, HEK293 cells were freshly thawed. HEK293 cells were prepared at a confluency of 80 % on 20 15cm cell culture plates. For infection, 20 MOI of the G2 stock diluted in 4 ml DMEM infection medium per cell culture dish were used. After one hour of infection, 10 ml DMEM growth medium were added on every plate. 45-50 hours after infection, cells were carefully rinsed of the cell culture plate. Virus containing cells were pelleted at 1000 g for 5 minutes and supernatant was withdrawn. Cell pellets were resuspended in 8 ml lysis buffer and stored at -80° C until caesium chloride purification.

2.2.4.4 Virus purification using caesium chloride density gradient

To release the virus from the cells, the HEK293 cell pellet (see 2.2.4.3) was repeatedly frozen and thawed for three times to destroy the cells. The solution was centrifuged at 3000 g for 15 minutes to separate the virus from the cell debris. The virus containing supernatant was transferred into a new tube and incubated with 12.5 U/ml Benzonase and 1 mM $MgCl_2$ for 2 hours at room temperature to digest the remaining cellular DNA. Afterwards, the virus was purified in a caesium chloride density gradient. Therefore, the gradient was built in an ultracentrifugation tube using 17 ml of 1.33 g/ml caesium chloride solution and 9 ml of 1.45 g/ml caesium chloride solution. The virus solution was carefully added on top of the gradient and tubes were centrifuged in an ultracentrifuge at 53 000 g for 3 h at 10°C. The virus band was taken off using a syringe and applied to a second caesium chloride density gradient for further purification. Therefore, the gradient was centrifuged for 18 h. Finally, the purified virus band was taken off, finally desalted using disposable PD-10 desalting columns. Viruses were obtained in virus storage buffer and aliquots were stored at -80° C.

2.2.5 *In vitro* assays using virus

2.2.5.1 Infection of cells with virus

24 hours before virus infection, cells were seeded at concentrations of $2x10^4$, $5x10^4$, $1x10^5$, $1x10^6$ cells on 24 well, 12 well, 6 well and 10 cm dish, respectively. Viruses were thawed on ice and appropriate working dilutions were prepared freshly using infection medium. For infection, growth medium was aspired and cells were infected in reduced volume of infection medium containing the diluted virus. Cells on 24 well, 12 well, 6 well or 10 cm dish were infected with 150µl, 200µl, 200µl, 2ml, respectively. Cells were swayed every 15 minutes for one hour and infection was terminated by adding growth medium to the cells.

For infection with magnetic nanoparticles, $1x10^4$ cells were seeded on a 12 well plate in 1 ml growth medium 24 hours before treatment. For coating of viral particles, a ratio of 5 fg magnetic nanoparticles (PEI-Mag2) per viral particle was used. Therefore, the virus was diluted to an appropriate concentration using DMEM and the nanoparticles were diluted in sterile deionized water. 90 µl of diluted virus was added to 10 µl of magnetic nanoparticles, carefully mixed by pipetting up and down and incubated at room temperature for 15 minutes. Then, a magnetic field was applied by positioning the cell culture plate on a 12 well magnetic plate. The coated virus was added to the cells and incubated for 15 minutes. Finally, cell culture plates were put back in the incubator.

2.2.5.2 Potency assay

$5x10^4$ cells were seeded on a 12 well plate. 24 hours after seeding, cells were treated as desired. Four days after infection, the medium was aspired, cells were washed three times with PBS and fixed for 30 minutes at 4° C using 1 ml ice cold 10 % TCA. Then TCA was removed and cell layers were washed four times with tap water. Cells were stained with 1 ml of 0.5 % SRB solution for 30 minutes. Unbound SRB was removed by washing five times with 1 % acetic acid and plates were air dried. Dried plates were scanned and bound SRB was solubilized in 1 ml 10 mM Tris base and diluted 1:10 with PBS in a 96 well plate. Finally, SRB absorbance was measured at 560 nm using the plate reader protocol SRB-absorbance 560 nm 0.1 s.

2.2.5.3 Analysis of viral replication

For analysis of viral replication, $1x10^5$ cells were seeded on a 6 well cell culture dish and infected the next day with various MOIs as described in 2.2.5.1. 4, 24, 48 and 72 hours after infection, cells were washed with PBS and DNA lysates were prepared as described in 2.2.1.3. Fiber DNA was quantified by performing a fiber qPCR (2.2.1.9).

2.2.5.4 Quick titer test

To analyze the titer of the G2 stock, $5x10^5$ HEK293 cells were seeded on two 6 well cell culture plates. 24 hours after seeding, cells were infected with 1, 3, 5, 10, 15, 20, 50, 100 and 200 µl of 1:10 diluted G2 stock. Uninfected cells served as control. Cells were observed under the microscope daily. As soon as 100 % CPE was visible in one of the infected wells, the titer was calculated according to the used infection volume.

2.2.5.5 Viral particle formation

5x104 MB49 cells were seeded on a 6 well plate and 24 hours later, the cells were treated with inhibitor or left untreated as described in 2.2.3.1. After another 24 hours, the cells were infected with 200 MOI of indicated viruses. At 72 hours after infection, cells and supernatant were harvested, and viruses were released from cells by three thaw-freeze circles. Finally, samples were centrifuged for 5 minutes at 1000 g and formation of viral particles was quantified by performing and hexon titer test as described in 2.2.5.5.

2.2.5.6 Hexon titer test

Low passage HEK293 cells were seeded on a 24 well plate at a concentration of $2x10^5$ cells per well in 500 µl. Purified virus was added to HEK293 in dilutions ranging from 10^{-1} to 10^{-6} in volumes of 10 µl and 50 µl. After 40 to 48 hours, HEK293 cells were fixed and stained according to the AdEasy Viral Titer Kit instruction manual (Agilent Technologies,972500).

2.2.5.7 IFNγ-coculture assay

PBMCs were isolated from whole blood by Ficoll density gradient separation. PBMCs were counted and cultured on 15 cm dishes for 2 days under IL2 stimulation (100 U/ml). On the third day, PBMCs were centrifuged, resuspended in fresh medium and cultured for another 3 days. On the same day, 50 000 UMUC3 cells per well were plated on a 12 well plate. After 24 hours, UMUC3 cells were infected with various doses of different viruses, treated with 100 ng/ml LPS or left untreated. On day six, UMUC3 cells were treated with 10 µg/ml aPD-L1 antibody or left untreated and 1 million PBMCs were added to each well. UMUC3 cells and PBMCs were cocultured for 48 hours. Then, the cell free supernatant was analyzed for the IFNγ content using an IFNγ ELISA. The ELISA was performed according to the BioLegend IFNγ Kit instruction manual.

2.2.6 Protein biochemical methods

2.2.6.1 Preparation of cellular protein lysates

The entire procedure was strictly carried out on ice. Cells were washed 3 times with ice cold PBS and lysed using cold protein lysis buffer containing phosphatase and protease inhibitors. 500 µl and 100 µl lysis buffer were used for 10 cm and 6 well plates, respectively. Cells were harvested using cell scrapers and the lysate was transferred to a microcentrifuge tube. When using RIPA protein lysis buffer or IP protein lysis buffer, samples were incubated in a rotator at 4° C for 10 minutes. When using SDS protein lysis buffer, samples were sheared to disrupt DNA protein complexes using a 27-gauge needle until no viscosity was observed. Lysates were centrifuged at 30 000 g for 30 minutes at 4° C in a pre-cooled centrifuge. Supernatant was transferred into a fresh tube and used either immediately or stored at -80° C.

2.2.6.2 Immunoprecipitation

The entire procedure was strictly carried out on ice. For immunoprecipitation against hPD-L1, 40 µl resin per sample were used. Resin was washed three times with IP lysis buffer. After the third washing step, beads were resuspended in 1 ml IP lysis buffer and incubated with 2,5 µg of aPD-L1-antibody per sample in a rotator at 4° C for 4 hours or overnight. Unbound antibody was removed by washing 3 times with IP lysis buffer and beads were resuspended in 200 µl IP lysis buffer per sample. Cellular protein lysates were prepared using IP lysis buffer as described in 2.2.6.1. and 500 µg lysed protein in a total volume of 800 µl were used for immunoprecipitation overnight at 4° C. Unbound protein was removed by washing 3 times with PBS. Bound protein was eluted by adding 50 µl of IP elution buffer and heating up the samples to 100°C for 5 min. Finally, beads were pelleted and lysate was used immediately for sodium dodecyl sulfate polyacrylamide gel electrophoresis (SDS-PAGE).

2.2.6.3 Quantification of protein concentration and sample preparation

Protein concentration was quantified using the BCA assay according to manufacturer's protocol in a 96 well format. For the measurement, all samples were prepared in duplicates and incubated within the working reagent for 30 minutes at 37° C. 30 µl of the protein lysate mixed with 10 µl of 4x loading buffer and DTT were used for each SDS-PAGE. Samples were denatured at 100° C for 5 minutes and were either used immediately or stored at -20° C.

2.2.6.4 Immunoblotting

2.2.6.4.1 Sodium dodecyl sulfate polyacrylamide gel electrophoresis (SDS-PAGE)

For protein separation, polyacrylamide gels were hand cast using gel casting chambers. 8, 10 or 12 % separating gels and stacking gels were prepared as described in Table 8 and 9. The separating gel was covered with 2 ml isopropanol during polymerization to ensure a shark demarcation. Once the separating gel was polymerized, the isopropanol was removed, the stacking gel was poured and a comb was inserted. After complete polymerization, gels were fixed into the electrophoresis assembly and loaded with 40 µl of protein sample per well. Electrophoresis was carried out at 90 V until proteins entered the separating gel. Electrophoresis was continued until loading front was running out at 150 V.

Table 8: Composition of separation gel.

Ingredient	8%	10%	12%
H_2O [ml]	4.78	4.12	3.45
1.5M Tris pH 8.8[ml]	2.5	2.5	2.5
30% acrylamide/Bis-acrylamide solution [ml]	2.67	3.33	4
10% APS [µl]	50	50	50
TEMED [µl]	10	10	10
Total	10ml	10ml	10ml

Table 9: Composition of stacking gel.

Ingredient	Volume
H_2O [ml]	3.07
0.5M Tris pH 8.8 [ml]	1.25
30% acrylamide/Bis-acrylamide solution [ml]	0.65
10% APS [µl]	25
TEMED [µl]	5
Total	5

2.2.6.4.2 Transfer and blocking

Following electrophoresis, proteins were transferred onto a PVDF membrane that was activated in a methanol bath for 5 minutes. Sponges and blotting paper were incubated in blotting buffer. The gel and the membrane were assembled in between two layers of blotting paper and sponges. Proteins were transferred for 1 to 2 hours at 100 V using cold blotting buffer. Following the transfer, membranes were blocked for nonspecific binding in blocking buffer for 1 hour at room temperature.

2.2.6.4.3 Immunodetection

Primary antibodies were diluted as required in antibody dilution buffer. Membranes were incubated in primary antibody solution overnight at 4° C or for 1 hour at room temperature. After washing 3 to 5 times with TBS-T, membranes were incubated with secondary antibody diluted in blocking solution for

30 minutes at room temperature. After 3 to 5 further washing steps with TBS-T, proteins were detected using the ECL reaction and chemiluminescent signal was visualized using autoradiography films.

2.2.7 Immunofluorescence staining

Coverslips were placed in 24 well plates, covered with ethanol for 5 minutes and washed with sterile PBS. The cells were seeded at the desired density (ranging from 5000 to 10000 cells/well) onto the coverslips. After 24 hours, cells were infected with desired MOIs of various viruses or left uninfected. After 24 to 48 hours of treatment, cells were fixed. Therefore, the medium was aspired and cells were gently washed with PBS. Cells were fixed with ice cold methanol:aceton (1:1) fixative solution for 20 minutes at -20° C. The fixative solution was aspired and cells were air dried for 45 minutes. To block unspecific binding sites, cells were incubated with 500 µl blocking solution per well for 30 minutes at room temperature. After three washing steps with PBS, staining with the primary antibody was performed in 150 µl blocking solution for 1 hour at room temperature. Unbound antibody was removed by washing three times with PBS. Staining with the secondary antibody was also done in 150 µl blocking solution for maximum 1 hour at room temperature in the dark. After 3 washing steps with PBS, DNA was stained with DAPI and cells were again washed with PBS for 3 times. Finally, cover slips were fixed on glass slides using water based mounting media. Immunofluorescence staining was immediately analyzed under the microscope or stored at 4°C.

2.2.8 *In vivo* experiments

7-week old athymic Foxn1$^{nu/nu}$ mice and C57BL6 were purchased from Charles River and kept at the animal facility of the Technical University of Munich. Mice were kept in IVCs in groups of maximum 5 animals per cage for one week to adjust to the environment before the experiment was started. All animal experiments were performed in accordance with the German law. The protocol was approved by the District Government of upper Bavaria.

2.2.8.1 Orthotopic, intramural injection of tumor cells into the bladder

Injections were performed according to the published protocol from (Jäger et al. 2014). In brief, 80 % confluent cells were passaged 1:3 to 1:2 one day before *in vivo* injections. For injections, cells were harvested and counted as described in 2.2.2.2. Desired amounts of cells were transferred into a new

tube, centrifuged and resuspended in a PBS-Matrigel mixture (1:1 ratio) in order to reach the desired cell concentration. The following cell numbers were used:

Mouse model	Cell number
UMUC3, FoxN1$^{nu/nu}$	200000 cells in 50µl Matrigel:PBS
MB49, C57BL6	70000 cells in 50µl Matrigel:PBS
MB49, C57BL6	100000 cells in 50µl Matrigel:PBS

The injection volume of tumor cell suspension was 50 µl per mouse. Cells, syringes and needles were kept on ice to avoid Matrigel polymerization.

Mice were anesthetized with medetomidine-midazolam-fentanyl mixture (MMF, medetomidine: 0.5 mg/kg, midazolam: 5 mg/kg, fentanyl: 0.05 mg/kg), proper anesthetization was confirmed by toe pinching. Mice were mounted on the imaging table, a bladder stabilization strap and ultrasound gel were applied and the bladder was visualized using the ultrasound. For the separation of the bladder wall layers, a 1.0 ml syringe filled with PBS and connected to a 30 gauge, ¾“ needle was used. When the needle was in the correct position between muscle layer and mucosa, sterile PBS was injected to create an artificial space. The needle was withdrawn and the syringe filled with the tumor cell suspension attached to a new 30 gauge, ¾“ needle was put into the syringe clamp and injected into the mouse in order to inject tumor cells into the artificially generated space. After successful injection, mouse was dismounted from the imaging table, and kept in a warm environment under continuous observation. When fully recovered from the anesthetic, mice were placed back in the home cage.

2.2.8.2 Monitoring of tumor growth by ultrasound

Monitoring of tumor growth was performed at least two times per week. Therefore, mice were anesthetized with a 2.5 % isoflurane-oxygen mixture and proper anesthetization was confirmed by toe pinching. The mouse was mounted on the imaging table, a bladder stabilization strap and ultrasound gel were applied and the bladder was visualized using the ultrasound. A 3D ultrasound was performed with scanning the whole bladder in 0.076 mm steps. The tumor volume was determined using the Visual Sonics imaging software by analyzing every fifth picture according to the manufacturer’s manual. After successful imaging, mouse was dismounted from the imaging table, and kept in a warm environment under continuous observation. When fully recovered from the anesthetic, mice were placed back in the home cage.

For tumor volume was measured using the Visual Sonics imaging software by analyzing every fifth picture according to the user manual (Jäger et al. 2014).

2.2.8.3 Intratumoral virus injection

When tumors reached an average size of 20 mm^3, mice were treated with virus or PBS every fourth day for a total of 3 times. For treatment of the tumor with virus or PBS, mice were anesthetized with a 2.5 % isoflurane-oxygen mixture and proper anesthetization was confirmed by toe pinching. The mouse was mounted on the imaging table, a bladder stabilization strap and ultrasound gel were applied and the bladder was visualized using the ultrasound. A 1.0 ml syringe filled with virus or PBS and connected to a 30 gauge, ¾ "needle. The needle was injected in the middle of the tumor and PBS or virus was injected very slowly under continuous retracting of the needle. $3x10^9$ viral particles of XVir-N-31 in a volume of 10 to 15µl or an equal volume of PBS were used for treatment.

After successful injection, mouse was dismounted from the imaging table and kept in a warm environment under continuous observation. When fully recovered from the anesthetic, mice were placed back in the home cage.

2.2.9 Tissue processing and haematoxylin & eosin staining

Tissue was fixed in paraformaldehyde for 24 to 72 hours at 4°C, followed by dehydration in the tissue processor and embedding in paraffin. 3.5 µm thick sections were cut using a microtome and placed onto slides. For haematoxylin & eosin (H&E) staining, the protocol as described in Table 10 was used.

Table 10: Protocol for H&E staining.

Time	Solution	Step
10-15 min	Xylol	Deparaffinization
5 min	Isopropanol	
5 min	96% Ethanol	
5 min	70% Ethanol	
5 min	Bidest H_2O (ELGA)	
10 min	Hämalaun	Staining
10 min	Tap water	
2 min	ELGA water	
20 sec	96% Ethanol +HCl (2-3 drops)	
10 min	Eosin (+2 drops acetic acid/100 ml Eosin)	
30 sec	96% Ethanol	Rehydration
25 sec	100% Ethanol	
25 sec	Isopropanol	
1 min	Xylol	

2.2.10 Statistical comparison.

Graphs were plotted using arithmetic mean ± standard deviation (S.D.) or standard error (S.E.). A 2-tailed Student's t-test was used for statistical analysis and $p \leq 0.05$ was considered to be statistical significant.

3 Results

Based on the oncolytic capacity of virotherapy and the therapeutic relevance of ICB, we aimed to establish a new therapeutic approach for bladder cancer by combining the YB-1 dependent oncolytic virotherapy with a PD-L1 specific ICB. Hence, we began by cloning and generating a novel virus encoding for an anti PD-L1 antibody.

3.1 Construction of the recombinant adenovirus XVir-N-31-aPD-L1

3.1.1 Development of a cloning strategy and cloning of the viral plasmid

We started by cloning the plasmid encoding for the novel virus XVir-N-31-aPD-L1 which contains an anti-PD-L1 encoding transgene in its E3 region. Therefore, we first developed the transgene and created a cloning strategy.

The transgene we integrated consists of two parts, the epitope binding Fab fragment and the Fc part of the antibody (figure 3.1). The Fc part from the human IgG1 was provided by PD Laschinger within a plasmid. The Fab fragment was newly designed. Its main part consists of the variable light chain and the variable heavy chain connected by a glycine-serine linker ($(Gly_4Ser)_3$ linker). The sequence for this fragment was used from the patent US 20100203056 A1 (Irving et al. 2009). 5' to the epitope binding part, there is the Kozak sequence GCC ACC which is important for translation efficacy (Kozak 1984). The sequence is followed by the start codon ATG and the Igκ leader sequence (ATG GAG ACA GAC ACA CTC CTG CTA TGG GTA CTG CTG CTC TGG GTT CCA GGT TCC ACT GGT GAC) that is needed for active protein secretion. In addition, there is a sequence encoding for the HA tag 5' of the variable light chain. The HA tag was used for detecting the antibody.

After designing the sequence for the Fab fragment, it was synthesized (life technologies ®) and provided within a plasmid.

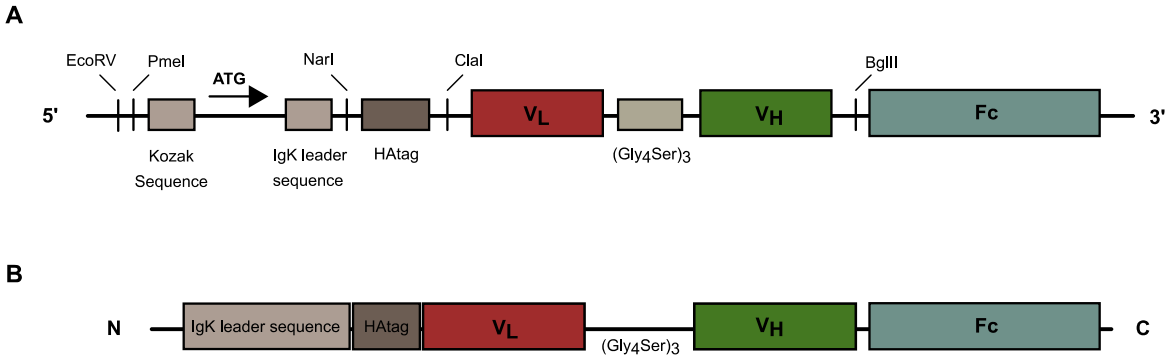

Figure 3.1: Structure of the anti PD-L1 transgene. A The anti-PD-L1 transgene is composed of a domain encoding the antigen binding Fab fragment which consists of the variable light chain, the $(Gly_4Ser)_3$ linker and the variable heavy chain, and a domain encoding for the Fc fragment of the antibody. At the 5' end, the transgene has a Kozak sequence, the start codon, an IgK leader sequence and an HA tag. **B** A schematic depiction of the encoded protein sequence. The protein can be detected via its N-terminal HA tag.

Then, we started to clone the plasmid encoding for the novel virus XVir-N-31-aPD-L1. Therefore, we first ligated the 3' end of the Fab fragment to the 5' end of the Fc part (Figure 3.2). The complete transgene was then cloned into a small, 1400bp containing section of the Wt E3 region. The Wt E3 part containing the transgene was then subsequently integrated into the complete Wt E3 region. Finally, the 11000 bp large WtAd E3 region including the anti-PD-L1 encoding transgene was ligated into the E3 region of the plasmid encoding for XVir-N-31.

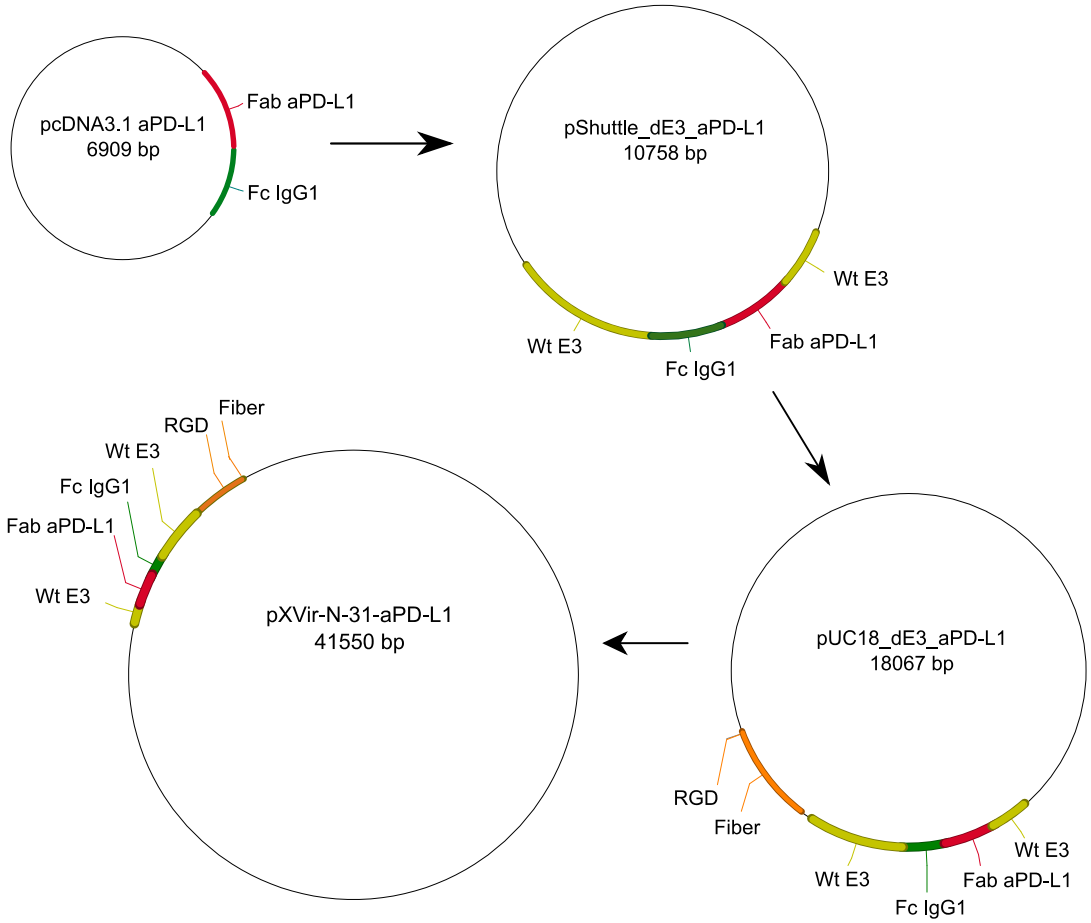

Figure 3.2: Cloning strategy for pXVir-N-31-aPD-L1. The Fab aPD-L1 encoding transgene was ligated to the Fc part of the human IgG1 within the plasmid pcDNA3.1. Via several cloning steps the transgene was finally integrated into the WtE3 region of pXVir-N-31.

Two different plasmids were cloned, pXVir-N-31-FL-aPD-L1 encoding for a full length (FL) anti PD-L1 antibody and pXVir-N-31-scFv-aPD-L1 encoding for a single chain variable fragment (scFv) anti PD-L1 antibody (Figure 3.3). This virus arose due to a shift in the reading frame of the transgene which led to a stop codon in the hinge region of the Fc part. In addition, a plasmid encoding for a control virus that expresses only the Fc part of the human IgG1 was constructed.

For simplification, the term XVir-N-31-aPD-L1 is from now on used when referring to XVir-N-31-FLaPD-L1 and XVir-N-31-scFvaPD-L1.

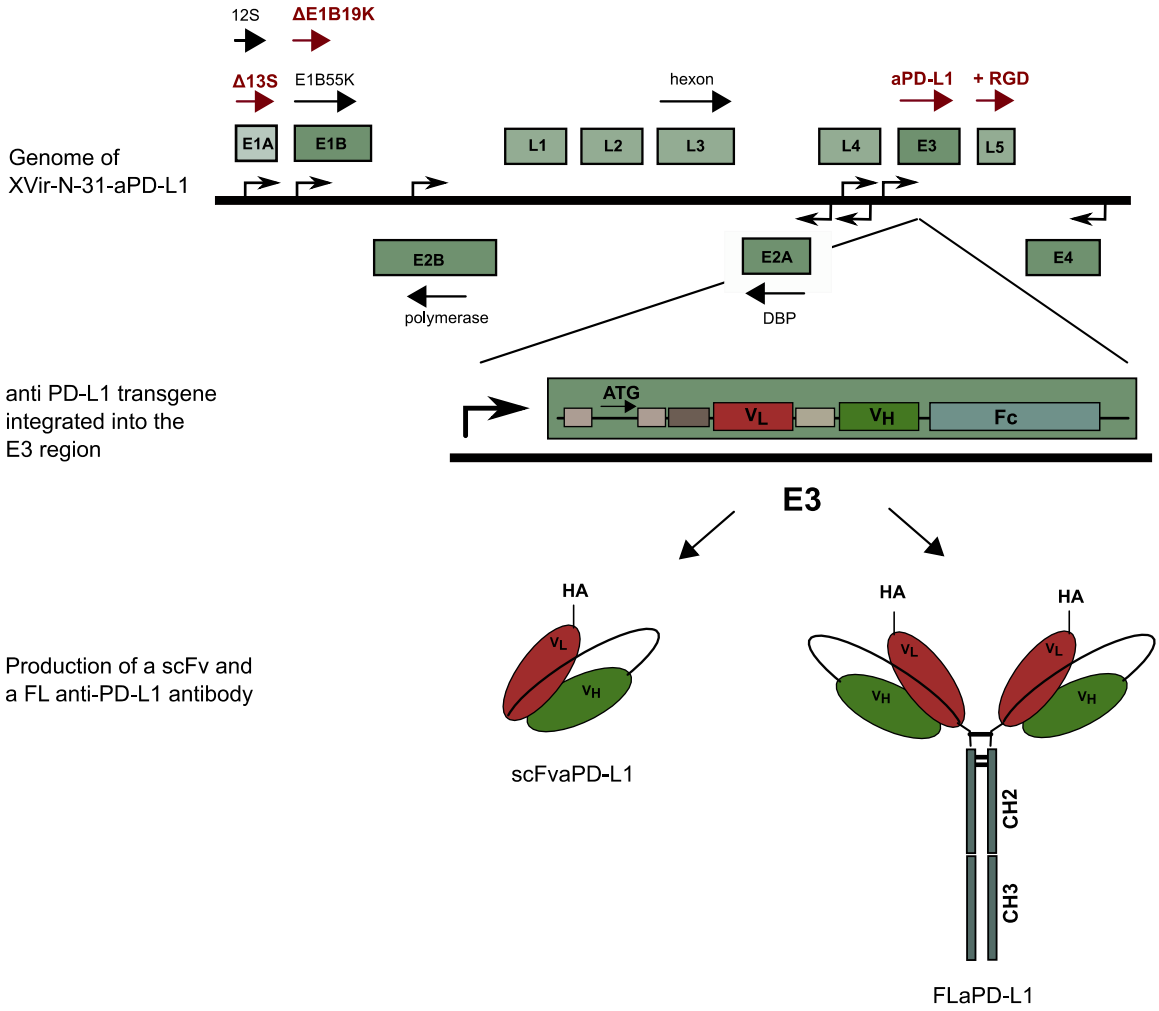

Figure 3.3: Genome of XVir-N-31-aPD-L1 and resulting antibodies. The genomic structure of XVir-N-31 and the anti-PD-L1 transgene. Two viruses differing only in 5 base pairs in the hinge region of the transgene were integrated into the E3 region. They encode for a scFvaPD-L1 and a FLaPD-L1 antibody.

3.1.2 Production of XVir-N-31-aPD-L1 in HEK293

After cloning of the viral plasmids, the viruses XVir-N-31-FLaPD-L1, XVir-N-31-Fc and XVir-N-31-scFvaPD-L1 were generated in HEK293 cells (figure 3.4 A). Therefore, the plasmids were linearized by PacI digestion and HEK293 cells were transfected with linearized plasmids. Plaques were detectable 10 to 14 days after transfection and cells showed a typical CPE. To produce the viral crude stocks, cells and supernatant were harvested and processed as described in 2.2.4.2. For large scale production of the virus, HEK293 cells were infected with 10 to 20 MOI of the G2 crude stock. At 48 to 50 hours post infection, the cells showed a CPE and were harvested by centrifugation (figure 3.4 B).

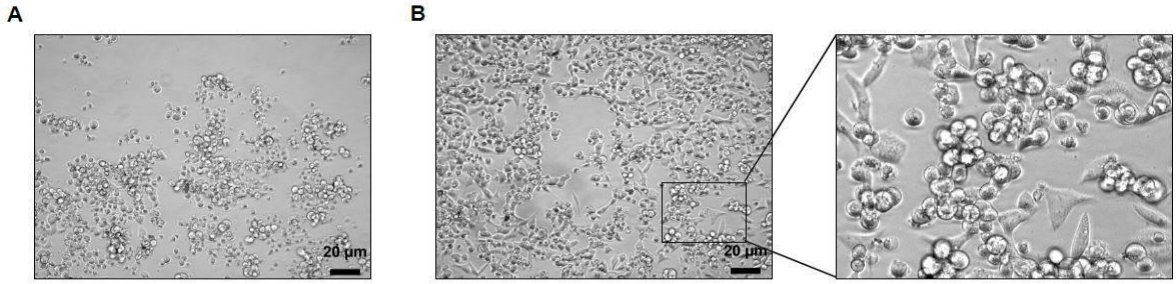

Figure 3.4: Virus production in HEK293 cells. A Representative picture of plaques after transfection of HEK293 cells with viral plasmids. **B** Production of the virus in HEK293 cells. 48 to 50 hours after infection, cells showed a CPE and were harvested for isolation and purification of the virus.

Subsequently, the viruses were isolated from the cells by repeated freeze thaw cycles and purified using CsCl density gradient centrifugation. Afterwards, the viral titers were measured. The hexon titer test revealed titers of 7.0 x 10^9 pfu/ml for XVir-N-31-scFvaPD-L1, 6.12 x 10^9 pfu/ml for XVir-N-31-FLaPD-L1 and 1.4 x 10^{11} pfu/ml for XVir-N-31-Fc. Analysis of viral particles per ml and the ratio of viral particles to infectious particles (P:I ratio) are summarized in table 11.

Table 11: Titers, viral particles per ml and P:I ratios of the generated viruses.

Virus	Titer [pfu/ml]	Vp/ml	P:I ratio
XVir-N-31-scFvaPD-L1	7.0 x 10^9	4.9x10^{11}	70
XVir-N-31-FLaPD-L1	6.12 x 10^9	5.67x10^{11}	93
XVir-N-31-Fc	1.4 x 10^{11}	1.0x10^{13}	72

Once we had produced the viruses and verified their titers we proofed their identity. Therefore, a specific PCR was developed that targets regions of XVir-N-31 differing from the WtAd genome (Figure 3.5). The PCR proved the correct identity of the newly generated viruses. In detail, it could be shown that all tested viruses have the E1A region (540 bp band), but only the WtAd has the E1A13S region (548 pb band). The deleted E1B19K region (WtAd: 587 bp band, XVir-N-31: 387 bp) was detectable only in the XVir-N-31 based viruses. The presence of E3 ADP (384bp band) was confirmed in XVir-N-31-aPD-L1 and XVir-N-31-Fc which are not deleted in E3. The RGD motif (176 bp) was proven in all XVir-N-31 based viruses. The presence of the anti-PD-L1 transgene (613 bp) and the Fc transgene (337 bp) was also shown. This PCR reaction can identify both XVir-N-31-FLaPD-L1 and XVir-N-31scFvaPD-L1, however, due to the difference of only 5 bp, it cannot distinguish the two viruses.

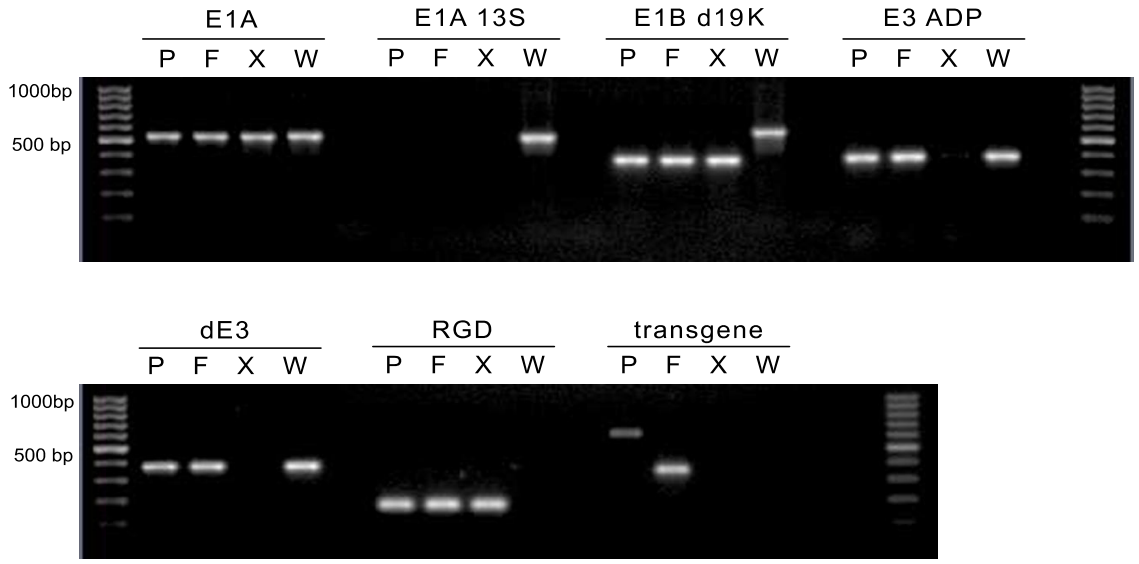

Figure 3.5: PCR to test the identity of the generated viruses. Gel electrophoresis of PCR amplified products. CsCl purified viruses were heat denatured by 10 minutes incubation at 100° C and 5 µl were used as template DNA. The newly generated viruses were tested for E1A, the deletion in E1A13S and E1B19K, for E3 ADP and the deletion in E3 as well as the RGD motif and the presence of the transgene. P: XVir-N-31scFvaPD-L1, F: XVir-N-31-Fc, X: XVir-N-31, W: WtAd This is a representative result, data for XVir-N-31-FLaPD-L1 are not shown.

3.2 in vitro characterization of XVir-N-31-aPD-L1

After successful cloning and production of XVir-N-31-scFvaPD-L1 and XVir-N-31-FLaPD-L1, we characterized the viruses in various *in vitro* assays. We started by evaluating the YB-1 status of the three bladder cancer cell lines UMUC3, T24 and J82 in order to choose the best cell line for the analysis of XVir-N-31 based viruses. Immunofluorescence staining revealed that all three cell lines show a cytoplasmatic, perinuclear localization of YB-1 (figure 3.6). To investigate the subcellular localization of YB-1 upon infection with XVir-N-31, we stained the cells for adenoviral E1A and YB-1 and could observe a distinct translocation of YB-1 into the nucleus in E1A positive cells. Based on the dominant translocation of YB-1 into the nucleus and the high susceptibility for adenoviral infection, we choose the cell line UMUC3 for the *in vitro* analysis of both XVir-N-31-scFvaPD-L1 and XVir-N-31-FLaPD-L1.

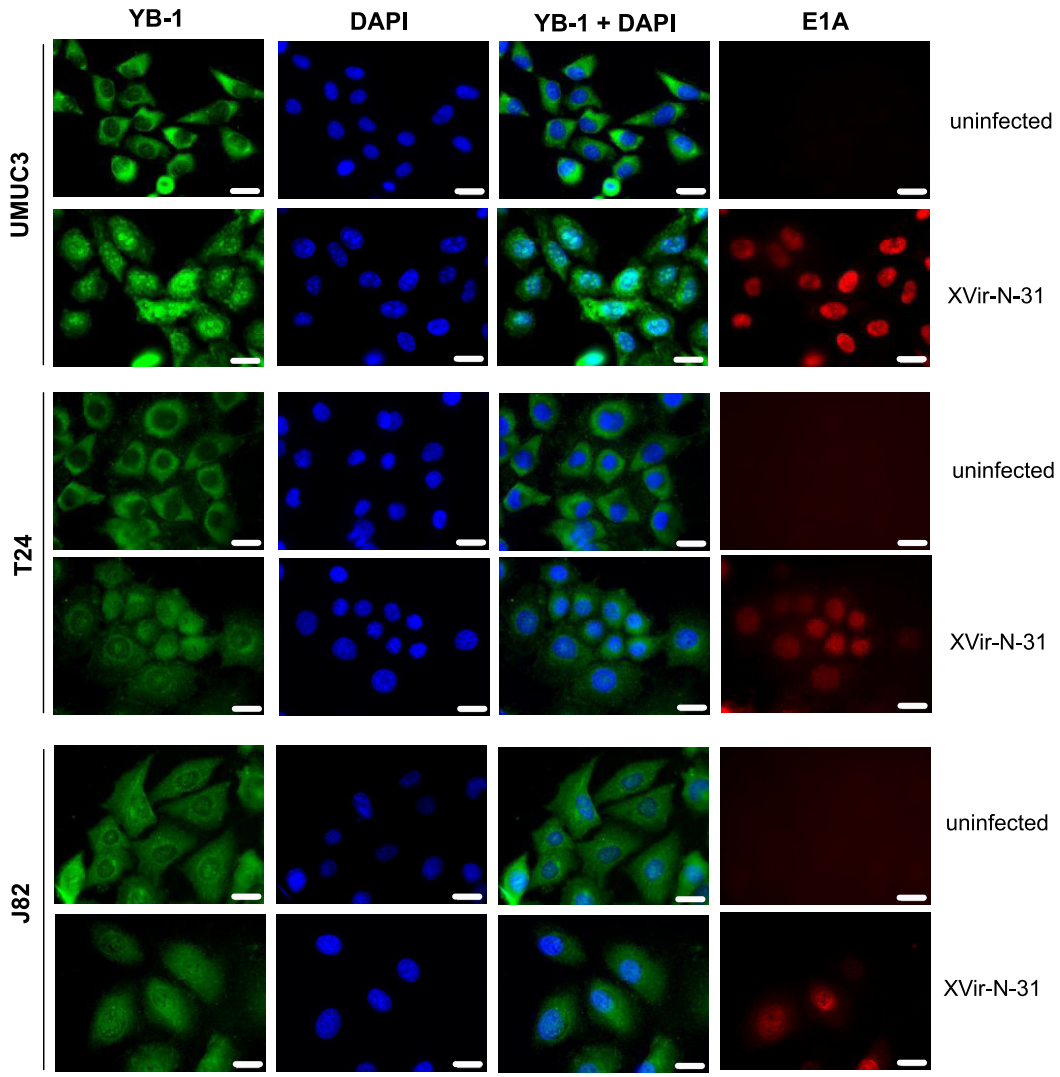

Figure 3.6: Subcellular localization of YB-1 in bladder cancer cell lines. UMUC3, T24 and J82 cells were seeded and infected with 30, 100 and 40 MOI of XVir-N-31. At 40 hours after infection, cells were fixed and stained for YB-1 and adenoviral E1A. Scale bar corresponds to 10 µm.

3.2.1 Analysis of replication of XVir-N-31-aPD-L1

Viral replication in UMUC3 cells was analyzed by quantifying fiber DNA at 4, 24 and 48 hours after infection (figure 3.7). The qPCR results showed that both XVir-N-31-FLaPD-L1 and XVir-N-31-scFvaPD-L1 replicate in the human bladder cancer cell line and that their replicative capacity is comparable. At 24 hours after infection, WtAd showed the highest replication values which increased about 10-fold after 48 hours. Replication of all XVir-N-31 based viruses was roughly 100-fold lower than WtAd at 24 hours after infection and roughly 10-fold lower at 48 hours after infection.

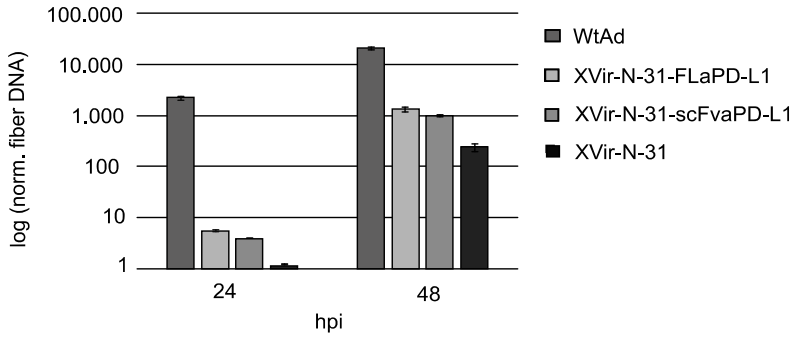

Figure 3.7: XVir-N-31-aPD-L1 replicates in the human bladder cancer cell line UMUC3. UMUC3 cells were infected with 10 MOI of indicated viruses. At 4, 24 and 48 hours after infection, cells were lysed and DNA was purified. Fiber DNA was quantified by qPCR and normalized to the 4 hours value. GAPDH and actin served as reference genes.

3.2.2 Investigation of the oncolytic activity of XVir-N-31-aPD-L1

Next, we investigated the cell killing capacity of XVir-N-31-aPD-L1 in UMUC3 cells (figure 3.8 A and B). A potency assay showed that both XVir-N-31-FLaPD-L1 and XVir-N-31-scFvaPD-L1 are oncolytic. Infection of cells with XVir-N-31-FLaPD-L1 and XVir-N-31-scFvaPD-L1 using MOIs between 8 and 18 induced oncolysis in 50 % of the cells and a complete cell lysis was seen upon infection with 40 MOI. The IC50 value of XVir-N-31 was 30 MOI and virus concentrations of 60 MOI induced oncolysis in all cells showing a strong oncolytic effect of XVir-N-31-FLaPD-L1 and XVir-N-31-scFvaPD-L1 in the bladder cancer cell line UMUC3. Additionally, these results showed a slightly higher potency of both XVir-N-31-FLaPD-L1 and XVir-N-31-scFvaPD-L1 compared to XVir-N-31 which might have been caused by minor variations in viral titers.

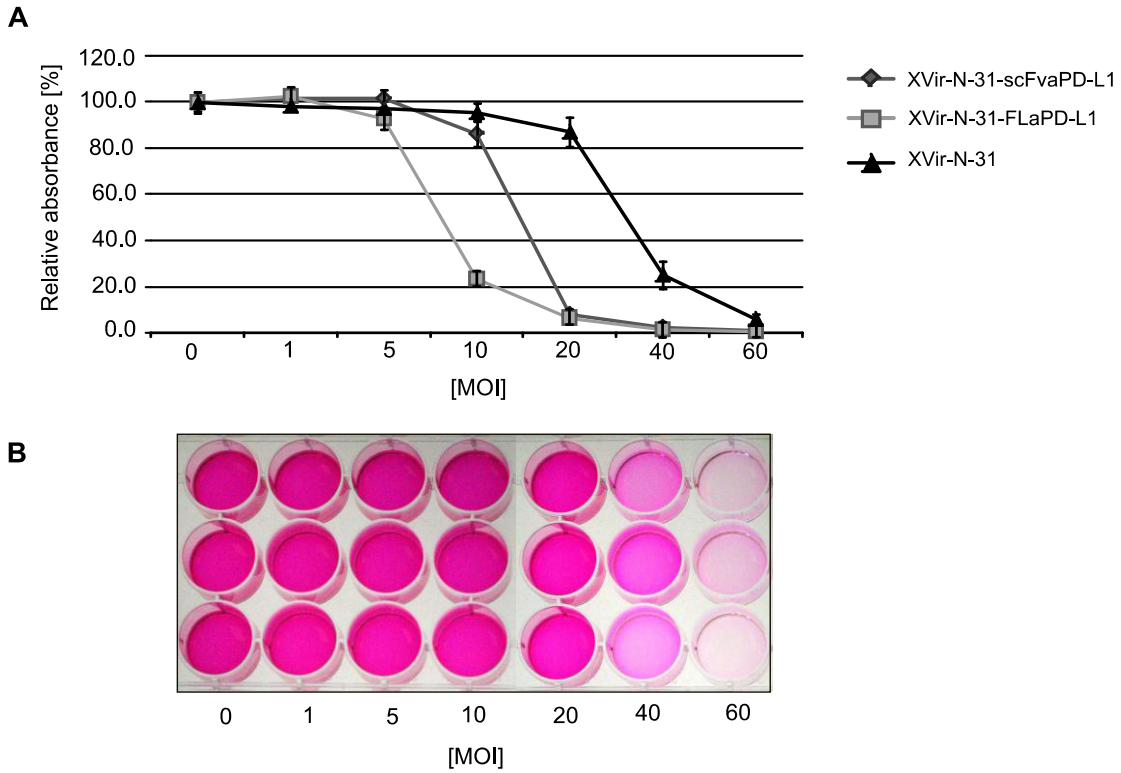

Figure 3.8: XVir-N-31-FLaPD-L1 and XVir-N-31-scFvaPD-L1 have oncolytic activity in UMUC3 cells. A To analyze the viral cell killing capacity, UMUC3 cells were infected with various MOIs of indicated viruses. At 96 hours after infection, cells were fixed and cell killing was measured by SRB staining. **B** A representative picture showing SRB stained cells at 96 hours after infection with XVir-N-31-scFvaPD-L1.

3.2.3 Verification of synthesis, secretion and functionality of the scFvaPD-L1 antibody

Furthermore, we investigated the synthesis and secretion of the scFv-aPD-L1 antibody in UMUC3 cells (figure 3.9). The denatured scFvaPD-L1 antibody had a size of 32 kDa. It was detectable in the cellular lysate as early as 24 hours after infection and antibody synthesis reached its maximum after another 24 hours. Secretion was first detectable at 48 hours after infection and increased strongly at 72 hours after infection.

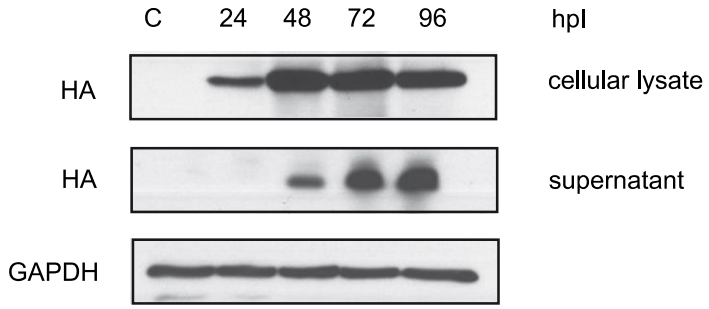

Figure 3.9: Synthesis and secretion of the scFvaPD-L1 antibody in UMUC3 cells. UMUC3 cells were infected with 20 MOI of XVir-N-31-scFvaPD-L1. After indicated time points cells were harvested and the supernatant was used for protein precipitation. Expression of the HA tagged antibody was analyzed by immunoblotting.

The specific binding of the scFvaPD-L1 antibody to PD-L1 was analyzed by immunoprecipitation. Therefore, we first showed that both infected and uninfected UMUC3 cells express PD-L1 in a similar manner (figure 3.10 B). Additionally, immunoblotting against the HA tagged antibody confirmed a suitable antibody production in infected UMUC3 cells (figure 3.10 C). The precipitation of scFvaPD-L1 against cellular PD-L1 and the subsequent immunoblotting clearly showed the specific recognition and binding of scFvaPD-L1 to its antigen PD-L1 (figure 3.10 A).

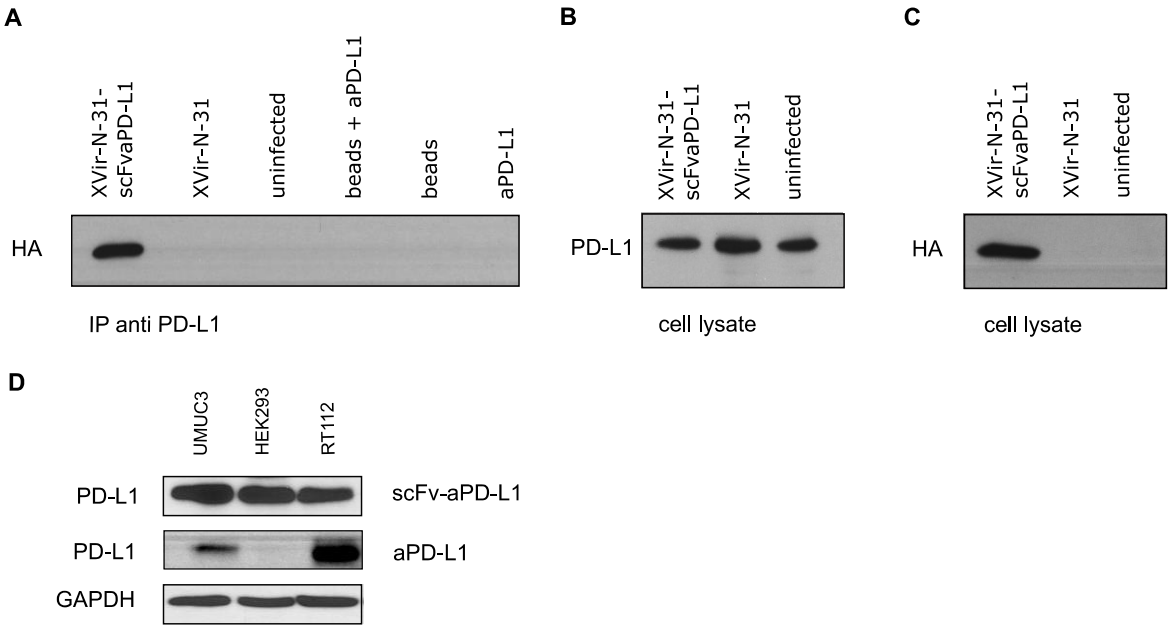

Figure 3.10: The scFvaPD-L1 antibody specifically binds to cellular PD-L1. A For immunoprecipitation, UMUC3 cells were infected with indicated viruses or left uninfected. Lysates were precipitated against PD-L1 and subsequently analyzed for the HA tagged antibody by immunoblotting. Beads+aPD-L1, beads alone and aPD-L1 alone were analyzed as controls. **B** Cellular lysates of infected and uninfected cells were analyzed for PD-L1 expression and antibody production (**C**) by immunoblotting. **D** The scFvaPD-L1 antibody and a commercial aPD-L1 antibody were used to detect PD-L1 in UMUC3, HEK293 and RT112 cells.

Further on, we could show that the scFvaPD-L1 antibody is also useable as a detection antibody in immunoblotting (figure 3.10 D). Both the commercial antibody and the scFvaPD-L1 antibody showed a specific band at 46 kDa. The scFvaPD-L1 antibody revealed a strong expression of PD-L1 in the tested cell lines whereas the commercial antibody detected no PD-L1 expression in HEK293 cells and a low expression level in UMUC3 cells. Albeit the signal intensity between the two antibodies was different in the three tested cell lines, we concluded that scFv-aPD-L1 can detect denatured PD-L1.

3.2.4 An attempt to develop an *in vitro* assay to verify the functional blocking of PD-L1

In addition to the specific binding to and the detection of PD-L1, we wanted to investigate if the scFvaPD-L1 antibody is able to functionally block PD-L1. Therefore, we developed an *in vitro* coculture assay as described in 2.2.5.7. The principle of this assay is based on the immune stimulatory effect of adenoviruses. It is known that adenoviral infections induce the production of various cytokines, chemokines and immune stimulatory proteins like IFNy (Schagen et al. 2004). Further on, it has been shown that IFNy induces PD-L1 expression (Blank et al. 2004). Hence, we hypothesized that infected UMUC3 cells induce IFNy expression in PBMCs and that this effect can be enhanced by blocking the PD-1/PD-L1 checkpoint. Thus, we tried to use the IFNy production for measuring the functionality of scFvaPD-L1.

We performed numerous assays and tried different settings. Nevertheless, we had problems to reproduce our results which was most likely due to various factors, e.g. concentration of the viruses, PBMC donors, incubation period for the PBMCs-UMUC3 coculture and effector cell to target cell ratio. Three representative results are depicted in figure 3.11. In general, we could see that both WtAd and XVir-N-31 induce IFNy production and that this effect could be increased by adding an anti-PD-L1 antibody. We also observed IFNy production upon infection with XVir-N-31-scFvaPD-L1 which could be further elevated by adding an additional anti-PD-L1 antibody. However, we were not able to standardize the protocol in order to obtain reliable and reproducible results. Thus, a final conclusion could not be made.

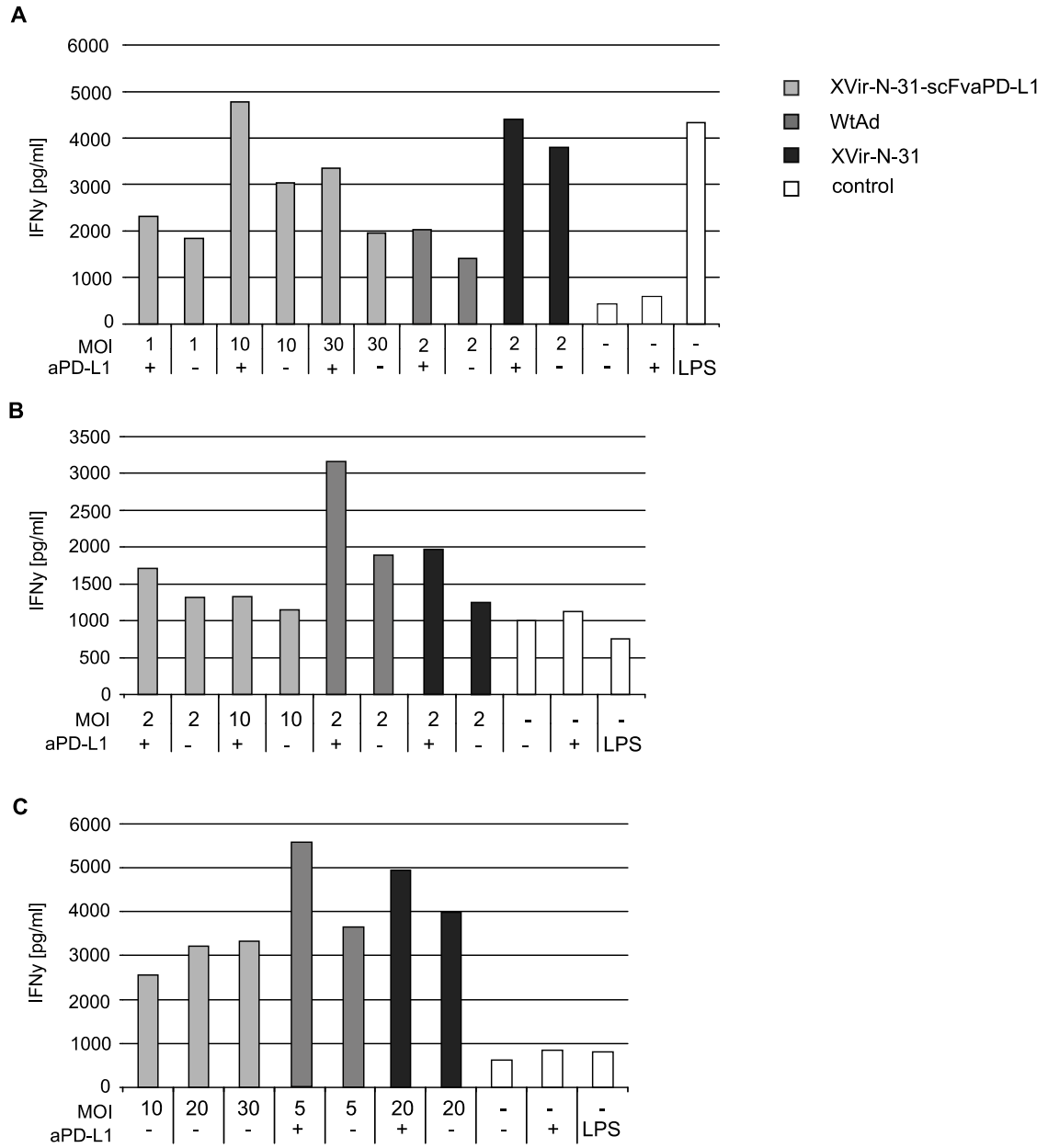

Figure 3.11: IFNy response to adenoviruses and PD-L1 blockade. A, **B** and **C** show three independent experiments. To measure IFNy response, UMUC3 cells were infected with various MOIs of indicated viruses or left uninfected. At 48 hours post infection, PBMCs were added to UMUC3 cells in an E:T ration of 1.25:1. After 48 hours of coculture, IFNy concentrations in the cell free supernatant were determined by ELISA.

3.3 Investigation of the murine cell line MB49 for adenoviral research

A major problem of adenoviral research is the difficulty of proper animal models for *in vivo* studies. So far, the humanized mouse model is the only possibility to analyze oncolytic adenoviruses in a human background (Shultz et al. 2012). However, this model is difficult to establish, extremely time intensive,

complicated and risky. To circumvent the humanized mouse model, we investigated if the murine bladder cancer cell line MB49 allows adenoviral replication and thus could be used in a syngeneic mouse model for adenoviral *in vivo* studies (Soloway 1975).

3.3.1 Analysis of viral replication in the murine bladder cancer cell line MB49

To verify if the murine cell line MB49 allows adenoviral replication, we first evaluated the YB-1 expression (figure 3.12 A). Immunoblotting showed that both infected and uninfected MB49 cells express YB-1 and that the expression levels were comparable to UMUC3 cells. Analysis of viral replication showed that the used viruses did not replicate within the first 24 hours after infection. At 48 hours post infection, only WtAd started to replicate.

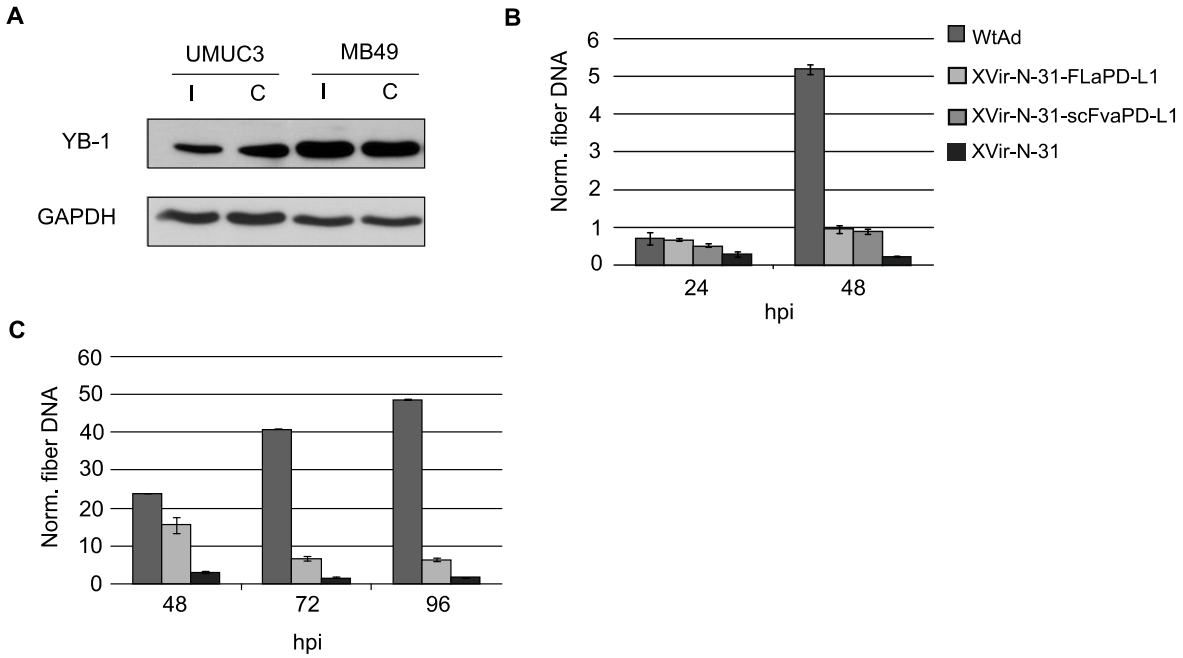

Figure 3.12: Replication capacity of WtAd and XVir-N-31 based viruses in MB49 cells. A Infected (I) and uninfected (C) MB49 cells were analyzed for YB-1 expression by immunoblotting and compared to UMUC3 cells. **B** MB49 cells were infected with 200 MOI of indicated viruses. At 4, 24, 48 hours and **C** at 4, 48, 72 and 96 hours after infection, cells were harvested, DNA was isolated and purified. Fiber DNA content was quantified by qPCR and normalized to the 4 hours value. Actin and GAPDH served as reference genes.

Additionally, replication analysis at 72 and 96 hours after infection showed a time dependent decrease of fiber DNA content for XVir-N-31 based viruses whereas fiber DNA clearly increased upon infection with WtAd (figure 3.12 C). This confirmed the replication deficiency of XVir-N-31 based viruses in MB49 cells compared to WtAd.

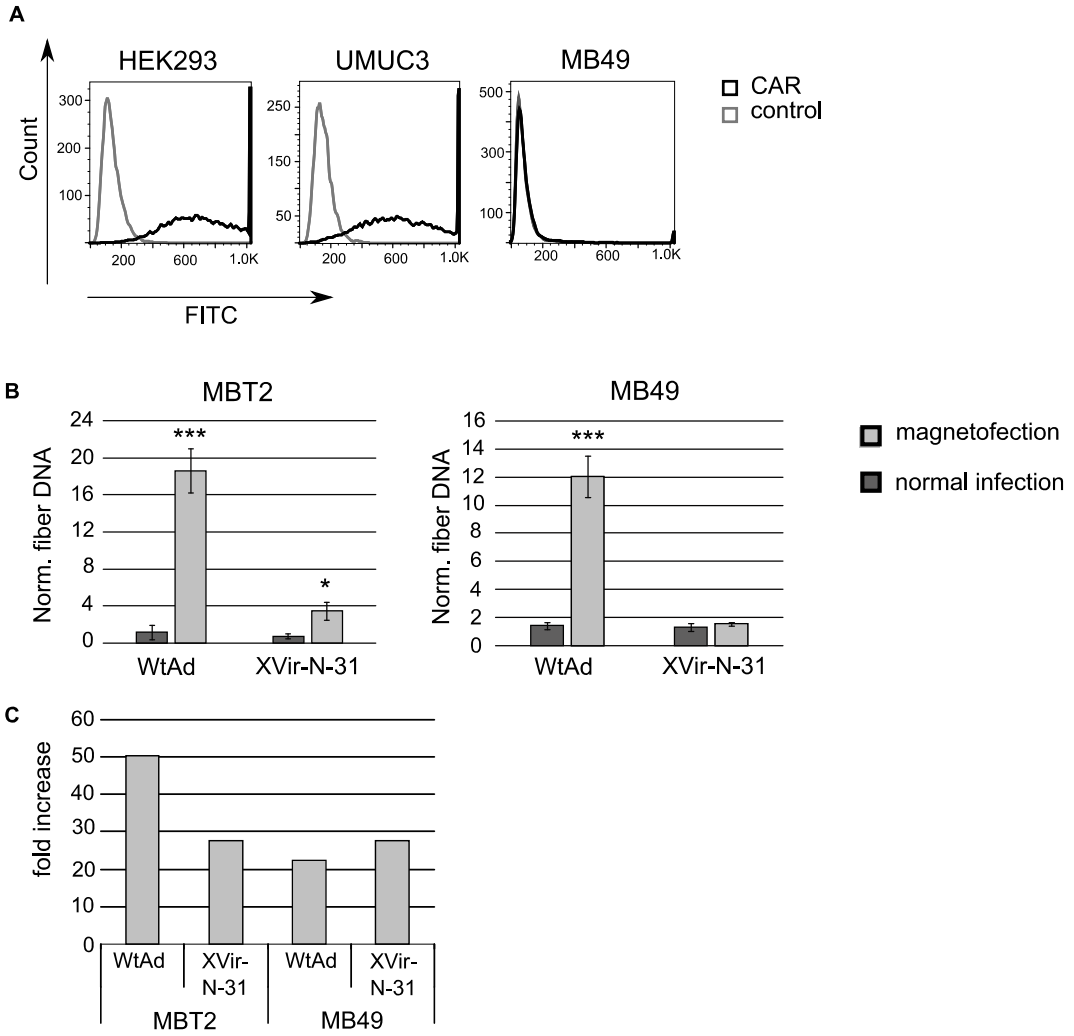

Figure 3.13: CAR expression of MB49 cells. A HEK293, UMUC3 and MB49 cells were analyzed for CAR expression. Staining with the FITC labeled secondary antibody served as control. **B** Replication analysis of indicated viruses in MBT2 and MB49 cells using normal infection and magnetofection. For magnetofection, the virus was coated with magnetic nanoparticles and cells were infected using a magnetic field. At 48 hours after infection, fiber DNA content was quantified and normalized to the 4 hours value. **C** Fold increase of infection rate using magnetofection referred to normal infection. Infection rate was measured by quantification of fiber DNA content at 4 hours after infection. GAPDH and actin were used as reference genes. *p≤ 0.05, ***p<0.001.

In order to investigate if the lack of replication of XVir-N-31 was due to low infection rates, we analyzed the CAR expression (figure 3.13 A). A FACS analysis showed that MB49 cells were negative for CAR compared to the CAR positive HEK293 and UMUC3 cells (Sabichi et al. 2006). This result indicated that the low replication capacity of WtAd was possibly due to reduced infection rates and that the replication deficit of XVir-N-31 based viruses is CAR independent. To verify if adenoviral replication is in principal possible, we infected MB49 and MBT2 cells using magnetofection and measured viral replication (figure 3.13 B). Here, we could show that replication of WtAd was increased up to 12-fold in both cell lines when using magnetofection compared to normal infection at 48 hours after infection. Replication of XVir-N-31 was slightly increased upon magnetofection in MBT2 cells, but not in MB49 cells. Further on, we were interested in the infection rates of both infection methods and therefore we quantified the fiber DNA content at 4 hours after infection. Magnetofection clearly improved infection of both viruses. In detail, infection with WtAd was increased 20-fold to 50-fold in MB49 and MBT2 cells, respectively and infection with XVir-N-31 was increased up to roughly 30-fold in both cell lines (figure 3.13 C).

3.3.2 Evaluation of oncolytic activity in MB49 cells

Although the replication analysis showed very limited replicative capacity of adenoviruses in MB49 cells, we were interested in the induction of cell death after infection with XVir-N-31 based viruses (figure 3.14 A and B). Therefore, we infected MB49 cells with XVir-N-31-based viruses and could show an MOI dependent induction of cell death with IC50 values ranging from 150 to 300 MOIs. We also observed a prominent change in cellular morphology (figure 3.14 C). The enormous swelling and agglutination of the cells was seen as soon as 24 hours after infection. We assumed that the cell killing effect was caused by a cytotoxic effect due to extremely high virus concentrations rather than induced by the oncolytic activity of XVir-N-31 in MB49.

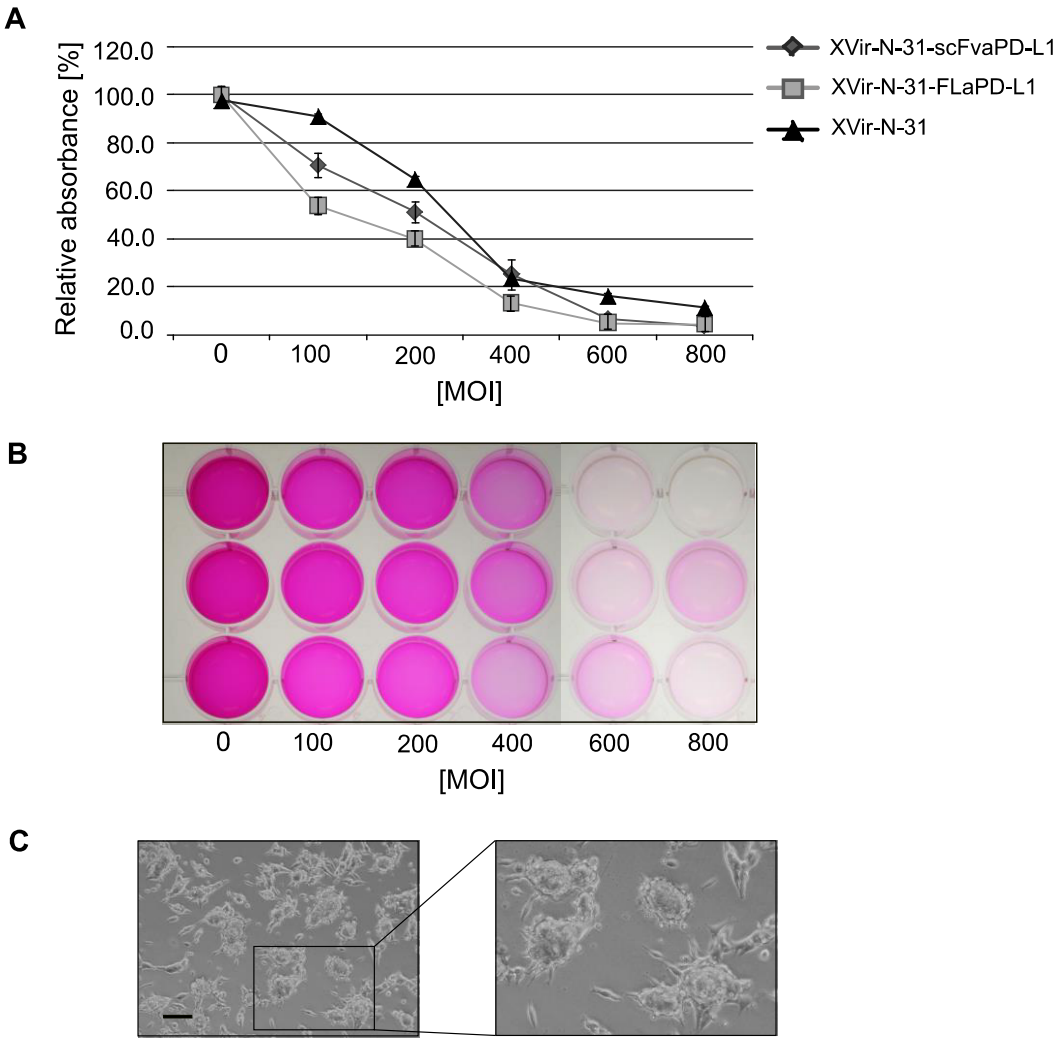

Figure 3.14: XVir-N-31 based viruses induce cell death in MB49. A MB49 cells were infected with various MOIs of indicated viruses. At 96 hours after infection, cells were fixed and cell killing was measured by SRB staining. **B** A representative picture of SRB stained cells infected with XVir-N-31-scFvaPD-L1. **C** MB49 cells showed noticeable chances in cellular morphology upon viral infection. Scale bar corresponds to 100 µm.

3.4 Combining XVir-N-31 and nutlin-3a in MB49 cells to improve virotherapeutic effects

Our experiments clearly demonstrated that murine MB49 cells are very limited in their permissiveness for YB-1 dependent adenoviral replication. To use this cell line in a syngeneic mouse model, it is necessary to improve adenoviral replication. Unpublished data from our lab indicated that virotherapeutic effects where dramatically enhanced upon combination with the Mdm2 inhibitor

nutlin-3a in human cell lines. Therefore, we were interested if we can overcome the low permissiveness of murine MB49 cells for YB-1 based adenoviral replication.

3.4.1 Biochemical effects of nutlin-3a in MB49

In order to analyze biochemical effects, we first determined the working concentration of nutlin-3a. Here, we also included the CDK4/6 inhibitor PD-0332991 (figure 3.15. A). Based on results of a dose response assay, we set the working concentration of nutlin-3a as a single inhibitor to 10 µM which had a 40 % effect on cell viability. The tested concentrations of PD-0332991 had only minor effects on cell viability. For the combination treatment, we used 5 µM nutlin-3a combined with 1 µM PD-0332991 which had a 40 % effect on cell viability. Next, we were interested in the biochemical effects of nutlin-3a (figure 3.15 B). At 24 and 48 hours after treatment, nutlin-3a induced a stabilization of p53. This was accompanied by a clear decrease of E2F1 at 24 hours and a complete downregulation at 48 hours upon concentrations of 10 µM and higher. We also observed a reduction of pRb levels at concentrations of 10 µM and higher at 24 hours and 48 hours after treatment. In addition, total Rb levels were clearly downregulated at 48 hours after treatment. The biochemical effects of PD-0332991 were investigated as part of another project in our lab and showed comparable effects (unpublished data, data are not shown).

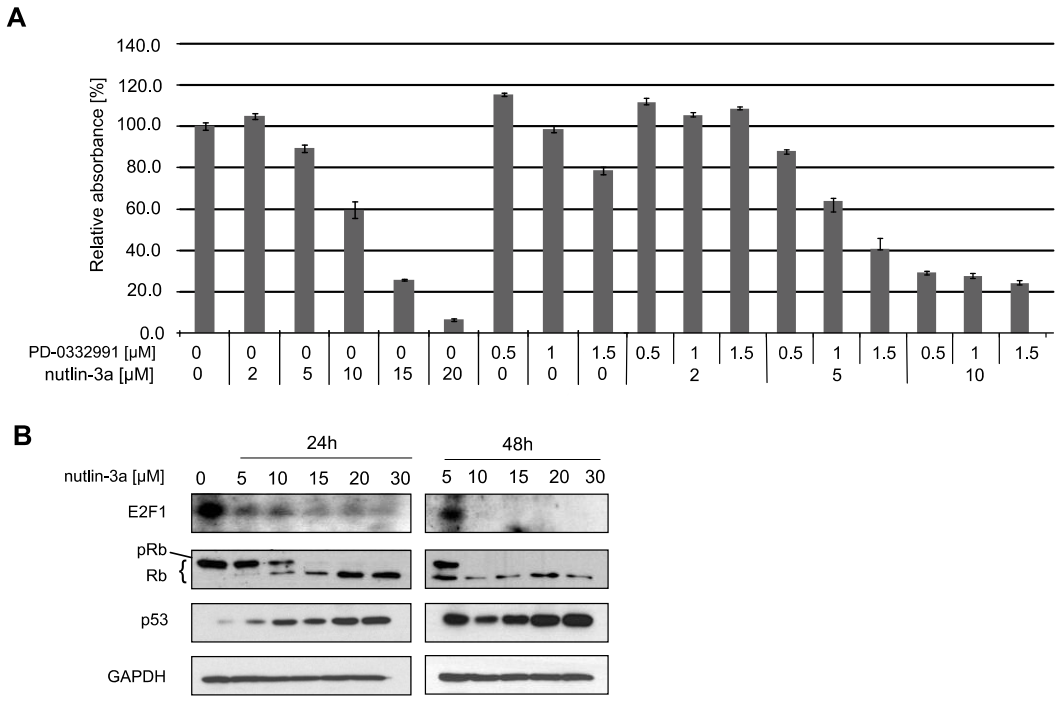

Figure 3.15: Nutlin-3a induces E2F1 downregulation and stabilizes p53 in MB49 cells. A To determine optimal working concentrations, MB49 cells were treated with various concentrations of nutlin-3a and PD-0332991. At 72 hours after treatment, cells were fixed and assayed by SRB staining. **B** MB49 cells were treated with various concentrations of nutlin-3a and the effects of treatment on E2F1, Rb, pRb and p53 were analyzed by immunoblotting.

A

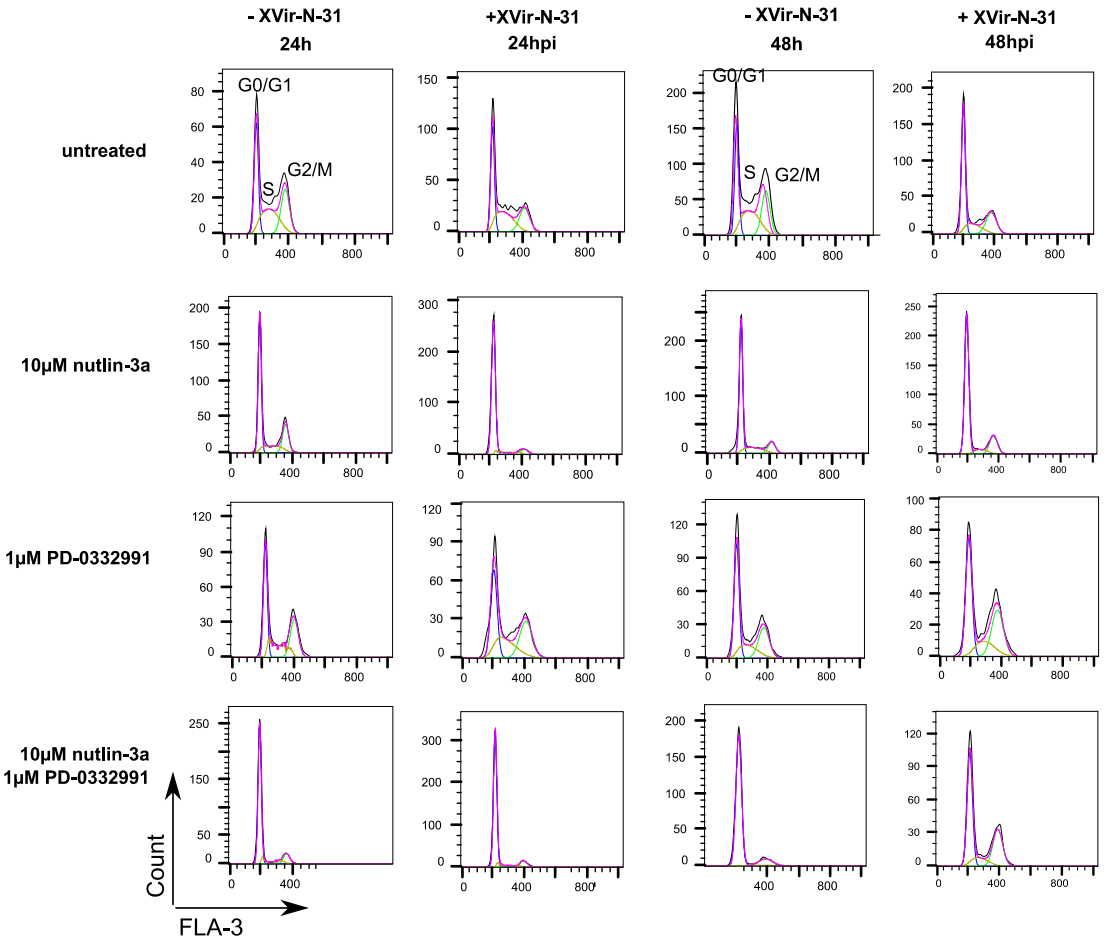

B

Percentage of cells in G0/G1 phase:

		untreated	10µM nutlin-3a	1µM PD-0332991	10µM nutlin-3a 1µM PD-0332991
- XVir-N-31	24h	36.3	58.2	43.2	79.7
+ XVir-N-31		39.7	89.7	38.6	86.8
- XVir-N-31	48h	37.5	65.9	49.1	87.5
+ XVir-N-31		54.3	75.6	45.8	55.6

Figure 3.16: Nutlin-3a induces a G1 arrest in MB49 cells. A MB49 cells were treated with indicated concentrations of nutlin-3a and PD-0332991 and infected with 200 MOI of XVir-N-31 or left uninfected. At 24 and 48 hours after treatment or infection, the cells were fixed and DNA was stained with 7-aminoactinomycin (7-AAD) for cell cycle analysis. **B** A tabular summery of the percentage of cells in G0/G1 phase.

Additionally, we evaluated the effects of nutlin-3a and PD-0332991 on the cell cycle (figure 3.16). A FACS analysis showed the induction of a G1 arrest at 24 hours after nutlin-3a treatment which became

more dominant at 48 hours. Treatment with 1µM PD-0332991 had no effects on the cell cycle. However, a combination of both inhibitors induced a G1 arrest at 24 hours and 48 hours after treatment. Further on, we were interested if this G1 arrest could be reversed upon virus infection and found that XVir-N-31 did not abrogate the G1 arrest in nutlin-3a and PD-0332991 treated cells. However, 48 hours after infection, XVir-N-31 was able to induce a shift towards G2/M phase in the combination treatment.

3.4.2 Analysis of virotherapeutic effects in combination with nutlin-3a and PD-0332991

After confirming the biochemical effects of nutlin-3a and PD-0332991, we analyzed if XVir-N-31-based virotherapy can be improved when combined with nutlin-3a or PD-0332991 (figure 3.17). We performed SRB assays to measure the cell killing capacity of XVir-N-31 alone and in combination with nutlin-3a and PD-0332991 (figure 3.17 A). Infection of untreated cells with 100 and 200 MOI of XVir-N-31 had a 20 % and 40 % cell killing effect, respectively, whereas infection with 50 MOI induced no cell lysis. Single treatment with 5 µM nutlin-3a and 1 µM PD-0332991 had only minor additional effects on cell killing and the strong lytic effect upon combination of 5 µM nutlin-3a and 1 µM PD-0332991 on infected cells could be ascribed to inhibitor induced effects. However, infection of cells treated with 10 µM nutlin-3a induced a significantly increased lytic effect compared to untreated cells. In detail, pretreatment of MB49 with 10 µM nutlin-3a resulted in an additional cell killing effect of 81 %, 93 % and 95 % when cells were infected with 50 MOI, 100 MOI and 200 MOI of XVir-N-31, respectively.

Next, we analyzed the viral replication upon inhibitor treatment (figure 3.17 B). Quantification of viral fiber DNA revealed an improved viral replication of XVir-N-31 and WtAd upon inhibitor treatment. XVir-N-31 replication was significantly improved upon treatment with 10 µM nutlin-3a, 1µM PD-0332991 and a combination of both compared to untreated control. Replication of WtAd was also increased upon inhibitor treatment, yet not significantly. Next, we were interested in transgene expression and viral particle formation upon inhibitor treatment. Here, we focused on the effects of nutlin-3a and found that nutlin-3a treatment clearly increased the expression of the HA-tagged scFvaPD-L1 antibody at 24 hours and 48 hours after infection (figure 3.17 C). However, nutlin-3a had no effect on viral particle formation (figure 3.17 D).

These results reveal that nutlin-3a induces a mechanism which improves adenoviral replication, protein expression and cell lysis in MB49 cells.

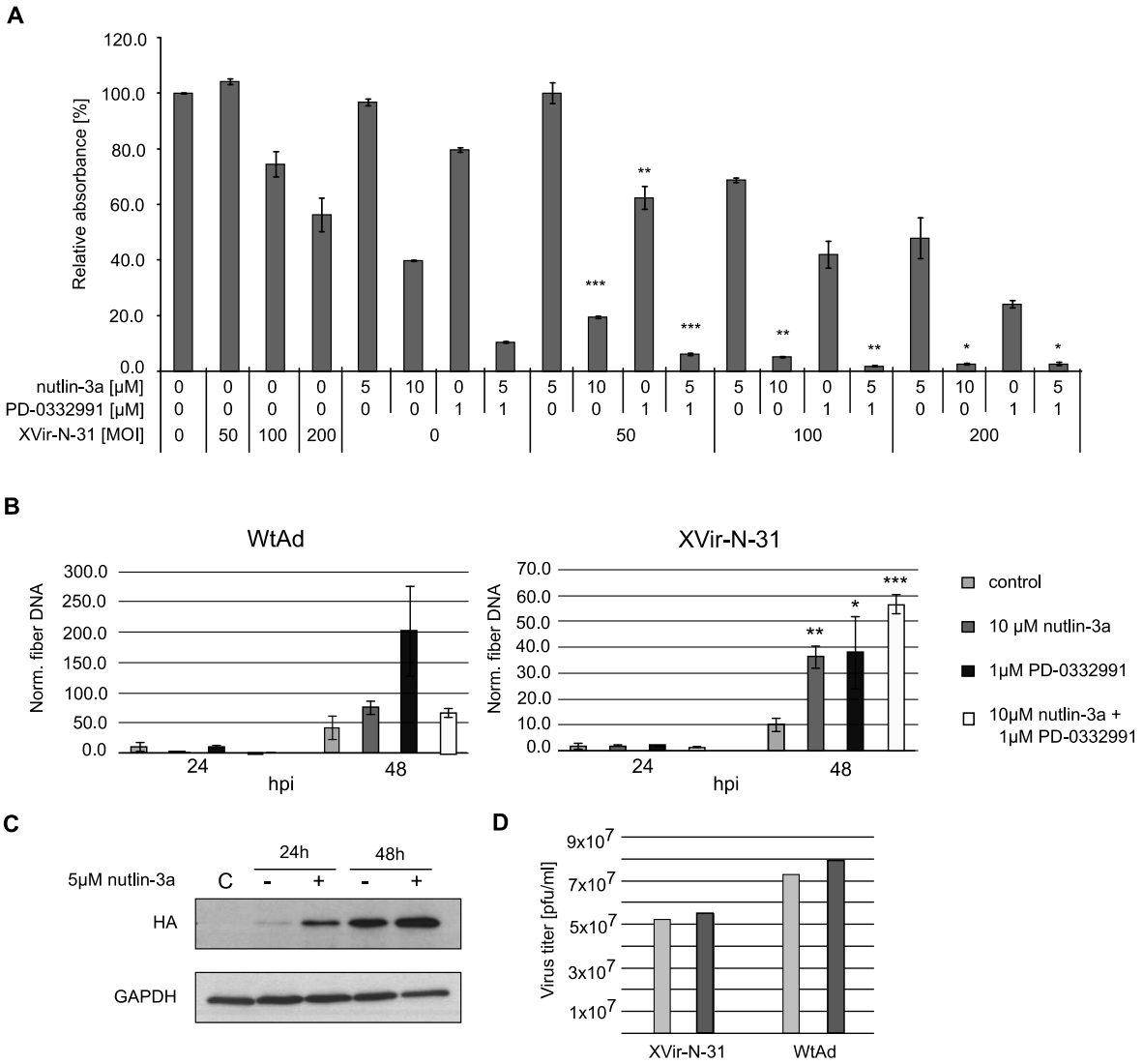

Figure 3.17: Nutlin-3a improves virotherapeutic effects of YB-1 based adenoviruses in MB49 cells. A Cells were pretreated with indicated concentrations of inhibitors and infected with various MOIs of XVir-N-31 at 24 hours after treatment. At 96 hours after infection, cells were fixed and stained with SRB and the cell killing effect was measured by SRB absorbance. **B** For quantification of viral replication, pretreated and untreated MB49 cells were infected with 200 MOI of XVir-N-31. At 4, 24 and 48 hours after infection the fiber DNA content was quantified by qPCR and normalized to the 4 hour value. Actin and GAPDH served as reference genes. **C** Pretreated and untreated MB49 cells were infected with 200 MOI of XVir-N-31-scFvaPD-L1. At 24 and 48 hours after infection, cells were lysed and expression of the scFvaPD-L1 antibody was analyzed by immunoblotting. **D** Nutlin-3a treated or untreated cells were infected with 200 MOI of indicated viruses. At 72 hours after infection, cells and supernatant were analyzed for viral particle formation by performing a hexon titer test *p≤ 0.05, **p<0.01, ***p<0.001. Infected, treated values were analyzed against corresponding infected, untreated samples.

Within another project in our lab, the effects of nutlin-3a in combination with XVir-N-31 in human bladder cancer cell lines were investigated. It was found that nutlin-3a could improve viral replication and that the nutlin-3a induced E2F1 and pRb downregulation were involved in the underlying mechanism. Further experiments within this project showed that the replication of XVir-N-31/E2Fm which is mutated in both E2F1 binding sites of its E2early promoter was improved compared to XVir-N-31 and that this could be further increased upon E2F1 downregulation. This finding indicated that E2F1 might have a repressive role on the adenoviral E2early promoter which contrasts with the common view of E2F1 as an activator of the E2early promoter. Therefore, we investigated if this is also true for the murine MB49 cells. However, quantification of viral replication showed that XVir-N-31/E2Fm replicates even less than XVir-N-31 although nutlin-3a treatment improved the replication of both viruses (figure 3.18). Based on this result, a final conclusion about the underlying mechanism is not possible and further experiments are needed.

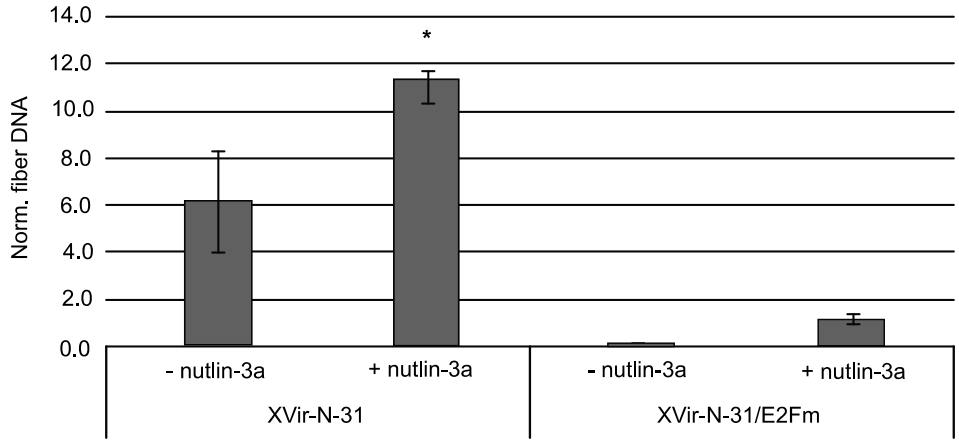

Figure 3.18: XVir-N-31/E2Fm barely replicates in MB49 cells. MB49 cells were treated with 10 µM nutlin-3a or left untreated. At 24 hours after treatment, cells were infected with 100 MOI of indicated viruses. Cells were harvested at 4 and 48 hours after infection. The fiber DNA content was quantified by qPCR and normalized to the 4-hour value. Actin and GAPDH served as reference genes. *p≤ 0.05. Infected, treated values were analyzed against corresponding infected, untreated samples.

3.5 The ultrasound guided orthotopic mouse model for bladder cancer

In order to extent our *in vitro* data, we established the ultrasound guided orthotopic mouse model for bladder cancer. This model was developed at the Prostate Cancer Center in Vancouver, Canada. It allows injection of tumor cells into the lamina propria of the bladder without surgical implantation and forms invasive bladder tumors (Jäger et al. 2014).

3.5.1 Establishment of a syngeneic and a xenograft orthotopic mouse model for bladder cancer

The orthotopic mouse model for bladder cancer is generated by injecting cancer cells into the lamina propria of the bladder which is called intramural injection. We established a syngeneic, immunocompetent model and a xenograft model. The xenograft model can be used to analyze the oncolytic effect of virotherapy whereas the syngeneic mouse model additionally allows the analysis of the immune stimulatory effect.

To perform the intramural injections, we generated an artificial space by injecting PBS into the 0.25 mm bladder wall (figure 3.19 A 1-3). Then, the tumor cells were injected into the proximal part of the artificial space. Therefore, the needle was exchanged by a needle filled with tumor cells resuspended in a Matrigel : PBS mixture. The needle was inserted into the generated space and 50 µl of the cell suspension containing the desired cell number were injected (figure 3.19 A 5, 6). Finally, the needle was rejected, and the mouse was recovered. For the whole procedure including anesthesia, roughly 45 to 60 minutes per mouse were needed.

To establish the syngeneic mouse model in C57BL/6, we first determined the ideal cell number of MB49 cells for tumor cell injections (figure 3.19 B, C, D). Using 700 000 MB49 cells resulted in tumor volumes of more than 70 mm^3 at day 7 after injection. Since we observed a very aggressive and fast tumor growth which was not suitable for treatment studies we tested lower cell numbers. Injection of 100 000 cells reached a tumor volume of 20 to 55 mm^3 and injection of 70 000 cells resulted in tumor volumes of 25 to 40 mm^3 at day 5 after injection. In general, we had 100 % tumor uptake and were able to show the aggressiveness and the extreme rapid growth behavior of MB49 which made this model very difficult.

For establishing the immunodeficient xenograft mouse model, we used UMUC3 cells in $Foxn1^{nu/nu}$ mice (figure 3.19 E). 200 000 UMUC3 cells were injected which led to an average tumor volume of 24 mm^3 at day 10 after injection. The tumor uptake rate was 100 % although one tumor did not exceed the size of 10 mm^3. In general, the used cell number resulted in tumors with appropriate growth behavior to apply intratumoral treatment.

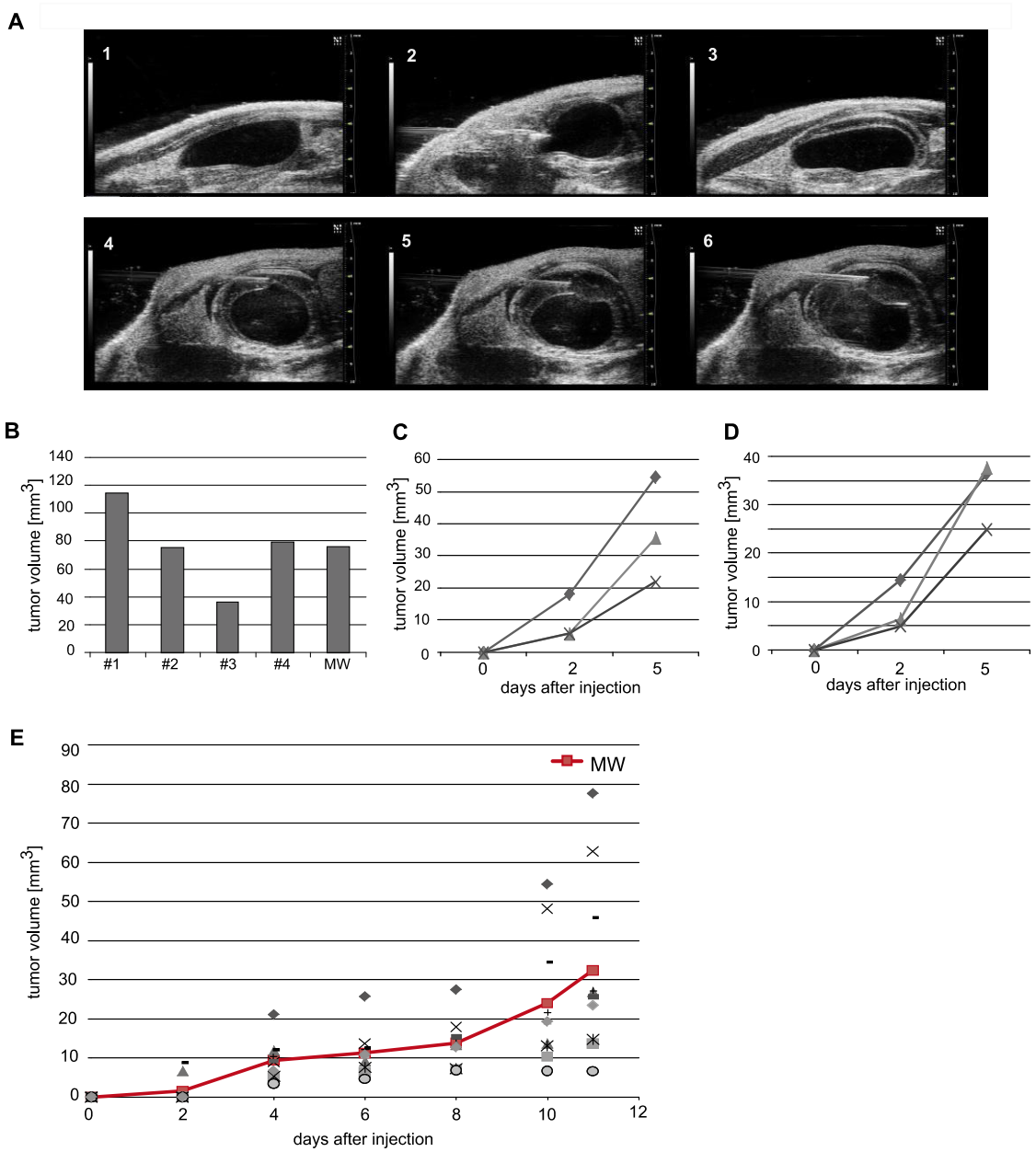

Figure 3.19: The orthotopic, ultrasound guided mouse model for bladder cancer. A The procedure for the intramural injections: 1) visualize the bladder on the ultrasound screen, 2) visualize the needle and insert the needle into the mouse, 3) injection of PBS to generate an artificial space, 4) insert the needle filled with tumor cells in the cavity, 5-6) inject cell suspension in the proximal part of the PBS filled space. **B** Tumor volumes of 4 mice bearing syngeneic tumors at day 7 after injection of 700 000 MB49 cells. Tumor growth after injection of **C** 100 000 MB49 cells and **D** 70 000 MB49 cells in the syngeneic mouse model. **E** Growth of xenograft tumors using 200 000 UMUC3 cells in immunodeficient mice. The tumor volume was determined using 3D ultrasound measurement.

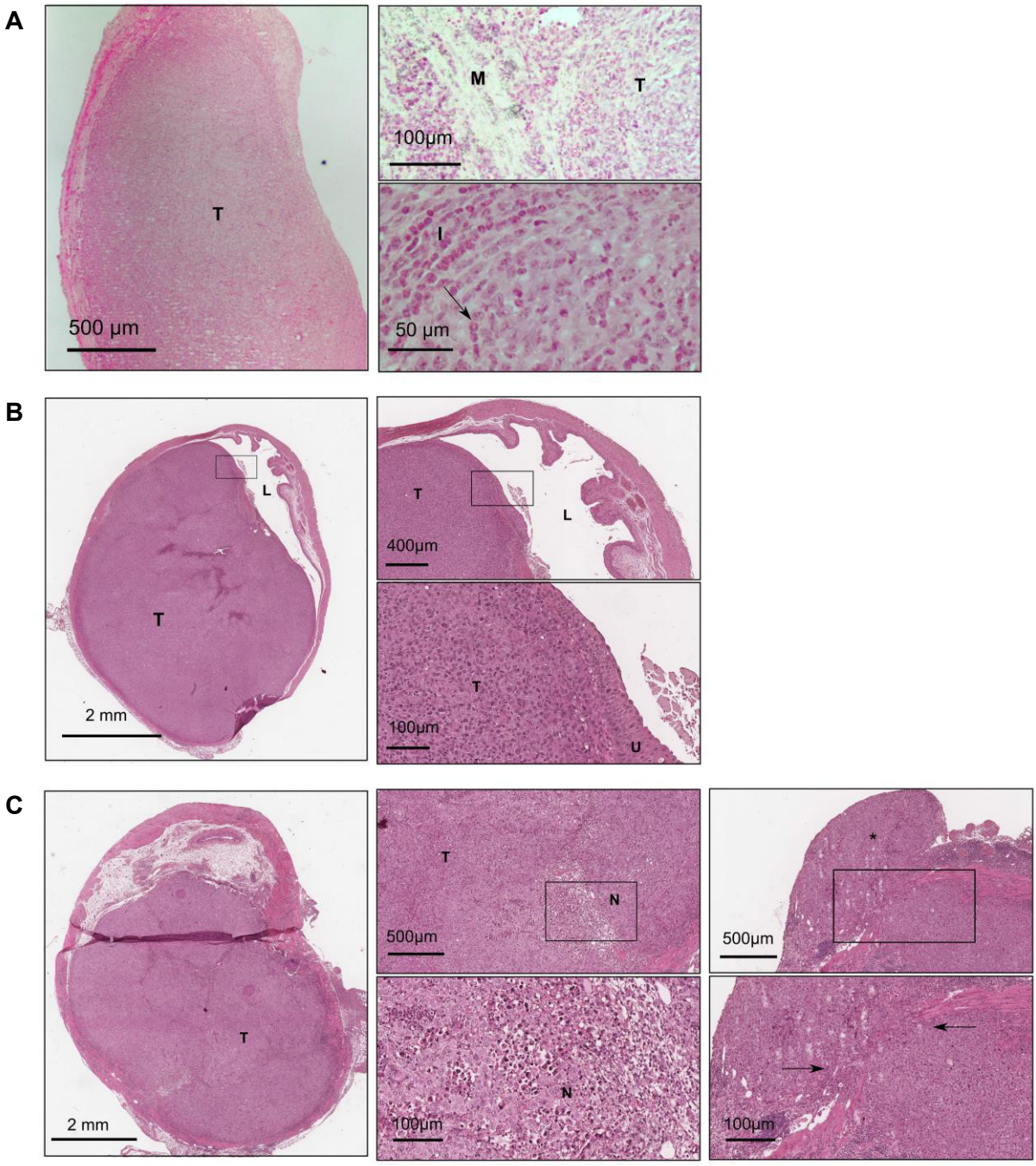

Figure 3.20: H&E stained sections of orthotopic bladder tumors show intramural and muscle invasive growth. **A** Representative sections of the syngeneic tumor model showed muscle invasive growth (M) and infiltration of immune cells. **B** A representative xenograft tumor (T) showed the correct location in the lamina propria and a slightly hyperplastic urothelium (U). **C** A virus treated xenograft tumor at day 17 after injection revealed necrotic areas (N) as well as muscle invasive tumor growth (arrows and asterisk).

After the mice were sacrificed, the tumors were examined on H&E sections to demonstrate the correct intramural injection and invasive tumor growth. Figure 3.20 A shows representative sections of syngeneic, orthotopic bladder tumors (T) which grew in the lamina propria. Additionally, it shows a moderate number of inflammatory cells like neutrophilic granulocytes, lymphocytes and macrophages which were adjacent (I) to or infiltrating (arrow) between the tumor cells (T) as well as infiltrative growth into the tunica muscularis (M). H&E stained sections of the orthotopically implanted xenograft carcinoma model showed an intact and slightly hyperplastic urothelium (U) covering the bladder lumen (L) and tumor cells (T) located in the lamina propria (figure 3.20 B). Further on, we detected small areas of necrosis (N) and apoptosis as well as tumor infiltration in (arrows) and through (asterisk) the tunica muscularis in a virus treated tumor (figure 3.20 C).

3.5.2 Ultrasound guided virotherapy using XVir-N-31 in the orthotopic bladder cancer model

After initial experiments in which we defined an appropriate cell number for the injections, we applied ultrasound guided intratumoral virotherapy using XVir-N-31 (figure 3.21 A). Tumor bearing animals were randomized into two groups (n= 4-5 per group) and treated with XVir-N-31 or PBS every fourth day for a total of three times. Establishing this treatment approach showed the difficulty of hitting the tumor and injecting equally into the tumor. Major issues were the insertion of the needle into the compact tumor and the intratumoral position. The central location of the needle within the tumor and a slow and careful application were important in order to ensure an optimal uptake of the virus by the tumor. Figure 3.21 B shows representative ultrasound images of the tumor growth (1-4), the intratumoral treatment (5) and the remaining tumor after virotherapy (6).

In this first experiment, we were able to show a significant reduction of tumor growth in the virus treated group compared to the PBS treated control group (figure 3.21 C). On day 17, animals treated with XVir-N-31 showed an average tumor volume of 124.1 mm^3 compared to an average tumor volume of 214.6 mm^3 in PBS treated animals which is equivalent to a reduction in tumor size of 42 %. For human reasons due to excessive tumor burden, nine out of ten animals had to be sacrificed on day 18 and could not be monitored until the end of the planned follow-up. However, one animal showed an almost complete response to XVir-N-31 based virotherapy (figure 3.21 D). This mouse had a tumor size of 35 mm^3 at treatment start which increased up to 40 mm^3 during therapy. 12 days after the last virus injection, the tumor size shrank to a size of 5 mm^3.

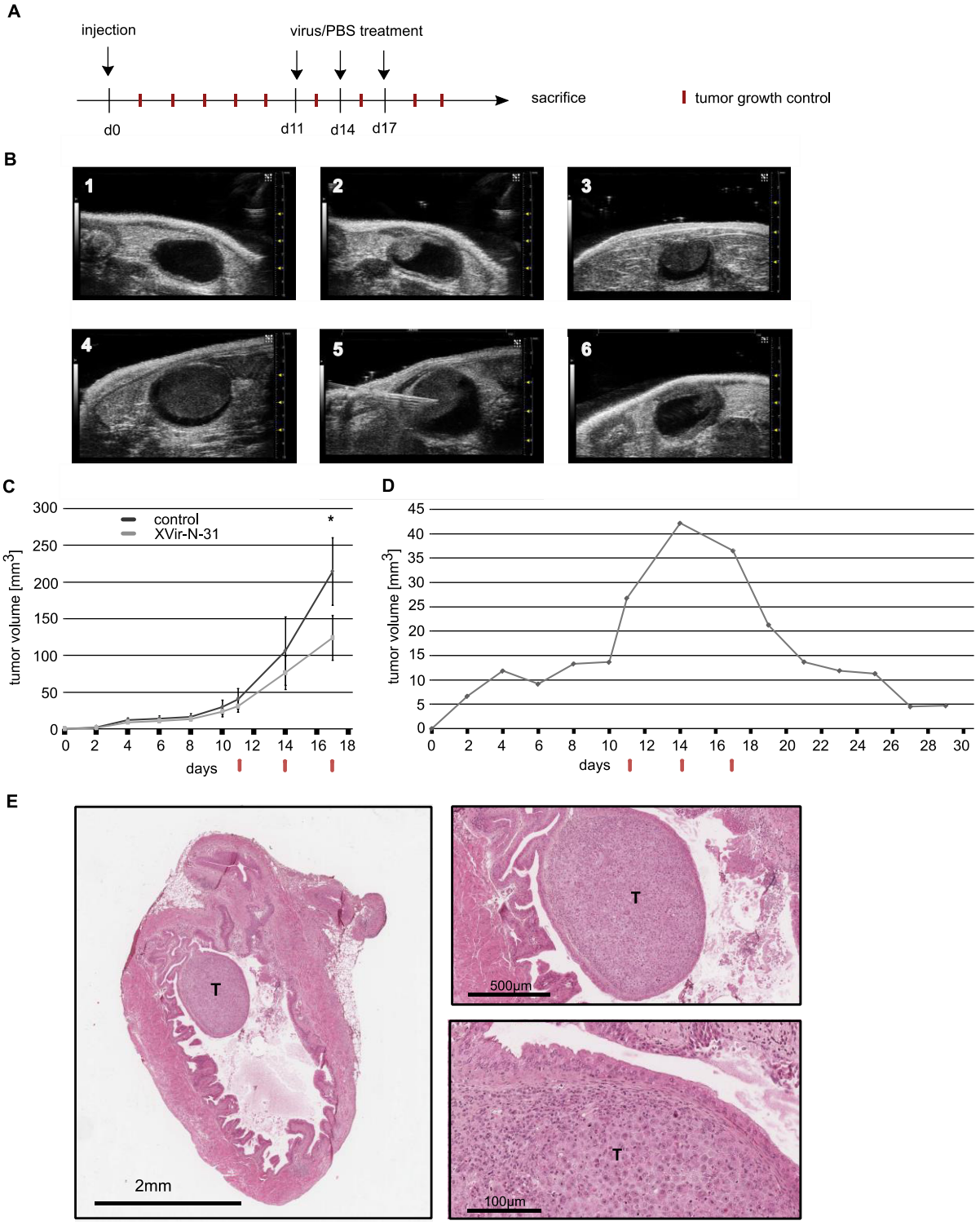

Figure 3.21: For figure legend see next page.

Figure 3.21: Ultrasound guided virotherapy using XVir-N-31. A Time table for the *in vivo* experiment. Nude mice were injected with 200 000 UMUC3 cells. Tumors were treated with $3x10^9$ viral particles on day 11, 14 and 17. Mice were monitored twice a week until sacrifice. **B** Ultrasound guided intratumoral injections. 1: Healthy bladder, 2-4: Growth of bladder tumor 4, 8 and 14 days after injections, 5: Intratumoral virus injection, 6: Remaining tumor after virotherapy (d27). **C** The tumor growth of virus treated animals compared to PBS treated animals (n=4-5 per group). The tumor volume was measured by 3D ultrasound imaging. Error bars indicate S.E. and *$p \leq 0.05$ **D** Reduction of tumor volume after virotherapy. **E** H&E staining of a remaining xenograft tumor (T) after virotherapy.

4 Discussion

4.1 Generation and production of the novel virus XVir-N-31-aPD-L1

In general, recombinant adenoviruses can be generated by homologous recombination or by cloning using multiple shuttle plasmids (Chartier et al. 1996; Graham und Prevec 1991). Here, we manipulated the adenoviral genome by integrating the transgene into a segment of the WtAd E3 region and cloning it into the backbone of XVir-N-31 via several shuttle plasmids. Within the adenoviral genome there are regions like the E3 gene which are not necessary for adenoviral replication and packaging. These regions are often deleted and are used for integration of large transgenes. Even undeleted WtAd can keep transgenes with a size of up to 1796 bp. This is according to the common rule that there is a constraint of DNA amount which is 105 % of the 35934 bp comprising WtAd genome that can be packed into virions (Sugarman B.J. et al. 2003). Viruses with genome sizes exceeding this limitation are difficult to produce and very unstable (Bett et al. 1993). Here, we used XVir-N-31 which has a size of 33114 bp and integrated the Wt E3 region including the aPD-L1 or Fc encoding transgene. Altogether, the newly generated viruses XVir-N-31scFvaPD-L1 and XVir-N-31-FLaPD-L1 had a size of 36971 bp and 36976 bp, respectively, and XVir-N-31-Fc comprised 36141 bp. This is in consensus with the rule from Bett et al. and should not influence virus production and viral titers (Bett et al. 1993). We were able to produce the newly cloned viruses using HEK293 cells, however, the viral titers were lower for XVir-N-31-scFvaPD-L1 and XVir-N-31-FLaPD-L1 compared to XVir-N-31. It is known that the size of transgenes as well as the protein they encode for can influence adenoviral packaging. And a recent publication showed that also the location of the transgene is influencing viral titers and that especially the transgene integration into the E3 region can have an influence on the titer (Suzuki et al. 2015). We assume that the size of the a-PD-L1 transgene and its location rather than the protein it encodes caused a lower titer of XVir-N-31-FLaPD-L1 and XVir-N-31-scFvaPD-L1 compared to XVir-N-31. The titer of XVir-N-31-Fc was normal which might indicate that transgene size is indeed crucial.

4.2 Characterization of XVir-N-31-aPD-L1 in UMUC3

After cloning and production of XVir-N-31-scFvaPD-L1 and XVir-N-31-FLaPD-L1, we characterized the viruses regarding their virotherapeutic effects in UMUC3 cells.

Analysis of viral replication revealed comparable values for XVir-N-31-scFvaPD-L1, XVir-N-31-FLaPD-L1 and XVir-N-31 showing that the integrated transgenes did not affect replicative activity. In general, values of XVir-N-31-based viruses were about 10-fold lower than values of WtAd. This is within our internal lab standards and can be attributed to the E1A13S deletion of XVir-N-31.

Further on, investigation of the viral potency showed an oncolytic effect of XVir-N-31-scFvaPD-L1 and XVir-N-31-FLaPD-L1. Here, we observed a slight trend indicating a higher cell killing effect of XVir-

N-31-scFvaPD-L1 and XVir-N-31-FLaPD-L1 compared to XVir-N-31. This finding might be due to the deletion of ADP in XVir-N-31. ADP induces efficient cell lysis in the late stages of infection and thereby ensures the release of viruses from infected cells. In keeping with these results, it has been shown before that ADP deleted viruses induce a slower cell lysis than viruses with wild type ADP without affecting viral replication (Tollefson et al. 1996). Additionally, it is important to mention that slight titer variations can influence *in vitro* experiments and especially the cell killing assay is very susceptible in this point.

Further on, we investigated the antibody synthesis of XVir-N-31-scFvaPD-L1. We showed an efficient synthesis of the HA tagged scFvaPD-L1 antibody starting at 24 hours after infection and a subsequent secretion of the antibody which was detectable as early as 48 hours after infection. We integrated the transgene into the E3 region and its transcription is controlled by the E3 promoter which is known to be activate about 12 hours after infection leading to detectable E3 proteins, e.g. ADP at 24 hours after infection (Bauzon et al. 2003; Hawkins und Hermiston 2001). Therefore, our results are in accordance with the activity of the E3 promoter and the expression of E3 gene products (Bauzon et al. 2003). Further on, our data are comparable with a similar viro-immunotherapeutic approach showing secretion of an anti-CTLA-4 antibody which was also integrated into the E3 region at 48 hours after infection (Dias et al. 2012).

Additionally, we showed the recognition and binding of the scFvaPD-L1 antibody to PD-L1 by immunoprecipitation. If this causes a functional blockade of the PD-L1/PD-1 axis resulting in elevated IFNy levels, IL-2 production and activation of immune cells has to be further investigated by cell based blocking assays (Blank et al. 2004; Peng et al. 2012; Sanmamed et al. 2015).

Several *in vivo* and *in vitro* experiments showed the strong lytic and replicative potential of XVir-N-31 in glioma cells (Rognoni et al. 2009; Kostova et al. 2015; Mantwill et al. 2013). Here, we demonstrated for the first time the virotherapeutic effects of XVir-N-31, XVir-N-31-scFvaPD-L1 and XVir-N-31-FLaPD-L1 in the bladder cancer cell line UMUC3.

4.3 The attempt to develop a coculture assay for measuring functional PD-L1 blockade

Recent publications showed that blocking the PD-1/PD-L1 axis led to elevated expression of IFNy (Blank et al. 2004; Peng et al. 2012; Sanmamed et al. 2015). These findings inspired us to develop an *in vitro* assay to proof the functional blockade of PD-L1. In all our experiments, viral infection led to titer dependent elevation of IFNy levels which could be enhanced by adding additional anti-PD-L1 antibody. However, despite many attempts and different conditions, we were not able to generate a stable experimental setup to reliably reproduce our results. There are several aspects which can explain our observations:

In our experiments, we cocultured PBMCs derived from colleagues with the established bladder cancer cell line UMUC3 disregarding HLA verification and matching. Furthermore, we used new PBMCs for every experiment and thus there might have been variations in activity and stimulation status of these cells.

Moreover, it is known that adenoviruses induce a strong immune reaction which is also characterized by IFNy production (Schagen et al. 2004). In this point many aspects can influence the read out: First, the replicative behavior which differs 10-fold between XVir-N-31 and WtAd has to be considered. Second, the genetic differences of XVir-N-31-scFvaPD-L1, XVir-N-31 and WtAd can lead to variations in IFNy stimulation making a comparison of these viruses difficult. And third, taking the IC50 values, the replicative potential and the cell killing effect of the viruses into account, we had to use varying virus concentrations and P:I ratios which might have additionally influenced the IFNy response.

To obtain reliable results in the future, it might be necessary to use tumor cells and PBMCs from the same donor. Alternatively, it would be worth trying to use the cell free supernatant of infected tumor cells to stimulate PBMCs from patients and healthy donors (Dias et al. 2012).

4.4 Translational aspects of viro-immunotherapy using XVir-N-31-aPD-L1

The recent clinical success and the multitude of clinical trials using oncolytic therapy demonstrate that virotherapy is about to become an integrative part of immune therapy for cancer treatment. Since the first studies on recombinant oncolytic viruses, clinical research has increased showing excellent tolerability and safety of oncolytic viruses, even at highest feasible doses. Additionally, virus transmission causing viral spread has not yet been seen and viremia after systemic injection is unlikely and has never been reported which is explained by the fast clearance of viruses by the liver, spleen and serum factors (Liu et al. 2007).

Oncolytic viruses were initially developed with the aim to induce high infection rates and massive tumor cell lysis to show the best effect and response. Latest research has shown that the immune stimulatory effect of virotherapy was underestimated but is inevitable and central for a systemic and long lasting immune response (Zamarin et al. 2014; Andtbacka et al. 2015). However, immune escape mechanisms represent limitations and their extent influences success or failure of oncolytic therapy.

ICB, e.g. against the PD-1/PD-L1 axis, represents an immunotherapeutic approach that has gained success in the last years. Nevertheless, the response rates to PD-1 blockade as a single therapy are still limited and many patients do not respond or develop resistance against it. This was seen when patients lacked intratumoral $CD8^+$ T cells or had low IFNy expression and thus showed reduced PD-L1/PD-1 expression (Ribas et al. 2017; Tumeh et al. 2014; Postow et al. 2015). It is hypothesized that limitations of both therapies can be overcome by combining the two strategies and the recent therapeutic success of virotherapy together with an anti-PD-1 ICB has confirmed the potential of this viro-immunotherapy (Ribas et al. 2017; Bourgeois-Daigneault et al. 2018). The rational for this well-working combination is the mutual stimulation and the following aspects are important when explaining viro-immunotherapy:

It has been shown that the immune stimulatory effect of OVT is essential for a successful cancer treatment. However, this effect is often inhibited by the immune suppressive tumor environment which can be overcome by relieving T cell inhibition by blocking negative immune checkpoints to enable a strong immune activation by oncolytic viruses. Additionally, it is known that oncolytic viruses cause an increase in circulating $CD8^+$ and $CD4^+$ immune cells, induce IFNy expression and thus have the potential to reverse the limitations to PD-1/PD-L1 blockade (Ribas et al. 2017). The recent study from Ribas et al.

demonstrated that a local injection of oncolytic viruses contributed to a systemic antitumor effect (Ribas et al. 2017). This supports the idea of a local administration of the virus directly into the tumor that can affect also distant metastasis. Moreover, it has been shown that oncolytic viruses have the capability to broaden the spectrum of neoantigen-directed $CD8^+$ T-cell response compared to PD-1 ICB (Woller et al. 2014; Woller et al. 2015). This finding has to be put in the context of publications showing a survival advantage of patients with missense mutations (Brown et al. 2014). Analyzing the patients from the study from Ribas et al. regarding their neoantigen directed immune activity would immensely contribute to a comprehensive understanding of this promising combination (Ribas et al. 2017).

Arming oncolytic viruses with immune stimulatory molecules, e.g. IL2 or GM-CSF has been studied since years but the idea of integrating antibodies against immune checkpoints into the viral genome is quite new and there are only a few publications. In 2014, Engeland et al. published a measles virus encoding for antibodies against CTLA-4 and PD-L1. They used fully immunocompetent mouse models and showed that their viruses were able to induce tumor regression. Additionally, they analyzed immunological aspects and found an increase of infiltrating T cells accompanied by a reduction of regulatory T cells. Moreover, they compared virotherapy with systemic anti-PD-L1 therapy and local, virus mediated anti-PD-L1 expression and obtained similar results (Engeland et al. 2014). Dias et al. published an oncolytic adenovirus armed with an anti-CTLA-4 antibody. They showed a significant antitumor activity of their virus in an immune deficient xenograft model and a virus mediated increase in IL-2 and IFNy production in patient derived PBMCS (Dias et al. 2012).

Our new virus XVir-N-31-aPD-L1 was characterized *in vitro*, but so far we were not able to test its immunological effects *in vivo*. We think that the direct combination of PD-L1 specific ICB and oncolytic therapy is a further development in the field of viro-immunotherapy. We hypothesize that the local administration into the bladder circumvents clearance of the virus, results in higher antibody concentrations within the tumor and an improved anti-tumor response while reducing side effects and systemic toxicity (Aznar et al. 2017). In addition, we speculate that the diffusion of a scFv antibody within the tumor might be better compared to a large full-length antibody. This question was addressed in a recent publication in which a FL aPD-L1 and a scFv aPD-L1 antibody vectorized in a vaccinia virus were compared. However, they could not see differences in the antitumor effects of the two constructs (Kleinpeter et al. 2016). A further important aspect is that the PD-1/PD-L1 axis regulates the effector phase of stimulated T cells in the periphery and that signaling is more important in later phases of T cell activation. Therefore, it is reasonable to exclusively inhibit PD-L1 signaling at the side of infection (Pardoll 2012).

The investigation of OVT focused mainly on resistant patients or end stage cancer patients. Recently, a new application of oncolytic viruses as neoadjuvant treatment has been published and obtained great results (Bourgeois-Daigneault et al. 2018). In this study, mouse models representing the highly aggressive and immune silent triple-negative breast cancer were used. The authors showed that virotherapy stimulated the immune system, generated a tumor specific memory and sensitized refractory tumors to ICB after surgery. This publication demonstrates once again the perfect match of virotherapy and ICB and gives reasons to test oncolytic viruses as a neoadjuvant treatment option. In the context of the present work, we argue that testing a neoadjuvant virotherapeutic approach for MIBC is reasonable. Using oncolytic viruses prior to radical cystectomy early in the diagnosis of MIBC

when patients have a low disease burden and stable immune system might help to reduce relapsing patients with metastatic disease (Bourgeois-Daigneault et al. 2018).

4.5 Generating a syngeneic *in vivo* model for adenoviral research

Since the immune aspect is playing an important role in the therapeutic response to oncolytic viruses, the understanding of virotherapy would benefit from the availability of suitable, immunocompetent mouse models (Ganly et al. 2000). The Syrian hamster model has been used as an *in vivo* system to test adenovirus-based therapy, although it allows only restricted adenoviral replication and immunological reagents are limited for this animal system (Wold und Toth 2012; Jiang et al. 2014). One possibility to analyze the oncolytic as well as the immune stimulatory effect of adenovirus-based therapy is the humanized mouse model. This model is very challenging and complex, its establishment is time intensive and experiments can vary due to differences in engraftment of the immune system (Shultz et al. 2012). Syngeneic mouse models offer an alternative and several systems representing different tumor entities (adenocarcinoma, hepatocarcinoma, bladder tumor) have been described (Kim et al. 2011; Diaconu et al. 2012; Cheng et al. 2015). To establish a syngeneic, orthotopic tumor model for bladder cancer, we tested if the murine bladder cancer cell line MB49 allows adenoviral replication.

4.5.1 Investigation of MB49 cells for YB-1 dependent adenoviral research

Many mouse cell lines are considered deficient for adenoviral replication (Ganly et al. 2000). This fact is based on data published decades ago which showed a limited permissiveness for adenoviral replication in normal mouse tissue (Ginsberg et al. 1991; Halldén et al. 2003). It is speculated that low CAR expression and the deficiency in viral particle formation are reasons, but this has not been clearly shown (Tomko et al. 2000; Younghusband et al. 1979). In contrast, there are some reports about murine tumor cells, e.g. glioma cells, showing permissiveness for adenoviral replication (Jiang et al. 2014; Halldén et al. 2003). We investigated if the murine MB49 cells allow replication of XVir-N-31 and found very limited replication rates for both XVir-N-31 and WtAd, whereby WtAd showed in general slightly higher replication values. We also showed that MB49 cells were CAR negative which is in line with literature (Tomko et al. 2000). This can explain the low replication values for WtAd, since it uses CAR to enter the cell. However, XVir-N-31 uses its RGD motif for infection and is thereby mostly CAR independent (Rognoni et al. 2009). Several ways to improve viral infection rates are known, e.g. polymer-enhanced delivery, pretreatment of viruses with a protein transduction domain fused to CAR or magnetofection (Kühnel et al. 2004; Tresilwised et al. 2012). We used magnetofection to improve infection rates and this increased the replication of WtAd but did not influence XVir-N-31 replication in MB49 cells indicating that replication of XVir-N-31 seems to be influenced by other cellular factors or signaling pathways. In this context we also showed the YB-1 positivity of MB49 cells.

To further understand and explain these observations, we looked at the oncolytic capacity of XVir-N-31 based viruses in MB49 cells and could observe a cell killing effect starting at 100 to 200 MOI. In context of our replication data, these results seemed to be contradictory since an oncolytic effect is caused by active viral replication. Additionally, we observed a very conspicuous change in morphology upon adenoviral infection which was different to the known CPE. Therefore, we speculate that these observations indicate a toxicity induced cell killing caused by too high virus concentrations instead of being induced by an oncolytic effect due to viral replication. All together these data confirm limited activity of XVir-N-31 in the murine bladder cancer cell line MB49 which might be owed to the strict species specificity of human adenoviruses, the low infection rates and possibly also differences in YB-1 location, regulation and activation of the E2 promoter (Robinson et al. 2013).

In contrast to our findings there is a study showing virotherapeutic activity of their recombinant adenovirus in MB49 cells. Han et al. could show an efficient expression of E1A and their transgene although using quite low MOIs (Han et al. 2013). Based on these data, it is worth testing if the deficiency of XVir-N-31 replication in MB49 cells is due to its YB-1 dependency.

4.5.2 Combining oncolytic virotherapy and nutlin-3a in MB49 cells

Unpublished data from our lab showed that virotherapeutic effects of XVir-N-31 can be tremendously improved upon combination with cell cycle inhibitors in human bladder cancer cell lines. These findings include enhanced replication, cell lysis, viral particle formation and protein expression. We explain these findings by hypothesizing that the downregulation of E2F1 and pRb play a major role in the improved virotherapeutic effects in human cell lines. We proposed a model which ascribes a repressive role of E2F1 on the E2-early promoter activation that can be overcome by E2F1 downregulation upon inhibitor treatment leading to a fully activated E2 early promoter and a consequent strong replication rate. This hypothesis could be further strengthened by data showing an increased replication of XVir-N-31/E2Fm compared to XVir-N-31 which increased even more upon E2F1 downregulation in human cells.

The interplay between E2Fs, pRb and E1A is not in detail understood. E2Fs are transcription factors that can be divided into activating E2Fs (E2F1 to 3) and repressing E2Fs (E2F4 to 7) (Attwooll et al. 2004). The adenoviral E1A protein is known to manipulate the host cell cycle by maintaining cell viability and inducing S phase entry which is achieved by binding of E1A to pocket proteins like pRb and p107 (Kaczmarek et al. 1986; Seifried et al. 2008). It was long though that binding of E1A to pRb releases E2F1 which than mediates cell viability by inducing DNA synthesis, DNA repair and cell proliferation (Helin et al. 1993; Fattaey et al. 1993). However, this mechanism has been questioned by findings showing that E1A selectively disrupts pRb-E2F4 complexes whereby leaving pRb-E2F1 interaction stable (Seifried et al. 2008). These data challenge the common knowledge that E1A releases E2F1 to mediate cellular viability and they strengthen our hypothesis that E2F1 has a repressive function on the adenoviral E2 early promoter (Bagchi et al. 1990).

Within this project, we analyzed if a combinatorial approach using nutlin-3a together with XVir-N-31 can enable YB-1 based adenoviral research in MB49 cells and further on, if the underlying mechanism in murine cells is, as in human cells, E2F1 dependent. We showed that nutlin-3a enhanced viral replication, transgene expression and also cell killing capacity. Further on, nutlin-3a induced downregulation of pRb and E2F1 and caused a cell cycle arrest in G1 which has been reported by many others in various human, p53 wild type cell lines (Walsh et al. 2015; Ambrosini et al. 2007; Du et al. 2009). In order to show that the model we developed for human cells is also true in a murine background, we measured the replication of XVir-N-31/E2Fm but could not see an increase in fiber DNA. This indicated that a E2F1-pRb independent regulation is responsible for the upregulated virotherapeutic effects in MB49. It is imaginable, that YB-1 plays a central role in this regard and it is important to consider the species specificity of human adenoviruses and that they might behave different in murine cells than in human cells. These differences in adenoviral regulation can include variations in the E2 gene activation via YB-1 and E2F1 and also in the interplay of E2F/pRb and E1A.

Although we were able to show an upregulation in virotherapeutic effects upon combination with nutlin-3a, this effect has to be further increased to investigate XVir-N-31 in a syngeneic *in vivo* model. Higher infection rates are for sure one factor that can improve adenoviral replication. But to cause a tremendous increase in replication rates it is inevitable to fully understand the involved mechanisms in order to accurately manipulate them. Further inhibitors have to be combined with XVir-N-31 to investigate if our findings are reproducible when using different cell cycle inhibitors. In this regard, we began to evaluate the CDK4/6 inhibitor PD-0332991 in a combinatorial approach. So far, we showed enhanced viral replication upon single treatment with PD-0332991 and PD-0332991 in combination with nutlin-3a. The biochemical effects of PD-0332991 combined with nutlin-3a have been explored only once showing an even stronger induction of G1 arrest and E2F1 downregulation compared to single treatment (Pollutri, 2014). The detailed effects and mechanisms of this combination and their relevance in our context remain to be explored.

Within this project, it was our aim to enable adenoviral replication in a murine cell line in order to generate a syngeneic mouse model that allows the immunological characterization of the novel viro-immunotherapy approach. With our *in vitro* findings, we are about to unleash the limitations of YB-1 based adenoviral replication in the murine cancer cell line MB49.

4.6 The ultrasound guided orthotopic bladder cancer mouse model

4.6.1 Establishment of the ultrasound guided orthotopic bladder cancer mouse model

In this project, we have established the ultrasound guided orthotopic mouse model for bladder cancer. Therefore, an imaging station consisting of an imaging platform and a highly precise mounting for the needle are needed. Initially we tried to build the needle mounting on our own using a photo tripod and a self-made construction to fix the needle. However, several attempts showed the enormous sensitivity

and preciosity that is needed to hit the lamina propria of the bladder. The self-made construction could not withstand these demands and thus we decided to use the professional mounting station. When establishing the model, we realized that the isoflurane anesthesia caused a bladder emptying which had the consequence that the bladder was very movable and flexible and intramural injections were not feasible. Therefore, we had to catheterize every bladder. We figured out that an MMF anesthesia did not induce a bladder emptying and we were able to inject one mouse in roughly 45 minutes. We are convinced that this huge time factor can be significantly decreased by intensive practicing.

In the original publication from Jäger et al. 2014, intramural injections were performed under isoflurane anesthesia and they needed an average time of 3 to 8 minutes per mouse. Here, the long experience and a perfectly organized mouse facility have to be considered when comparing with our data.

After we have established the experimental setup, we began to generate the xenograft model using UMUC3 cells on the one hand and the syngeneic mouse model using MB49 cells on the other hand. For the syngeneic mouse model, we tried various concentrations of MB49 cells. We had a tumor uptake of 100 %, however, the tested cell numbers were too high and led to an uncontrolled and extreme fast tumor growth. Even with as little as 70 000 MB49 cells, mice developed tumors with an average size of 32 mm^3 at day 5 after injection showing the aggressiveness of this cell line. Before using the syngeneic model to study XVir-N-31 based virotherapy in the future, an appropriate cell number leading to treatable tumors has to be found. Recently, this syngeneic, orthotopic bladder cancer mouse model was published for the first time showing that injection of 20 000 MB49 cells led to a consistent tumor growth (van Hooren et al. 2017).

For the xenograft mouse model, we used 200 000 UMUC3 cells for the injections which led to detectable tumors on day 4 in all animals (100 % tumor uptake) and an average tumor size of 24 mm^3 on day 10. Since there were variations in tumor growth and tumor volumes reached the experimental end point too fast, it might be worth testing lower cell concentrations in order to get a controllable tumor growth

4.6.2 Therapeutic effect of XVir-N-31 in the ultrasound guided, orthotopic bladder cancer mouse model

Within this project, we revealed the therapeutic potential of XVir-N-31 using the ultrasound guided orthotopic mouse model for bladder cancer. We could show that XVir-N-31 as a monotherapy significantly slowed down tumor growth in this sophisticated tumor model, although we used a relatively small number of animals per group. A complete tumor regression was not achieved which is in line with published data demonstrating the difficulty to completely eradicate tumors in immunodeficient xenograft models in which the immune response against the tumor is not present. This was confirmed in experiments where the ablation of T cells in an immunocompetent mouse model significantly reduced the efficacy of oncolysis (Tysome et al., 2012; Kleijn et al., 2017). In addition, since nuclear YB-1 is a prerequisite for viral replication of XVir-N-31, combination treatments with

chemotherapy or radiation therapy which translocate YB-1 into the nucleus are warranted and can help to further improve the therapeutic activity (Bieler et al., 2008).

4.7 Outlook

In this project, we began to investigate a viro-immunotherapeutic approach for bladder cancer. Therefore, we generated the novel virus XVir-N-31-aPD-L1 and provided the basis for further *in vivo* experiments. However, the most relevant and important questions remain to be answered. In the future, we want to address the immunological aspects of this therapy. Herein, we plan to analyze a broad spectrum ranging from basic questions like expression levels of PD-L1, IFNy and E2Fs pre-and post-infection till analysis of infiltrating immune cells and their function. Moreover, it is important to investigate if inhibiting PD-1/PD-L1 signaling and the consequent activation of the immune system remains the potency of XVir-N-31-aPD-L1 (Dias et al. 2012). Further on, we plan to evaluate the induction of a systemic anti-tumor immune response that can fight also distant metastasis. This aspect is of high clinical relevance and the generation of a systemic effect which enables the formation of memory T cells might be the key to a long lasting anti-tumor immune response. Thereby, deleting T cell subpopulations can help to identify important immune cells and understand the underlying mechanism of this novel therapeutic approach.

In order to analyze the above mentioned immunological aspects of virotherapy in an immunocompetent mouse model, we began to investigate YB-1 based adenoviral research in murine MB49 cells. Herein, we found that nutlin-3a improved replication of XVir-N-31 and that this effect seems, in contrast to human cells, independent of E2F1 and pRb downregulation. Various aspects should be studied in order to uncover this mechanism in detail. Herein, it would be interesting to analyze the activation of the E2 late promoter by looking at YB-1 expression, cellular localization and its nuclear translocation. Further on, expression of E2F1 and its influence on E2early promoter have to be studied. Additionally, based on the publication from Lasham et al. from 2012, it would be worth evaluating the regulation of E2F1 by YB-1 and their influence on adenovirus replication (Lasham et al. 2012). Moreover, it is necessary to explore the biochemical effects of nutlin-3a as well as the roles of cyclins, Rb and p53 in the context of XVir-N-31 in order to overcome the strict species specificity of human adenoviruses.

Altogether, the viro-immunotherapeutic approach is a novel and innovative strategy that is about to become an integrative part of cancer therapy and offers hope for a successful treatment of bladder cancer.

Bibliography

Aben, K.K.H., Witjes, J.A., Schoenberg, M.P., Hulsbergen-van de Kaa, C., Verbeek, A.L.M., and Kiemeney, L.A.L.M. (2002). Familial aggregation of urothelial cell carcinoma. International journal of cancer *98*, 274-278.

Adkins, I., Fucikova, J., Garg, A.D., Agostinis, P., and Špíšek, R. (2014). Physical modalities inducing immunogenic tumor cell death for cancer immunotherapy. Oncoimmunology *3*, e968434.

Alemany, R., Balagué, C., and Curiel, D.T. (2000). Replicative adenoviruses for cancer therapy. Nature biotechnology *18*, 723-727.

Ambrosini, G., Sambol, E.B., Carvajal, D., Vassilev, L.T., Singer, S., and Schwartz, G.K. (2007). Mouse double minute antagonist Nutlin-3a enhances chemotherapy-induced apoptosis in cancer cells with mutant p53 by activating E2F1. Oncogene *26*, 3473-3481.

Andtbacka, R.H.I., Kaufman, H.L., Collichio, F., Amatruda, T., Senzer, N., Chesney, J., Delman, K.A., Spitler, L.E., Puzanov, I., and Agarwala, S.S., et al. (2015). Talimogene Laherparepvec Improves Durable Response Rate in Patients with Advanced Melanoma. Journal of clinical oncology : official journal of the American Society of Clinical Oncology *33*, 2780-2788.

Apolo, A.B. (2016). PDL1: The Illusion of an Ideal Biomarker. European urology focus *1*, 269-271.

Apolo, A.B., Infante, J.R., Balmanoukian, A., Patel, M.R., Wang, D., Kelly, K., Mega, A.E., Britten, C.D., Ravaud, A., and Mita, A.C., et al. (2017). Avelumab, an Anti-Programmed Death-Ligand 1 Antibody, In Patients with Refractory Metastatic Urothelial Carcinoma: Results from a Multicenter, Phase Ib Study. Journal of clinical oncology : official journal of the American Society of Clinical Oncology *35*, 2117-2124.

Arnberg, N., Kidd, A.H., Edlund, K., Olfat, F., and Wadell, G. (2000). Initial Interactions of Subgenus D Adenoviruses with A549 Cellular Receptors: Sialic Acid versus αv Integrins. Journal of Virology *74*, 7691-7693.

Asghar, U., Witkiewicz, A.K., Turner, N.C., and Knudsen, E.S. (2015). The history and future of targeting cyclin-dependent kinases in cancer therapy. Nature reviews. Drug discovery *14*, 130-146.

Attwooll, C., Lazzerini Denchi, E., and Helin, K. (2004). The E2F family. Specific functions and overlapping interests. The EMBO journal *23*, 4709-4716.

Aznar, M.A., Tinari, N., Rullán, A.J., Sánchez-Paulete, A.R., Rodriguez-Ruiz, M.E., and Melero, I. (2017). Intratumoral Delivery of Immunotherapy-Act Locally, Think Globally. Journal of immunology (Baltimore, Md. : 1950) *198*, 31-39.

Bagchi, S., Raychaudhuri, P., and Nevins, J.R. (1990). Adenovirus E1A proteins can dissociate heteromeric complexes involving the E2F transcription factor. A novel mechanism for E1A trans-activation. Cell *62*, 659-669.

Bandara, L.R., and La Thangue, N.B. (1991). Adenovirus E1a prevents the retinoblastoma gene product from complexing with a cellular transcription factor. Nature *351*, 494-497.

Barber, G.N. (2011). Cytoplasmic DNA innate immune pathways. Immunological reviews *243*, 99-108.

Barber, G.N. (2011). Innate immune DNA sensing pathways: STING, AIMII and the regulation of interferon production and inflammatory responses. Current opinion in immunology *23*, 10-20.

Bargou, R.C., Jürchott, K., Wagener, C., Bergmann, S., Metzner, S., Bommert, K., Mapara, M.Y., Winzer, K.J., Dietel, M., and Dörken, B., et al. (1997). Nuclear localization and increased levels of transcription factor YB-1 in primary human breast cancers are associated with intrinsic MDR1 gene expression. Nature medicine *3*, 447-450.

Bauzon, M., Castro, D., Karr, M., Hawkins, L.K., and Hermiston, T.W. (2003). Multigene expression from a replicating adenovirus using native viral promoters. Molecular Therapy *7*, 526-534.

Bellacchio, E., and Paggi, M.G. (2013). Understanding the targeting of the RB family proteins by viral oncoproteins to defeat their oncogenic machinery. Journal of cellular physiology *228*, 285-291.

Ben-Israel, H. (2002). Adenovirus and cell cycle control. Front Biosci *7*, d1369.

Bernt, K.M., Ni, S., Tieu, A.-T., and Lieber, A. (2005). Assessment of a Combined, Adenovirus-Mediated Oncolytic and Immunostimulatory Tumor Therapy. Cancer Res *65*, 4343-4352.

Bett, A.J., Haddara, W., Prevec, L., and Graham, F.L. (1994). An efficient and flexible system for construction of adenovirus vectors with insertions or deletions in early regions 1 and 3. Proceedings of the National Academy of Sciences of the United States of America *91*, 8802-8806.

Bett, A.J., Prevec, L., and Graham, F.L. (1993). Packaging capacity and stability of human adenovirus type 5 vectors. Journal of Virology *67*, 5911-5921.

Bieler, A., Mantwill, K., Holzmüller, R., Jürchott, K., Kaszubiak, A., Stärk, S., Glockzin, G., Lage, H., Grosu, A.-L., and Gansbacher, B., et al. (2008). Impact of radiation therapy on the oncolytic adenovirus dl520. Implications on the treatment of glioblastoma. Radiotherapy and oncology : journal of the European Society for Therapeutic Radiology and Oncology *86*, 419-427.

Bidnur, S., Savdie, R., and Black, P.C. (2016). Inhibiting Immune Checkpoints for the Treatment of Bladder Cancer. Bladder cancer (Amsterdam, Netherlands) *2*, 15-25.

Bischoff, J.R., Kirn, D.H., Williams, A., Heise, C., Horn, S., Muna, M., Ng, L., Nye, J.A., Sampson-Johannes, A., and Fattaey, A., et al. (1996). An Adenovirus Mutant That Replicates Selectively in p53- Deficient Human Tumor Cells. Science *274*, 373-376.

Blank, C., Brown, I., Peterson, A.C., Spiotto, M., Iwai, Y., Honjo, T., and Gajewski, T.F. (2004). PD-L1/B7H-1 inhibits the effector phase of tumor rejection by T cell receptor (TCR) transgenic CD8+ T cells. Cancer research *64*, 1140-1145.

Boorjian, S.A., Sheinin, Y., Crispen, P.L., Farmer, S.A., Lohse, C.M., Kuntz, S.M., Leibovich, B.C., Kwon, E.D., and Frank, I. (2008). T-cell coregulatory molecule expression in urothelial cell carcinoma: clinicopathologic correlations and association with survival. Clinical cancer research : an official journal of the American Association for Cancer Research *14*, 4800-4808.

Boozari, B., Mundt, B., Woller, N., Strüver, N., Gürlevik, E., Schache, P., Kloos, A., Knocke, S., Manns, M.P., and Wirth, T.C., et al. (2010). Antitumoural immunity by virus-mediated immunogenic apoptosis inhibits metastatic growth of hepatocellular carcinoma. Gut *59*, 1416-1426.

Boulanger, P.A., and Blair, G.E. (1991). Expression and interactions of human adenovirus oncoproteins. Biochem. J. *275*, 281-299.

Bourgeois-Daigneault, M.-C., Roy, D.G., Aitken, A.S., El Sayes, N., Martin, N.T., Varette, O., Falls, T., St-Germain, L.E., Pelin, A., and Lichty, B.D., et al. (2018). Neoadjuvant oncolytic virotherapy before surgery sensitizes triple-negative breast cancer to immune checkpoint therapy. Science translational medicine *10*.

Braithwaite, A.W., and Russell, I.A. (2001). Induction of cell death by adenoviruses. Apoptosis : an international journal on programmed cell death *6*, 359-370.

Breitbach, C.J., Lichty, B.D., and Bell, J.C. (2016). Oncolytic Viruses: Therapeutics with an Identity Crisis. EBioMedicine *9*, 31-36.

Brennan, P., Bogillot, O., Cordier, S., Greiser, E., Schill, W., Vineis, P., Lopez-Abente, G., Tzonou, A., Chang-Claude, J., and Bolm-Audorff, U., et al. (2000). Cigarette smoking and bladder cancer in men: a pooled analysis of 11 case-control studies. International journal of cancer *86*, 289-294.

Bressy, C., and Benihoud, K. (2014). Association of oncolytic adenoviruses with chemotherapies. An overview and future directions. Biochemical pharmacology *90*, 97-106.

Brown, S.D., Warren, R.L., Gibb, E.A., Martin, S.D., Spinelli, J.J., Nelson, B.H., and Holt, R.A. (2014). Neo-antigens predicted by tumor genome meta-analysis correlate with increased patient survival. Genome Research *24*, 743-750.

Burger, M., Catto, J.W.F., Dalbagni, G., Grossman, H.B., Herr, H., Karakiewicz, P., Kassouf, W., Kiemeney, L.A., La Vecchia, C., and Shariat, S., et al. (2013). Epidemiology and risk factors of urothelial bladder cancer. European urology *63*, 234-241.

Burke, J. (2010). Virus therapy for bladder cancer. Cytokine & growth factor reviews *21*, 99-102.

Chartier, C., Degryse, E., Gantzer, M., Dieterle, A., Pavirani, A., and Mehtali, M. (1996). Efficient generation of recombinant adenovirus vectors by homologous recombination in Escherichia coli. Journal of Virology *70*, 4805-4810.

Chaurushiya, M.S., and Weitzman, M.D. (2009). Viral manipulation of DNA repair and cell cycle checkpoints. DNA repair *8*, 1166-1176.

Chen, J., Jiang, C.C., Jin, L., and Zhang, X.D. (2016). Regulation of PD-L1: a novel role of pro-survival signalling in cancer. Annals of oncology : official journal of the European Society for Medical Oncology *27*, 409-416.

Cheng, P.-H., Rao, X.-M., Wechman, S.L., Li, X.-F., McMasters, K.M., and Zhou, H.S. (2015). Oncolytic adenovirus targeting cyclin E overexpression repressed tumor growth in syngeneic immunocompetent mice. BMC cancer *15*, 716.

Cheng, P.-H., Wechman, S.L., McMasters, K.M., and Zhou, H.S. (2015). Oncolytic Replication of E1b-Deleted Adenoviruses. Viruses *7*, 5767-5779.

Chinai, J.M., Janakiram, M., Chen, F., Chen, W., Kaplan, M., and Zang, X. (2015). New immunotherapies targeting the PD-1 pathway. Trends in pharmacological sciences *36*, 587-595.

Cogdill, A.P., Andrews, M.C., and Wargo, J.A. (2017). Hallmarks of response to immune checkpoint blockade. British journal of cancer *117*, 1-7.

Cohen, C.J., Shieh, J.T., Pickles, R.J., Okegawa, T., Hsieh, J.T., and Bergelson, J.M. (2001). The coxsackievirus and adenovirus receptor is a transmembrane component of the tight junction. Proceedings of the National Academy of Sciences of the United States of America *98*, 15191-15196.

Coyne, C.B., and Bergelson, J.M. (2005). CAR: a virus receptor within the tight junction. Advanced drug delivery reviews *57*, 869-882.

Curiel, D.T. (2000). The development of conditionally replicative adenoviruses for cancer therapy. Clinical Cancer Research, 3395-3399.

Davarpanah, N.N., Yuno, A., Trepel, J.B., and Apolo, A.B. (2017). Immunotherapy. A new treatment paradigm in bladder cancer. Current opinion in oncology.

Di Iasio, M.G., and Zauli, G. (2013). The non-genotoxic activator of the p53 pathway Nutlin-3 shifts the balance between E2F7 and E2F1 transcription factors in leukemic cells. Investigational New Drugs *31*, 458-460.

Diaconu, I., Cerullo, V., Hirvinen, M.L.M., Escutenaire, S., Ugolini, M., Pesonen, S.K., Bramante, S., Parviainen, S., Kanerva, A., and Loskog, A.S.I., et al. (2012). Immune Response Is an Important Aspect of the Antitumor Effect Produced by a CD40L-Encoding Oncolytic Adenovirus. Cancer Res *72*, 2327-2338.

Dias, J.D., Hemminki, O., Diaconu, I., Hirvinen, M., Bonetti, A., Guse, K., Escutenaire, S., Kanerva, A., Pesonen, S., and Löskog, A., et al. (2012). Targeted cancer immunotherapy with oncolytic adenovirus coding for a fully human monoclonal antibody specific for CTLA-4. Gene therapy *19*, 988-998.

Diaz, R.M., Galivo, F., Kottke, T., Wongthida, P., Qiao, J., Thompson, J., Valdes, M., Barber, G., and Vile, R.G. (2007). Oncolytic immunovirotherapy for melanoma using vesicular stomatitis virus. Cancer research *67*, 2840-2848.

Dmitriev, I., Krasnykh, V., Miller, C.R., Wang, M., Kashentseva, E., Mikheeva, G., Belousova, N., and Curiel, D.T. (1998). An adenovirus vector with genetically modified fibers demonstrates expanded tropism via utilization of a coxsackievirus and adenovirus receptor-independent cell entry mechanism. Journal of Virology *72*, 9706-9713.

Dotti, G., Gottschalk, S., Savoldo, B., and Brenner, M.K. (2014). Design and development of therapies using chimeric antigen receptor-expressing T cells. Immunological reviews *257*, 107-126.

Drakos, E., Singh, R.R., Rassidakis, G.Z., Schlette, E., Li, J., Claret, F.X., Ford, R.J., JR, Vega, F., and Medeiros, L.J. (2011). Activation of the p53 pathway by the MDM2 inhibitor nutlin-3a overcomes BCL2 overexpression in a preclinical model of diffuse large B-cell lymphoma associated with t(14;18) (q32;q21). Leukemia *25*, 856-867.

Du, W., Wu, J., Walsh, E.M., Zhang, Y., Chen, C.Y., and Xiao, Z.-X.J. (2009). Nutlin-3 affects expression and function of retinoblastoma protein. Role of retinoblastoma protein in cellular response to nutlin-3. The Journal of biological chemistry *284*, 26315-26321.

Dyson, N. (1998). The regulation of E2F by pRB-family proteins. Genes & development *12*, 2245-2262.

Efficacy Study of Recombinant Adenovirus for Non Muscle Invasive Bladder Cancer - Full Text View - ClinicalTrials.gov. https://clinicaltrials.gov/ct2/show/NCT01438112. 13.07.2017.

Eliseeva, I.A., Kim, E.R., Guryanov, S.G., Ovchinnikov, L.P., and Lyabin, D.N. (2011). Y-box-binding protein 1 (YB-1) and its functions. Biochemistry. Biokhimiia *76*, 1402-1433.

Engeland, C.E., Grossardt, C., Veinalde, R., Bossow, S., Lutz, D., Kaufmann, J.K., Shevchenko, I., Umansky, V., Nettelbeck, D.M., and Weichert, W., et al. (2014). CTLA-4 and PD-L1 checkpoint blockade enhances oncolytic measles virus therapy. Molecular therapy : the journal of the American Society of Gene Therapy *22*, 1949-1959.

Ewen, M.E., Sluss, H.K., Sherr, C.J., Matsushime, H., Kato, J., and Livingston, D.M. (1993). Functional interactions of the retinoblastoma protein with mammalian D-type cyclins. Cell *73*, 487-497.

Farkona, S., Diamandis, E.P., and Blasutig, I.M. (2016). Cancer immunotherapy: the beginning of the end of cancer? BMC medicine *14*, 73.

Fattaey, A.R., Harlow, E., and Helin, K. (1993). Independent regions of adenovirus E1A are required for binding to and dissociation of E2F-protein complexes. Molecular and cellular biology *13*, 7267-7277.

Fausther-Bovendo, H., and Kobinger, G.P. (2014). Pre-existing immunity against Ad vectors: humoral, cellular, and innate response, what's important? Human vaccines & immunotherapeutics *10*, 2875-2884.

Ferlay, J., Soerjomataram, I., Dikshit, R., Eser, S., Mathers, C., Rebelo, M., Parkin, D.M., Forman, D., and Bray, F. (2015). Cancer incidence and mortality worldwide: sources, methods and major patterns in GLOBOCAN 2012. International journal of cancer *136*, E359-86.

Freedman, N.D., Silverman, D.T., Hollenbeck, A.R., Schatzkin, A., and Abnet, C.C. (2011). Association between smoking and risk of bladder cancer among men and women. JAMA *306*, 737-745.

Freeman, G.J., Long, A.J., Iwai, Y., Bourque, K., Chernova, T., Nishimura, H., Fitz, L.J., Malenkovich, N., Okazaki, T., and Byrne, M.C., et al. (2000). Engagement of the PD-1 immunoinhibitory receptor by a novel B7 family member leads to negative regulation of lymphocyte activation. The Journal of experimental medicine *192*, 1027-1034.

Freytag, S.O., Stricker, H., Lu, M., Elshaikh, M., Aref, I., Pradhan, D., Levin, K., Kim, J.H., Peabody, J., and Siddiqui, F., et al. (2014). Prospective randomized phase 2 trial of intensity modulated radiation therapy with or without oncolytic adenovirus-mediated cytotoxic gene therapy in intermediate-risk prostate cancer. International journal of radiation oncology, biology, physics *89*, 268-276.

Fueyo, J., Alemany, R., Gomez-Manzano, C., Fuller, G.N., Khan, A., Conrad, C.A., Liu, T.-J., Jiang, H., Lemoine, M.G., and Suzuki, K., et al. (2003). Preclinical characterization of the antiglioma activity of a tropism-enhanced adenovirus targeted to the retinoblastoma pathway. Journal of the National Cancer Institute *95*, 652-660.

Fuge, O., Vasdev, N., Allchorne, P., and Green, J.S. (2015). Immunotherapy for bladder cancer. Research and reports in urology *7*, 65-79.

Fukuhara, H., Ino, Y., and Todo, T. (2016). Oncolytic virus therapy: A new era of cancer treatment at dawn. Cancer science *107*, 1373-1379.

Galanis, E., Markovic, S.N., Suman, V.J., Nuovo, G.J., Vile, R.G., Kottke, T.J., Nevala, W.K., Thompson, M.A., Lewis, J.E., and Rumilla, K.M., et al. (2012). Phase II Trial of Intravenous Administration of Reolysin(®) (Reovirus Serotype-3-dearing Strain) in Patients with Metastatic Melanoma. Molecular therapy : the journal of the American Society of Gene Therapy *20*, 1998-2003.

Gangi, A., and Zager, J.S. (2017). The safety of talimogene laherparepvec for the treatment of advanced melanoma. Expert opinion on drug safety *16*, 265-269.

Ganly, I., Mautner, V., and Balmain, A. (2000). Productive Replication of Human Adenoviruses in Mouse Epidermal Cells. Journal of Virology *74*, 2895-2899.

Ghebremedhin, B. (2014). Human adenovirus: Viral pathogen with increasing importance. European journal of microbiology & immunology *4*, 26-33.

Giberson, A.N., Davidson, A.R., and Parks, R.J. (2012). Chromatin structure of adenovirus DNA throughout infection. Nucleic acids research *40*, 2369-2376.

Ginsberg, H.S., Moldawer, L.L., Sehgal, P.B., Redington, M., Kilian, P.L., Chanock, R.M., and Prince, G.A. (1991). A mouse model for investigating the molecular pathogenesis of adenovirus pneumonia. Proceedings of the National Academy of Sciences of the United States of America *88*, 1651-1655.

Gong, A.-Y., Zhou, R., Hu, G., Li, X., Splinter, P.L., O'Hara, S.P., LaRusso, N.F., Soukup, G.A., Dong, H., and Chen, X.-M. (2009). MicroRNA-513 regulates B7-H1 translation and is involved in IFN-gamma-induced B7-H1 expression in cholangiocytes. Journal of immunology (Baltimore, Md. : 1950) *182*, 1325-1333.

Gosnell, H., Kasman, L.M., Potta, T., Vu, L., Garrett-Mayer, E., Rege, K., and Voelkel-Johnson, C. (2014). Polymer-enhanced delivery increases adenoviral gene expression in an orthotopic model of bladder cancer. Journal of controlled release : official journal of the Controlled Release Society *176*, 35-43.

Graham, F.L., and Prevec, L. (1991). Manipulation of adenovirus vectors. Methods in molecular biology (Clifton, N.J.) *7*, 109-128.

Green, D.R., Ferguson, T., Zitvogel, L., and Kroemer, G. (2009). Immunogenic and tolerogenic cell death. Nature reviews. Immunology *9*, 353-363.

Gronostajski, R.M., Nagata, K., and Hurwitz, J. (1984). Isolation of human DNA sequences that bind to nuclear factor I, a host protein involved in adenovirus DNA replication. Proceedings of the National Academy of Sciences of the United States of America *81*, 4013-4017.

Guo, Z.S., Liu, Z., Kowalsky, S., Feist, M., Kalinski, P., Lu, B., Storkus, W.J., and Bartlett, D.L. (2017). Oncolytic Immunotherapy: Conceptual Evolution, Current Strategies, and Future Perspectives. Frontiers in immunology *8*, 555.

Halldén, G., Hill, R., Wang, Y., Anand, A., Liu, T.-C., Lemoine, N.R., Francis, J., Hawkins, L., and Kirn, D. (2003). Novel immunocompetent murine tumor models for the assessment of replication-competent oncolytic adenovirus efficacy. Molecular Therapy *8*, 412-424.

Han, C., Hao, L., Chen, M., Hu, J., Shi, Z., Zhang, Z., Dong, B., Fu, Y., Pei, C., and Wu, Y. (2013). Target expression of Staphylococcus enterotoxin A from an oncolytic adenovirus suppresses mouse bladder tumor growth and recruits CD3+ T cell. Tumour biology : the journal of the International Society for Oncodevelopmental Biology and Medicine *34*, 2863-2869.

Hanahan, D., and Weinberg, R.A. (2000). The Hallmarks of Cancer. Cell *100*, 57-70.

Hawkins, L.K., and Hermiston, T.W. (2001). Gene delivery from the E3 region of replicating human adenovirus. Evaluation of the ADP region. Gene therapy *8*, 1132-1141.

Hay, R.T., Freeman, A., Leith, I., Monaghan, A., and Webster, A. (1995). Molecular interactions during adenovirus DNA replication. Current topics in microbiology and immunology *199 (Pt 2)*, 31-48.

Helin, K., Harlow, E., and Fattaey, A. (1993). Inhibition of E2F1 transactivation by direct binding of the retinoblastoma protein. Molecular and cellular biology *13*, 6501-6508.

Hendrickx, R., Stichling, N., Koelen, J., Kuryk, L., Lipiec, A., and Greber, U.F. (2014). Innate immunity to adenovirus. Human gene therapy *25*, 265-284.

Hengel, H., Koszinowski, U.H., and Conzelmann, K.-K. (2005). Viruses know it all: new insights into IFN networks. Trends in immunology *26*, 396-401.

Herbst, R.S., Soria, J.-C., Kowanetz, M., Fine, G.D., Hamid, O., Gordon, M.S., Sosman, J.A., McDermott, D.F., Powderly, J.D., and Gettinger, S.N., et al. (2014). Predictive correlates of response to the anti-PD-L1 antibody MPDL3280A in cancer patients. Nature *515*, 563-567.

Hoeben, R.C., and Uil, T.G. (2013). Adenovirus DNA replication. Cold Spring Harbor perspectives in biology *5*, a013003.

Holm, P.S., Bergmann, S., Jurchott, K., Lage, H., Brand, K., Ladhoff, A., Mantwill, K., Curiel, D.T., Dobbelstein, M., and Dietel, M., et al. (2002). YB-1 relocates to the nucleus in adenovirus-infected cells and facilitates viral replication by inducing E2 gene expression through the E2 late promoter. J. Biol. Chem. *277*, 10427-10434.

Holm, P.S., Lage, H., Bergmann, S., Jürchott, K., Glockzin, G., Bernshausen, A., Mantwill, K., Ladhoff, A., Wichert, A., and Mymryk, J.S., et al. (2004). Multidrug-resistant cancer cells facilitate E1-independent adenoviral replication: impact for cancer gene therapy. Cancer research *64*, 322-328.

Horinaga, M., Fukuyama, R., Nishiyama, T., Harsch, K.M., Cicek, M., Heston, W., Sizemore, N., Casey, G., and Larchian, W. (2005). Novel enhanced lung-colonizing variant of murine MBT-2 bladder cancer cells. Urology *66*, 676-681.

Inman, B.A., Sebo, T.J., Frigola, X., Dong, H., Bergstralh, E.J., Frank, I., Fradet, Y., Lacombe, L., and Kwon, E.D. (2007). PD-L1 (B7-H1) expression by urothelial carcinoma of the bladder and BCG-induced granulomata: associations with localized stage progression. Cancer *109*, 1499-1505.

Irving, B., Chiu, H., Maecker, H., Mariathasan, S., Lehar, S.M., Wu, Y. and Cheung, J. (2009). Anti-pd-l1 antibodies and their use to enhance t-cell function (United States Patent Application Publication). http://www.google.ch/patents/US20100203056.

Iwai, Y., Terawaki, S., Ikegawa, M., Okazaki, T., and Honjo, T. (2003). PD-1 inhibits antiviral immunity at the effector phase in the liver. The Journal of experimental medicine *198*, 39-50.

Jäger, W., Moskalev, I., Janssen, C., Hayashi, T., Gust, K.M., Awrey, S., and Black, P.C. (2014). Minimally invasive establishment of murine orthotopic bladder xenografts. Journal of visualized experiments : JoVE, e51123.

Jiang, H., Clise-Dwyer, K., Ruisaard, K.E., Fan, X., Tian, W., Gumin, J., Lamfers, M.L., Kleijn, A., Lang, F.F., and Yung, W.-K.A., et al. (2014). Delta-24-RGD Oncolytic Adenovirus Elicits Anti-Glioma Immunity in an Immunocompetent Mouse Model. PLoS ONE *9*.

Jiang, H., Gomez-Manzano, C., Rivera-Molina, Y., Lang, F.F., Conrad, C.A., and Fueyo, J. (2015). Oncolytic adenovirus research evolution: from cell-cycle checkpoints to immune checkpoints. Current opinion in virology *13*, 33-39.

Jounaidi, Y., Doloff, J.C., and Waxman, D.J. (2007). Conditionally replicating adenoviruses for cancer treatment. Current cancer drug targets *7*, 285-301.

Juric, M.K., Ghimire, S., Ogonek, J., Weissinger, E.M., Holler, E., van Rood, J.J., Oudshoorn, M., Dickinson, A., and Greinix, H.T. (2016). Milestones of Hematopoietic Stem Cell Transplantation - From First Human Studies to Current Developments. Frontiers in immunology *7*, 470.

Kaczmarek, L., Ferguson, B., Rosenberg, M., and Baserga, R. (1986). Induction of cellular DNA synthesis by purified adenovirus E1A proteins. Virology *152*, 1-10.

Kandoth, C., McLellan, M.D., Vandin, F., Ye, K., Niu, B., Lu, C., Xie, M., Zhang, Q., McMichael, J.F., and Wyczalkowski, M.A., et al. (2013). Mutational landscape and significance across 12 major cancer types. Nature *502*, 333-339.

Kaufman, H.L., Kohlhapp, F.J., and Zloza, A. (2015). Oncolytic viruses: a new class of immunotherapy drugs. Nature reviews. Drug discovery *14*, 642-662.

Kawai, T., and Akira, S. (2009). The roles of TLRs, RLRs and NLRs in pathogen recognition. International immunology *21*, 317-337.

Kepp, O., Menger, L., Vacchelli, E., Locher, C., Adjemian, S., Yamazaki, T., Martins, I., Sukkurwala, A.Q., Michaud, M., and Senovilla, L., et al. (2013). Crosstalk between ER stress and immunogenic cell death. Cytokine & growth factor reviews *24*, 311-318.

Kim, W., Seong, J., Oh, H.J., Koom, W.S., Choi, K.-J., and Yun, C.-O. (2011). A novel combination treatment of armed oncolytic adenovirus expressing IL-12 and GM-CSF with radiotherapy in murine hepatocarcinoma. Journal of radiation research *52*, 646-654.

Kirn, D. (2005). Oncolytic virotherapy for cancer with the adenovirus dl1520 (Onyx-015). Results of Phase I and II trials. Expert Opinion on Biological Therapy *1*, 525-538.

Kleinpeter, P., Fend, L., Thioudellet, C., Geist, M., Sfrontato, N., Koerper, V., Fahrner, C., Schmitt, D., Gantzer, M., and Remy-Ziller, C., et al. (2016). Vectorization in an oncolytic vaccinia virus of an antibody, a Fab and a scFv against programmed cell death -1 (PD-1) allows their intratumoral delivery and an improved tumor-growth inhibition. Oncoimmunology *5*, e1220467.

Kleijn, A., van den Bossche, W., Haefner, E.S., Belcaid, Z., Burghoorn-Maas, C., Kloezeman, J.J., Pas, S.D., Leenstra, S., Debets, R., and Vrij, J. de, et al. (2017). The Sequence of Delta24-RGD and TMZ Administration in Malignant Glioma Affects the Role of CD8+T Cell Anti-tumor Activity. Molecular therapy oncolytics *5*, 11-19.

Knowles, M.A., and Hurst, C.D. (2015). Molecular biology of bladder cancer. New insights into pathogenesis and clinical diversity. Nature reviews. Cancer *15*, 25-41.

Kohlhapp, F.J., Zloza, A., and Kaufman, H.L. (2015). Talimogene laherparepvec (T-VEC) as cancer immunotherapy. Drugs of today (Barcelona, Spain : 1998) *51*, 549-558.

Kohno, K., Izumi, H., Uchiumi, T., Ashizuka, M., and Kuwano, M. (2003). The pleiotropic functions of the Y-box-binding protein, YB-1. BioEssays : news and reviews in molecular, cellular and developmental biology *25*, 691-698.

Kostova, Y., Mantwill, K., Holm, P.S., and Anton, M. (2015). An armed, YB-1-dependent oncolytic adenovirus as a candidate for a combinatorial anti-glioma approach of virotherapy, suicide gene therapy and chemotherapeutic treatment. Cancer gene therapy *22*, 30-43.

Kovesdi, I., Reichel, R., and Nevins, J.R. (1987). Role of an adenovirus E2 promoter binding factor in E1A-mediated coordinate gene control. Proceedings of the National Academy of Sciences of the United States of America *84*, 2180-2184.

Kozak, M. (1984). Point mutations close to the AUG initiator codon affect the efficiency of translation of rat preproinsulin in vivo. Nature *308*, 241-246.

Kroemer, G., Galluzzi, L., Kepp, O., and Zitvogel, L. (2013). Immunogenic cell death in cancer therapy. Annual review of immunology *31*, 51-72.

Kühnel, F., Schulte, B., Wirth, T., Woller, N., Schäfers, S., Zender, L., Manns, M., and Kubicka, S. (2004). Protein Transduction Domains Fused to Virus Receptors Improve Cellular Virus Uptake and Enhance Oncolysis by Tumor-Specific Replicating Vectors. J. Virol. *78*, 13743-13754.

Lasham, A., Print, C.G., Woolley, A.G., Dunn, S.E., and Braithwaite, A.W. (2013). YB-1: oncoprotein, prognostic marker and therapeutic target? The Biochemical journal *449*, 11-23.

Lasham, A., Samuel, W., Cao, H., Patel, R., Mehta, R., Stern, J.L., Reid, G., Woolley, A.G., Miller, L.D., and Black, M.A., et al. (2012). YB-1, the E2F pathway, and regulation of tumor cell growth. Journal of the National Cancer Institute *104*, 133-146.

Le, D.T., Durham, J.N., Smith, K.N., Wang, H., Bartlett, B.R., Aulakh, L.K., Lu, S., Kemberling, H., Wilt, C., and Luber, B.S., et al. (2017). Mismatch repair deficiency predicts response of solid tumors to PD-1 blockade. Science (New York, N.Y.) *357*, 409-413.

Leach, D.R., Krummel, M.F., and Allison, J.P. (1996). Enhancement of antitumor immunity by CTLA-4 blockade. Science *271*, 1734-1736.

Lee, S., and Margolin, K. (2011). Cytokines in cancer immunotherapy. Cancers *3*, 3856-3893.

Leonard, G.T., and Sen, G.C. (1997). Restoration of interferon responses of adenovirus E1A-expressing HT1080 cell lines by overexpression of p48 protein. Journal of Virology *71*, 5095-5101.

Li, E., Stupack, D., Bokoch, G.M., and Nemerow, G.R. (1998). Adenovirus endocytosis requires actin cytoskeleton reorganization mediated by Rho family GTPases. Journal of Virology *72*, 8806-8812.

Li, E., Stupack, D., Klemke, R., Cheresh, D.A., and Nemerow, G.R. (1998). Adenovirus endocytosis via alpha(v) integrins requires phosphoinositide-3-OH kinase. Journal of Virology *72*, 2055-2061.

Li, Y., Li, F., Jiang, F., Lv, X., Zhang, R., Lu, A., and Zhang, G. (2016). A Mini-Review for Cancer Immunotherapy: Molecular Understanding of PD-1/PD-L1 Pathway & Translational Blockade of Immune Checkpoints. International journal of molecular sciences *17*.

Lichtenstein, D.L., Krajcsi, P., Esteban, D.J., Tollefson, A.E., and Wold, W.S.M. (2002). Adenovirus RID Subunit Contains a Tyrosine Residue That Is Critical for RID-Mediated Receptor Internalization and Inhibition of Fas- and TRAIL-Induced Apoptosis. Journal of Virology *76*, 11329-11342.

Lichty, B.D., Breitbach, C.J., Stojdl, D.F., and Bell, J.C. (2014). Going viral with cancer immunotherapy. Nature reviews. Cancer *14*, 559-567.

Limbourg, F.P., Städtler, H., Chinnadurai, G., Baeuerle, P.A., and Schmitz, M.L. (1996). A Hydrophobic Region within the Adenovirus E1B 19 kDa Protein Is Necessary for the Transient Inhibition of NF-κB Activated by Different Stimuli. J. Biol. Chem. *271*, 20392-20398.

Liu, Q., and Muruve, D.A. (2003). Molecular basis of the inflammatory response to adenovirus vectors. Gene therapy *10*, 935-940.

Liu, T.-C., Galanis, E., and Kirn, D. (2007). Clinical trial results with oncolytic virotherapy. A century of promise, a decade of progress. Nature clinical practice. Oncology *4*, 101-117.

Livak, K.J., and Schmittgen, T.D. (2001). Analysis of relative gene expression data using real-time quantitative PCR and the 2(-Delta Delta C(T)) Method. Methods (San Diego, Calif.) *25*, 402-408.

Loskog, A., Dzojic, H., Vikman, S., Ninalga, C., Essand, M., Korsgren, O., and Totterman, T.H. (2004). Adenovirus CD40 ligand gene therapy counteracts immune escape mechanisms in the tumor Microenvironment. Journal of immunology (Baltimore, Md. : 1950) *172*, 7200-7205.

Loskog, A., Ninalga, C., Hedlund, T., Alimohammadi, M., Malmström, P.-U., and Tötterman, T.H. (2005). Optimization of the MB49 mouse bladder cancer model for adenoviral gene therapy. Laboratory animals *39*, 384-393.

Mahdavifar, N., Ghoncheh, M., Pakzad, R., Momenimovahed, Z., and Salehiniya, H. (2016). Epidemiology, Incidence and Mortality of Bladder Cancer and their Relationship with the Development Index in the World. Asian Pacific Journal of Cancer Prevention *17*, 381-386.

Mahr, J.A., and Gooding, L.R. (1999). Immune evasion by adenoviruses. Immunological reviews *168*, 121-130.

Makkouk, A., and Weiner, G.J. (2015). Cancer immunotherapy and breaking immune tolerance. New approaches to an old challenge. Cancer research *75*, 5-10.

Mantwill, K., Köhler-Vargas, N., Bernshausen, A., Bieler, A., Lage, H., Kaszubiak, A., Surowiak, P., Dravits, T., Treiber, U., and Hartung, R., et al. (2006). Inhibition of the multidrug-resistant phenotype by targeting YB-1 with a conditionally oncolytic adenovirus: implications for combinatorial treatment regimen with chemotherapeutic agents. Cancer research *66*, 7195-7202.

Mantwill, K., Naumann, U., Seznec, J., Girbinger, V., Lage, H., Surowiak, P., Beier, D., Mittelbronn, M., Schlegel, J., and Holm, P.S. (2013). YB-1 dependent oncolytic adenovirus efficiently inhibits tumor growth of glioma cancer stem like cells. Journal of translational medicine *11*, 216.

Martin, K., Trouche, D., Hagemeier, C., Sorensen, T.S., La Thangue, N.B., and Kouzarides, T. (1995). Stimulation of E2F1/DP1 transcriptional activity by MDM2 oncoprotein. Nature *375*, 691-694.

Martin, M.E., and Berk, A.J. (1998). Adenovirus E1B 55K represses p53 activation in vitro. Journal of Virology *72*, 3146-3154.

Massard, C., Gordon, M.S., Sharma, S., Rafii, S., Wainberg, Z.A., Luke, J., Curiel, T.J., Colon-Otero, G., Hamid, O., and Sanborn, R.E., et al. (2016). Safety and Efficacy of Durvalumab (MEDI4736), an Anti-Programmed Cell Death Ligand-1 Immune Checkpoint Inhibitor, in Patients with Advanced Urothelial Bladder Cancer. Journal of clinical oncology : official journal of the American Society of Clinical Oncology *34*, 3119-3125.

Matthews, D.A., and Russell, W.C. (1994). Adenovirus protein-protein interactions: hexon and protein VI. Journal of General Virology *75*, 3365-3374.

McDaniel, A.S., Alva, A., Zhan, T., Xiao, H., Cao, X., Gursky, A., Siddiqui, J., Chinnaiyan, A.M., Jiang, H., and Lee, C.T., et al. (2016). Expression of PDL1 (B7-H1) Before and After Neoadjuvant Chemotherapy in Urothelial Carcinoma. European urology focus *1*, 265-268.

Mell, L.K., Brumund, K.T., Daniels, G.A., Advani, S.J., Zakeri, K., Wright, M.E., Onyeama, S.-J., Weisman, R.A., Sanghvi, P.R., and Martin, P.J., et al. (2017). PHASE I TRIAL OF INTRAVENOUS ONCOLYTIC VACCINIA VIRUS (GL-ONC1) WITH CISPLATIN AND RADIOTHERAPY IN PATIENTS WITH LOCOREGIONALLY ADVANCED HEAD AND NECK CARCINOMA. Clinical cancer research : an official journal of the American Association for Cancer Research.

Meng, R.D., Phillips, P., and El-Deiry, W.S. (1999). p53-independent increase in E2F-1 expression enhances the cytotoxic effects of etoposide and of adriamycin. International journal of oncology *14*, 5-14.

Miyazaki, J., and Nishiyama, H. (2017). Epidemiology of urothelial carcinoma. International journal of urology : official journal of the Japanese Urological Association.

Moore, A.E. (1952). VIRUSES WITH ONCOLYTIC PROPERTIES AND THEIR ADAPTATION TO TUMORS. Annals of the New York Academy of Sciences *54*, 945-952.

Morales, A., Eidinger, D., and Bruce, A.W. (1976). Intracavitary Bacillus Calmette-Guerin in the treatment of superficial bladder tumors. The Journal of urology *116*, 180-183.

Nemajerova, A., Talos, F., Moll, U.M., and Petrenko, O. (2008). Rb function is required for E1A-induced S-phase checkpoint activation. Cell death and differentiation *15*, 1440-1449.

Nemerow, G.R. (2000). Cell receptors involved in adenovirus entry. Virology *274*, 1-4.

Nervins, J.R. (1987). Regulation of Early Adenovirus Gene Expression. Microbiological Reviews *51*, 419-430.

Nettelbeck, D.M. (2003). Virotherapeutics: conditionally replicative adenoviruses for viral oncolysis. Anti-cancer drugs *14*, 577-584.

Nevins, J.R. (1992). E2F. A link between the Rb tumor suppressor protein and viral oncoproteins. Science *258*, 424-429.

Nirschl, C.J., and Drake, C.G. (2013). Molecular pathways: coexpression of immune checkpoint molecules: signaling pathways and implications for cancer immunotherapy. Clinical cancer research : an official journal of the American Association for Cancer Research *19*, 4917-4924.

Nishino, M., Ramaiya, N.H., Hatabu, H., and Hodi, F.S. (2017). Monitoring immune-checkpoint blockade: response evaluation and biomarker development. Nature reviews. Clinical oncology.

Noonan, A.M., Farren, M.R., Geyer, S.M., Huang, Y., Tahiri, S., Ahn, D., Mikhail, S., Ciombor, K.K., Pant, S., and Aparo, S., et al. (2016). Randomized Phase 2 Trial of the Oncolytic Virus Pelareorep (Reolysin) in Upfront Treatment of Metastatic Pancreatic Adenocarcinoma. Molecular therapy : the journal of the American Society of Gene Therapy *24*, 1150-1158.

Okazaki, T., and Honjo, T. (2007). PD-1 and PD-1 ligands: from discovery to clinical application. International immunology *19*, 813-824.

Pardoll, D.M. (2012). The blockade of immune checkpoints in cancer immunotherapy. Nature reviews. Cancer *12*, 252-264.

Patel, M.R., and Kratzke, R.A. (2013). Oncolytic virus therapy for cancer: the first wave of translational clinical trials. Translational research : the journal of laboratory and clinical medicine *161*, 355-364.

Peng, W., Liu, C., Xu, C., Lou, Y., Chen, J., Yang, Y., Yagita, H., Overwijk, W.W., Lizée, G., and Radvanyi, L., et al. (2012). PD-1 Blockade Enhances T-cell Migration to Tumors by Elevating IFN-γ Inducible Chemokines. Cancer Res *72*, 5209-5218.

Pesonen, S., Kangasniemi, L., and Hemminki, A. (2011). Oncolytic adenoviruses for the treatment of human cancer: focus on translational and clinical data. Molecular pharmaceutics *8*, 12-28.

Philipson, L., and Pettersson, R.F. (2004). The coxsackie-adenovirus receptor--a new receptor in the immunoglobulin family involved in cell adhesion. Current topics in microbiology and immunology *273*, 87-111.

Pico de Coaña, Y., Choudhury, A., and Kiessling, R. (2015). Checkpoint blockade for cancer therapy: revitalizing a suppressed immune system. Trends in molecular medicine *21*, 482-491.

Polager, S., and Ginsberg, D. (2009). p53 and E2f: partners in life and death. Nature reviews. Cancer *9*, 738-748.

Pollutri, D. (2014). Drugs down - regulati ng E2F - 1 expression hinder s cell proliferation through a p53 Drugs down-regulating E2F-1 expression hinders cell proliferation through a p53-independent mechanism. Dissertation (Bologna).

Postow, M.A., Callahan, M.K., and Wolchok, J.D. (2015). Immune Checkpoint Blockade in Cancer Therapy. Journal of clinical oncology : official journal of the American Society of Clinical Oncology *33*, 1974-1982.

Potts, K.G., Hitt, M.M., and Moore, R.B. (2012). Oncolytic viruses in the treatment of bladder cancer. Advances in urology *2012*, 404581.

Prestwich, R.J., Errington, F., Ilett, E.J., Morgan, R.S.M., Scott, K.J., Kottke, T., Thompson, J., Morrison, E.E., Harrington, K.J., and Pandha, H.S., et al. (2008). Tumor infection by oncolytic reovirus primes adaptive antitumor immunity. Clinical cancer research : an official journal of the American Association for Cancer Research *14*, 7358-7366.

Purcell, A.W., and Elliott, T. (2008). Molecular machinations of the MHC-I peptide loading complex. Current opinion in immunology *20*, 75-81.

Puzanov, I., Milhem, M.M., Minor, D., Hamid, O., Li, A., Chen, L., Chastain, M., Gorski, K.S., Anderson, A., and Chou, J., et al. (2016). Talimogene Laherparepvec in Combination with Ipilimumab in Previously

Untreated, Unresectable Stage IIIB-IV Melanoma. Journal of clinical oncology : official journal of the American Society of Clinical Oncology *34*, 2619-2626.

Qian, Y., Deng, J., Geng, L., Xie, H., Jiang, G., Zhou, L., Wang, Y., Yin, S., Feng, X., and Liu, J., et al. (2008). TLR4 signaling induces B7-H1 expression through MAPK pathways in bladder cancer cells. Cancer investigation *26*, 816-821.

Querido, E., Marcellus, R.C., Lai, A., Charbonneau, R., Teodoro, J.G., Ketner, G., and Branton, P.E. (1997). Regulation of p53 levels by the E1B 55-kilodalton protein and E4orf6 in adenovirus-infected cells. Journal of Virology *71*, 3788-3798.

Ramesh, N., Ge, Y., Ennist, D.L., Zhu, M., Mina, M., Ganesh, S., Reddy, P.S., and Yu, D.-C. (2006). CG0070, a conditionally replicating granulocyte macrophage colony-stimulating factor--armed oncolytic adenovirus for the treatment of bladder cancer. Clinical cancer research : an official journal of the American Association for Cancer Research *12*, 305-313.

Rehman, H., Silk, A.W., Kane, M.P., and Kaufman, H.L. (2016). Into the clinic: Talimogene laherparepvec (T-VEC), a first-in-class intratumoral oncolytic viral therapy. Journal for immunotherapy of cancer *4*, 53.

Reolysin ClinicalTrials.gov.
https://clinicaltrials.gov/ct2/results?cond=&term=Reolysin&cntry=&state=&city=&dist=. 18.01.2018.

Ressing, M.E., Luteijn, R.D., Horst, D., and Wiertz, E.J. (2013). Viral interference with antigen presentation: trapping TAP. Molecular immunology *55*, 139-142.

Ribas, A., and Hu-Lieskovan, S. (2016). What does PD-L1 positive or negative mean? The Journal of experimental medicine *213*, 2835-2840.

Ribas, A., Dummer, R., Puzanov, I., VanderWalde, A., Andtbacka, R.H.I., Michielin, O., Olszanski, A.J., Malvehy, J., Cebon, J., and Fernandez, E., et al. (2017). Oncolytic Virotherapy Promotes Intratumoral T Cell Infiltration and Improves Anti-PD-1 Immunotherapy. Cell *170*, 1109-1119.e10.

Ritprajak, P., and Azuma, M. (2015). Intrinsic and extrinsic control of expression of the immunoregulatory molecule PD-L1 in epithelial cells and squamous cell carcinoma. Oral oncology *51*, 221-228.

Rizvi, N.A., Hellmann, M.D., Snyder, A., Kvistborg, P., Makarov, V., Havel, J.J., Lee, W., Yuan, J., Wong, P., and Ho, T.S., et al. (2015). Cancer immunology. Mutational landscape determines sensitivity to PD-1 blockade in non-small cell lung cancer. Science (New York, N.Y.) *348*, 124-128.

Robinson, C.M., Singh, G., Lee, J.Y., Dehghan, S., Rajaiya, J., Liu, E.B., Yousuf, M.A., Betensky, R.A., Jones, M.S., and Dyer, D.W., et al. (2013). Molecular evolution of human adenoviruses. Scientific reports *3*, 1812.

Rognoni, E., Widmaier, M., Haczek, C., Mantwill, K., Holzmüller, R., Gansbacher, B., Kolk, A., Schuster, T., Schmid, R.M., and Saur, D., et al. (2009). Adenovirus-based virotherapy enabled by cellular YB-1 expression in vitro and in vivo. Cancer gene therapy *16*, 753-763.

Rothmann, T., Hengstermann, A., Whitaker N., J., Scheffner M., and Hausen, H. (1998). Replication of ONYX-015, a potential anticancer adenovirus, is independent of p53 status in tumor biology. Journal of Virology *72*, 9470-9478.

Russell, S.J., Peng, K.-W., and Bell, J.C. (2012). Oncolytic virotherapy. Nature biotechnology *30*, 658-670.

Russell, W.C. (2000). Update on adenovirus and its vectors. The Journal of general virology *81*, 2573-2604.

Russell, W.C. (2009). Adenoviruses: update on structure and function. The Journal of general virology *90*, 1-20.

Sabichi, A., Keyhani, A., Tanaka, N., Delacerda, J., Lee, I.-l., Zou, C., Zhou, J.-h., Benedict, W.F., and Grossman, H.B. (2006). Characterization of a Panel of Cell Lines Derived from Urothelial Neoplasms. Genetic Alterations, Growth In Vivo and the Relationship of Adenoviral Mediated Gene Transfer to Coxsackie Adenovirus Receptor Expression. The Journal of urology *175*, 1133-1137.

Safety and Efficacy of CG0070 Oncolytic Virus Regimen for High Grade NMIBC After BCG Failure - Full Text View - ClinicalTrials.gov. https://clinicaltrials.gov/ct2/show/NCT02365818. 13.07.2017.

Saha, B., Wong, C.M., and Parks, R.J. (2014). The adenovirus genome contributes to the structural stability of the virion. Viruses *6*, 3563-3583.

Saluja, M., and Gilling, P. (2017). Intravesical bacillus Calmette-Guérin instillation in non-muscle-invasive bladder cancer: A review. International journal of urology : official journal of the Japanese Urological Association.

Sanmamed, M.F., Rodriguez, I., Schalper, K.A., Onate, C., Azpilikueta, A., Rodriguez-Ruiz, M.E., Morales-Kastresana, A., Labiano, S., Perez-Gracia, J.L., and Martin-Algarra, S., et al. (2015). Nivolumab and Urelumab Enhance Antitumor Activity of Human T Lymphocytes Engrafted in Rag2-/-IL2Rgammanull Immunodeficient Mice. Cancer research *75*, 3466-3478.

Sathe, A., Koshy, N., Schmid, S.C., Thalgott, M., Schwarzenböck, S.M., Krause, B.J., Holm, P.S., Gschwend, J.E., Retz, M., and Nawroth, R. (2016). CDK4/6 Inhibition Controls Proliferation of Bladder Cancer and Transcription of RB1. The Journal of urology *195*, 771-779.

Schagen, F.H.E., Ossevoort, M., Toes, R.E.M., and Hoeben, R.C. (2004). Immune responses against adenoviral vectors and their transgene products. A review of strategies for evasion. Critical Reviews in Oncology / Hematology *50*, 51-70.

Schroder, K., Hertzog, P.J., Ravasi, T., and Hume, D.A. (2004). Interferon-gamma. An overview of signals, mechanisms and functions. Journal of leukocyte biology *75*, 163-189.

Schumacher, T.N., and Schreiber, R.D. (2015). Neoantigens in cancer immunotherapy. Science (New York, N.Y.) *348*, 69-74.

Scosyrev, E., Noyes, K., Feng, C., and Messing, E. (2009). Sex and racial differences in bladder cancer presentation and mortality in the US. Cancer *115*, 68-74.

Seifried, L.A., Talluri, S., Cecchini, M., Julian, L.M., Mymryk, J.S., and Dick, F.A. (2008). pRB-E2F1 complexes are resistant to adenovirus E1A-mediated disruption. Journal of Virology *82*, 4511-4520.

Sharma, A., Li, X., Bangari, D.S., and Mittal, S.K. (2009). Adenovirus receptors and their implications in gene delivery. Virus research *143*, 184-194.

Sharma, P., and Allison, J.P. (2015). The future of immune checkpoint therapy. Science (New York, N.Y.) *348*, 56-61.

Sharma, S., Ksheersagar, P., and Sharma, P. (2009). Diagnosis and treatment of bladder cancer. American family physician *80*, 717-723.

Shaw, P.H. (1996). The Role of p53 in Cell Cycle Regulation. Pathology - Research and Practice *192*, 669-675.

Shen, Z., Shen, T., Wientjes, M.G., O'Donnell, M.A., and Au, J.L.-S. (2008). Intravesical treatments of bladder cancer: review. Pharmaceutical research *25*, 1500-1510.

Sherr, C.J., and McCormick, F. (2002). The RB and p53 pathways in cancer. Cancer Cell *2*, 103-112.

Shultz, L.D., Brehm, M.A., Garcia, J.V., and Greiner, D.L. (2012). Humanized mice for immune system investigation. Progress, promise and challenges. Nature reviews. Immunology *12*, 786-798.

Shultz, L.D., Ishikawa, F., and Greiner, D.L. (2007). Humanized mice in translational biomedical research. Nature reviews. Immunology *7*, 118-130.

Sim, G.C., and Radvanyi, L. (2014). The IL-2 cytokine family in cancer immunotherapy. Cytokine & growth factor reviews *25*, 377-390.

Snyder, A., Makarov, V., Merghoub, T., Yuan, J., Zaretsky, J.M., Desrichard, A., Walsh, L.A., Postow, M.A., Wong, P., and Ho, T.S., et al. (2014). Genetic basis for clinical response to CTLA-4 blockade in melanoma. The New England journal of medicine *371*, 2189-2199.

Sobol, P.T., Boudreau, J.E., Stephenson, K., Wan, Y., Lichty, B.D., and Mossman, K.L. (2011). Adaptive antiviral immunity is a determinant of the therapeutic success of oncolytic virotherapy. Molecular therapy : the journal of the American Society of Gene Therapy *19*, 335-344.

Soloway, M.S. (1975). Single and combination chemotherapy for primary murine bladder cancer. Cancer *36*, 333-340.

Study of Pembrolizumab with REOLYSIN® and Chemotherapy in Patients With Advanced Pancreatic Adenocarcinoma - Full Text View - ClinicalTrials.gov. https://clinicaltrials.gov/ct2/show/NCT02620423. 01.10.2017.

Stuiver, M.H., and Vliet, P C van der (1990). Adenovirus DNA-binding protein forms a multimeric protein complex with double-stranded DNA and enhances binding of nuclear factor I. J. Virol. *64*, 379-386.

Stuiver, M.H., and Vliet, P C van der (1990). Adenovirus DNA-binding protein forms a multimeric protein complex with double-stranded DNA and enhances binding of nuclear factor I. J. Virol. *64*, 379-386.

Sugarman B.J., Hutchins B.M., McAllister D.L.: Lu F., and Thomas K.B. (2003). The Complete Nucleic Acid Sequence of the Adenovirus Type 5 Reference Material (ARM) Genome. BioProcessing Journal *5*, 27-33.

Summerhayes, I.C., and Franks, L.M. (1979). Effects of donor age on neoplastic transformation of adult mouse bladder epithelium in vitro. Journal of the National Cancer Institute *62*, 1017-1023.

Suzuki, M., Kondo, S., Pei, Z., Maekawa, A., Saito, I., and Kanegae, Y. (2015). Preferable sites and orientations of transgene inserted in the adenovirus vector genome. The E3 site may be unfavorable for transgene position. Gene therapy *22*, 421-429.

Taguchi, S., Fukuhara, H., Homma, Y., and Todo, T. (2017). Current status of clinical trials assessing oncolytic virus therapy for urological cancers. International journal of urology : official journal of the Japanese Urological Association *24*, 342-351.

Tanaka, T., Miyazawa, K., Tsukamoto, T., Kuno, T., and Suzuki, K. (2011). Pathobiology and chemoprevention of bladder cancer. Journal of oncology *2011*, 528353.

Tesniere, A., Panaretakis, T., Kepp, O., Apetoh, L., Ghiringhelli, F., Zitvogel, L., and Kroemer, G. (2008). Molecular characteristics of immunogenic cancer cell death. Cell death and differentiation *15*, 3-12.

Thaci, B., Ulasov, I.V., Wainwright, D.A., and Lesniak, M.S. (2011). The challenge for gene therapy: innate immune response to adenoviruses. Oncotarget *2*, 113-121.

Tollefson, A.E., Ryerse, J.S., Scaria, A., Hermiston, T.W., and Wold, W.S. (1996). The E3-11.6-kDa Adenovirus Death Protein (ADP) Is Required for Efficient Cell Death. Virology *220*, 152-162.

Tollefson, A.E., Scaria, A., Hermiston, T.W., Ryerse, J.S., Wold, L.J., and Wold, W.S. (1996). The adenovirus death protein (E3-11.6K) is required at very late stages of infection for efficient cell lysis and release of adenovirus from infected cells. Journal of Virology *70*, 2296-2306.

Tollefson, A.E., Scaria, A., Saha, S.K., and Wold, W.S. (1992). The 11,600-MW protein encoded by region E3 of adenovirus is expressed early but is greatly amplified at late stages of infection. Journal of Virology *66*, 3633-3642.

Tomko, R.P., Johansson, C.B., Totrov, M., Abagyan, R., Frisen, J., and Philipson, L. (2000). Expression of the adenovirus receptor and its interaction with the fiber knob. Experimental cell research *255*, 47-55.

Tresilwised, N., Pithayanukul, P., Holm, P.S., Schillinger, U., Plank, C., and Mykhaylyk, O. (2012). Effects of nanoparticle coatings on the activity of oncolytic adenovirus-magnetic nanoparticle complexes. Biomaterials *33*, 256-269.

Trimarchi, J.M., and Lees, J.A. (2002). Sibling rivalry in the E2F family. Nature reviews. Molecular cell biology *3*, 11-20.

Tumeh, P.C., Harview, C.L., Yearley, J.H., Shintaku, I.P., Taylor, E.J.M., Robert, L., Chmielowski, B., Spasic, M., Henry, G., and Ciobanu, V., et al. (2014). PD-1 blockade induces responses by inhibiting adaptive immune resistance. Nature *515*, 568-571.

Turnbull, S., West, E.J., Scott, K.J., Appleton, E., Melcher, A., and Ralph, C. (2015). Evidence for Oncolytic Virotherapy: Where Have We Got to and Where Are We Going? Viruses *7*, 6291-6312.

Tysome, J.R., Li, X., Wang, S., Wang, P., Gao, D., Du, P., Chen, D., Gangeswaran, R., Chard, L.S., and Yuan, M., et al. (2012). A novel therapeutic regimen to eradicate established solid tumors with an effective induction of tumor-specific immunity. Clinical cancer research : an official journal of the American Association for Cancer Research *18*, 6679-6689.

van Hooren, L., Sandin, L.C., Moskalev, I., Ellmark, P., Dimberg, A., Black, P., Tötterman, T.H., and Mangsbo, S.M. (2017). Local checkpoint inhibition of CTLA-4 as a monotherapy or in combination with anti-PD1 prevents the growth of murine bladder cancer. European journal of immunology *47*, 385-393.

van Maerken, T., Speleman, F., Vermeulen, J., Lambertz, I., Clercq, S. de, Smet, E. de, Yigit, N., Coppens, V., Philippé, J., and Paepe, A. de, et al. (2006). Small-molecule MDM2 antagonists as a new therapy concept for neuroblastoma. Cancer research *66*, 9646-9655.

Vassilev, L.T., Vu, B.T., Graves, B., Carvajal, D., Podlaski, F., Filipovic, Z., Kong, N., Kammlott, U., Lukacs, C., and Klein, C., et al. (2004). In vivo activation of the p53 pathway by small-molecule antagonists of MDM2. Science (New York, N.Y.) *303*, 844-848.

Velcheti, V., and Schalper, K. (2016). Basic Overview of Current Immunotherapy Approaches in Cancer. American Society of Clinical Oncology educational book. American Society of Clinical Oncology. Meeting *35*, 298-308.

virotherapy - ClinicalTrials.gov.
https://clinicaltrials.gov/ct2/results?cond=&term=virotherapy&cntry1=&state1=&Search=Search.
25.07.2017.

Vorburger, S.A., and Hunt, K.K. (2002). Adenoviral gene therapy. The oncologist *7*, 46-59.

Vroni Girbinger (2013). Immunological aspects of YB-1-dependent oncolytic virotherapy. Dissertation (München).

Walsh, E.M., Niu, M., Bergholz, J., and Xiao, Z.-X.J. (2015). Nutlin-3 down-regulates retinoblastoma protein expression and inhibits muscle cell differentiation. Biochemical and biophysical research communications *461*, 293-299.

Wang, Y., Hallden, G., Hill, R., Anand, A., Liu, T.-C., Francis, J., Brooks, G., Lemoine, N., and Kirn, D. (2003). E3 gene manipulations affect oncolytic adenovirus activity in immunocompetent tumor models. Nature biotechnology *21*, 1328-1335.

Whyte, P., Williamson, N.M., and Harlow, E. (1989). Cellular targets for transformation by the adenovirus E1A proteins. Cell *56*, 67-75.

Witjes, J.A., Compérat, E., Cowan, N.C., Santis, M. de, Gakis, G., Lebret, T., Ribal, M.J., van der Heijden, A.G., and Sherif, A. (2014). EAU guidelines on muscle-invasive and metastatic bladder cancer: summary of the 2013 guidelines. European urology *65*, 778-792.

Wohlleber, D., Kashkar, H., Gärtner, K., Frings, M.K., Odenthal, M., Hegenbarth, S., Börner, C., Arnold, B., Hämmerling, G., and Nieswandt, B., et al. (2012). TNF-induced target cell killing by CTL activated through cross-presentation. Cell reports *2*, 478-487.

Wold, W.S. (1993). Adenovirus genes that modulate the sensitivity of virus-infected cells to lysis by TNF. Journal of cellular biochemistry *53*, 329-335.

Wold, W.S., Tollefson, A.E., and Hermiston, T.W. (1995). E3 transcription unit of adenovirus. Current topics in microbiology and immunology *199 (Pt 1)*, 237-274.

Wold, W.S.M., and Toth, K. (2012). Chapter three--Syrian hamster as an animal model to study oncolytic adenoviruses and to evaluate the efficacy of antiviral compounds. Advances in cancer research *115*, 69-92.

Wolffe, A.P., Tafuri, S., Ranjan, M., and Familari, M. (1992). The Y-box factors: a family of nucleic acid binding proteins conserved from Escherichia coli to man. The New biologist *4*, 290-298.

Woller, N., Gürlevik, E., Fleischmann-Mundt, B., Schumacher, A., Knocke, S., Kloos, A.M., Saborowski, M., Geffers, R., Manns, M.P., and Wirth, T.C., et al. (2015). Viral Infection of Tumors Overcomes Resistance to PD-1-immunotherapy by Broadening Neoantigenome-directed T-cell Responses. Molecular therapy : the journal of the American Society of Gene Therapy *23*, 1630-1640.

Woller, N., Gürlevik, E., Ureche, C.-I., Schumacher, A., and Kühnel, F. (2014). Oncolytic viruses as anticancer vaccines. Frontiers in oncology *4*, 188.

Workenhe, S.T., and Mossman, K.L. (2014). Oncolytic virotherapy and immunogenic cancer cell death: sharpening the sword for improved cancer treatment strategies. Molecular therapy : the journal of the American Society of Gene Therapy *22*, 251-256.

Wu, C.-L., Shieh, G.-S., Chang, C.-C., Yo, Y.-T., Su, C.-H., Chang, M.-Y., Huang, Y.-H., Wu, P., and Shiau, A.-L. (2008). Tumor-selective replication of an oncolytic adenovirus carrying oct-3/4 response elements in murine metastatic bladder cancer models. Clinical cancer research : an official journal of the American Association for Cancer Research *14*, 1228-1238.

Yamamoto, M., and Curiel, D.T. (2005). Cancer gene therapy. Technology in cancer research & treatment *4*, 315-330.

Younghusband, H.B., Tyndall, C., and Bellett, A.J. (1979). Replication and interaction of virus DNA and cellular DNA in mouse cells infected by a human adenovirus. The Journal of general virology *45*, 455-467.

Yun, C.-O., Kim, E., Koo, T., Kim, H., Lee, Y.-s., and Kim, J.-H. (2005). ADP-overexpressing adenovirus elicits enhanced cytopathic effect by induction of apoptosis. Cancer gene therapy *12*, 61-71.

Zaiss, A.K., Machado, H.B., and Herschman, H.R. (2009). The influence of innate and pre-existing immunity on adenovirus therapy. Journal of cellular biochemistry *108*, 778-790.

Zamarin, D., Holmgaard, R.B., Subudhi, S.K., Park, J.S., Mansour, M., Palese, P., Merghoub, T., Wolchok, J.D., and Allison, J.P. (2014). Localized oncolytic virotherapy overcomes systemic tumor resistance to immune checkpoint blockade immunotherapy. Science translational medicine *6*, 226ra32.

Zhang, L., Hedjran, F., Larson, C., Perez, G.L., and Reid, T. (2015). A novel immunocompetent murine model for replicating oncolytic adenoviral therapy. Cancer gene therapy *22*, 17-22.

Zhang, Y., Xiong, Y., and Yarbrough, W.G. (1998). ARF promotes MDM2 degradation and stabilizes p53: ARF-INK4a locus deletion impairs both the Rb and p53 tumor suppression pathways. Cell *92*, 725-734.

Affidavit

I hereby declare that the dissertation titled
Establishment of an orthotopic bladder cancer mouse model for the assessment of a novel YB-1 based viro-immunotherapy *in vivo*
prepared under the guidance and supervision of
PD Dr. Per Sonne Holm at the Department of Urology
and submitted to the degree-awarding institution of Medicine at the Technical University Munich is my own, original work undertaken in partial fulfillment of the requirements of the doctoral degree. I have made no use of sources, materials or assistance other than those specified in §6(6) and (7), clause 2.
[X] I have not employed the service of an organization that provides dissertation supervisors in return for payment or that fulfills, in whole or in part, the obligations incumbent on me in connection with my dissertation.
[X] I have not submitted the dissertation, either in the present or in a similar form, as part of another examination process.
[ ] The complete dissertation was published in _____
The degree- awarding institution _____
has approved prior publication of the dissertation.
[ ] I have not yet been awarded the desired doctoral degree nor have I failed the last possible attempt to obtain the desired degree in a previous doctoral program.
[ ] I have already applied for admission to a doctoral program at the school or college of
_____
at (university) _____
by submitting the dissertation on the topic _____
_____
with the result: _____
I am familiar with the publicly available regulations of the Award of Doctoral Degrees of TUM, §28 (invalidation of doctoral degree) and §29 (revocation of doctoral degree). I am aware of the consequences of filling a false affidavit.

[X] I agree [ ] I do not agree
That my personal data is stored in the TUM alumni database.

Munich, 9.2.2018